Calhoun
Institutional Archive of the Naval Postgraduate School

**Calhoun: The NPS Institutional Archive**

**DSpace Repository**

Theses and Dissertations 1. Thesis and Dissertation Collection, all items

1999

# Low cost parachute guidance, navigation, and control

Dellicker, Scott Henry

Monterey, California. Naval Postgraduate School

http://hdl.handle.net/10945/8636

This publication is a work of the U.S. Government as defined in Title 17, United States Code, Section 101. Copyright protection is not available for this work in the United States.

*Downloaded from NPS Archive: Calhoun*

DUDLEY KNOX LIBRARY

Calhoun is the Naval Postgraduate School's public access digital repository for research materials and institutional publications created by the NPS community. Calhoun is named for Professor of Mathematics Guy K. Calhoun, NPS's first appointed -- and published -- scholarly author.

Dudley Knox Library / Naval Postgraduate School
411 Dyer Road / 1 University Circle
Monterey, California USA 93943

http://www.nps.edu/library

NPS ARCHIVE
1999.09
DELLICKER, S.

DUDLEY KNOX LIBRARY
NAVAL POSTGRADUATE SCHOOL
MONTEREY CA 93943-5101

# NAVAL POSTGRADUATE SCHOOL
## Monterey, California

# THESIS

## LOW COST PARACHUTE GUIDANCE, NAVIGATION, AND CONTROL

by

Scott Henry Dellicker

September 1999

Thesis Advisors: Richard M. Howard<br>
Isaac I. Kaminer

Approved for public release; distribution is unlimited.

# REPORT DOCUMENTATION PAGE

*Form Approved*
*OMB No. 0704-0188*

Public reporting burden for this collection of information is estimated to average 1 hour per response, including the time for reviewing instruction, searching existing data sources, gathering and maintaining the data needed, and completing and reviewing the collection of information. Send comments regarding this burden estimate or any other aspect of this collection of information, including suggestions for reducing this burden, to Washington headquarters Services, Directorate for Information Operations and Reports, 1215 Jefferson Davis Highway, Suite 1204, Arlington, VA 22202-4302, and to the Office of Management and Budget, Paperwork Reduction Project (0704-0188) Washington DC 20503.

**1. AGENCY USE ONLY *(Leave blank)***

**2. REPORT DATE**
September 1999

**3. REPORT TYPE AND DATES COVERED**
Master's Thesis

**4. TITLE AND SUBTITLE**
**LOW COST PARACHUTE GUIDANCE, NAVIGATION, AND CONTROL**

**5. FUNDING NUMBERS**

**6. AUTHOR(S)**
Dellicker, Scott Henry

**7. PERFORMING ORGANIZATION NAME(S) AND ADDRESS(ES)**
Naval Postgraduate School
Monterey, CA 93943-5000

**8. PERFORMING ORGANIZATION REPORT NUMBER**

**9. SPONSORING / MONITORING AGENCY NAME(S) AND ADDRESS(ES)**
US Army Yuma Proving Ground, STEYP-MT-EA, Yuma, AZ 85365

**10. SPONSORING / MONITORING AGENCY REPORT NUMBER**

**11. SUPPLEMENTARY NOTES**
The views expressed in this thesis are those of the author and do not reflect the official policy or position of the Department of Defense or the U S Government A multi-media version of this report can be requested from the Sponsoring/Monitoring Agency.

**12a. DISTRIBUTION / AVAILABILITY STATEMENT**
Approved for public release; distribution is unlimited.

**12b. DISTRIBUTION CODE**

**13. ABSTRACT *(maximum 200 words)***

The Affordable Guided Airdrop System (AGAS) integrates a low-cost guidance and control system into fielded cargo air delivery systems. This study evaluated the feasibility of this concept and included the design and execution of a flight test program to assess prototype system performance, as well as modeling efforts to develop initial guidance and control techniques leading to an evaluation of the feasibility of the AGAS concept. The flight test program provided adequate flight dynamic data for the AGAS system. The wind measurement techniques employed for this effort, through the use of a "calibration" parachute system, provided wind estimates that were not previously available. Flight test data demonstrated the actuator system could provide glide ratios of 0.4 to 0.5 for a flat circular parachute. A simulation was developed using a point mass model for parachute dynamics, sensor models, and a Bang-Bang type control system. Six hundred simulations demonstrated that the Affordable Guided Airdrop System shows strong potential of providing a low-cost alternative for precision airdrop. Further work is recommended to implement a six-degree of freedom dynamic model, assess the dynamic response of the production parachute system, and optimize the control algorithms to minimize fuel usage.

**14. SUBJECT TERMS**
Parachute, Guidance, Navigation, Control, Parameter Estimation

**15. NUMBER OF PAGES** 141

**16. PRICE CODE**

**17. SECURITY CLASSIFICATION OF REPORT**
Unclassified

**18. SECURITY CLASSIFICATION OF THIS PAGE**
Unclassified

**19. SECURITY CLASSIFI- CATION OF ABSTRACT**
Unclassified

**20. LIMITATION OF ABSTRACT**
UL

**Approved for public release; distribution is unlimited**

# LOW COST PARACHUTE GUIDANCE, NAVIGATION, AND CONTROL

Scott Henry Dellicker
United States Army
B.S., Rensselaer Polytechnic Institute, 1984

Submitted in partial fulfillment of the
requirements for the degree of

**MASTER OF SCIENCE IN AERONAUTICAL ENGINEERING**

from the

**NAVAL POSTGRADUATE SCHOOL**
**September 1999**

DUDLEY KNOX LIBRARY
NAVAL POSTGRADUATE SCHOOL
MONTEREY CA 93943-5101

# ABSTRACT

The Affordable Guided Airdrop System (AGAS) integrates a low-cost guidance and control system into fielded cargo air delivery systems. This study evaluated the feasibility of this concept and included the design and execution of a flight test program to assess prototype system performance, as well as modeling efforts to develop initial guidance and control techniques leading to an evaluation of the feasibility of the AGAS concept. The flight test program provided adequate flight dynamic data for the AGAS system. The wind measurement techniques employed for this effort, through the use of a "calibration" parachute system, provided wind estimates that were not previously available. Flight test data demonstrated the actuator system could provide glide ratios of 0.4 to 0.5 for a flat circular parachute. A simulation was developed using a point mass model for parachute dynamics, sensor models, and a Bang-Bang type control system. Six hundred simulations demonstrated that the Affordable Guided Airdrop System shows strong potential of providing a low-cost alternative for precision airdrop. Further work is recommended to implement a six-degree of freedom dynamic model, assess the dynamic response of the production parachute system, and optimize the control algorithms to minimize fuel usage.

This document was prepared as a multimedia presentation. There are several references to video clips and animations throughout the printed document. Multimedia versions of this document can be requested from U.S. Army Yuma Proving Ground, STEYP-MT-EA, Yuma, AZ 85365.

# TABLE OF CONTENTS

**I. INTRODUCTION** .......... **1**

**II. SYSTEM DESCRIPTION** .......... **3**

A. AFFORDABLE GUIDED AIRDROP SYSTEM (AGAS) .......... 3
B. PARACHUTE .......... 4
C. ACTUATORS .......... 5
D. MASS AND CENTER OF GRAVITY .......... 8
E. MOMENTS OF INERTIA .......... 8
*1. Parachute* .......... *9*
*2. Payload* .......... *10*
*3. Actuators and Suspension Lines* .......... *10*

**III. CONTROL SYSTEM** .......... **11**

**IV. TESTING** .......... **15**

A. INVESTIGATION OF APPARENT MASS EFFECTS .......... 15
B. FLIGHT TESTING .......... 19
C. INSTRUMENTATION .......... 20
D. WIND ESTIMATION .......... 21
E. DATA REDUCTION .......... 28

**V. FLIGHT TEST RESULTS** .......... **35**

A. SINGLE CONTROL INPUT .......... 36
B. TWO SIMULTANEOUS CONTROL INPUTS .......... 37
C. ATTITUDE RESPONSE .......... 39

**VI. NAVIGATION SENSOR MODELS** .......... **43**

A. GLOBAL POSITIONING SYSTEM (GPS) .......... 43
*1. Selective Availability* .......... *43*
*2. Model Without Selective Availability Errors* .......... *46*
B. HEADING SENSOR .......... 48

**VII. EQUATIONS OF MOTION** .......... **51**

A. NOTATION .......... 51
B. ASSUMPTIONS .......... 52
C. DERIVATION OF EQUATIONS OF MOTION .......... 52
D. APPARENT MASS .......... 56
*1. Estimation of Apparent Mass Terms* .......... *57*
*2. Effects on the Equations of Motion* .......... *57*
E. EXTERNAL FORCES AND MOMENTS .......... 59
*1. Aerodynamic Forces and Moments* .......... *59*
*2. Gravity* .......... *60*
*3. Total External Forces and Moments* .......... *61*
F. COMPLETE EQUATIONS OF MOTION .......... 61

VIII. ANALYSIS OF EQUATIONS OF MOTIONS .......... 63
- A. EQUATIONS OF MOTION EXPANSION .......... 63
- B. LONGITUDINAL EQUATIONS .......... 64
- C. LATERAL-DIRECTIONAL EQUATIONS .......... 65
- D. SUMMARY OF EQUATIONS .......... 67

IX. PARAMETER ESTIMATION .......... 69
- A. OVERVIEW .......... 69
- B. MODIFIED MAXIMUM LIKELIHOOD ESTIMATION .......... 69
- C. RESULTS .......... 70

X. SYSTEM MODEL .......... 73

XI. SIMULATION .......... 79
- A. OVERVIEW .......... 79
- B. INITIALIZATION .......... 80
- C. RESULTS .......... 81

XII. CONCLUSIONS AND RECOMMENDATIONS .......... 87
- A. CONCLUSIONS .......... 87
- B. RECOMMENDATIONS .......... 89

REFERENCES .......... 92

APPENDIX A. SIMULATION RESULTS .......... 93

APPENDIX B. SAMPLE SIMULATION RESULTS .......... 105

APPENDIX C. SIMULINK® REALIZATION .......... 113

APPENDIX D. AGAS INSTRUMENTATION DESCRIPTION .......... 117

APPENDIX E. MATLAB® SCRIPT FILES .......... 121

INITIAL DISTRIBUTION LIST .......... 127

# ACKNOWLEDGEMENTS

There is no doubt that I could not have completed this project without the help of many colleagues, friends, and my family. My thanks to Wade Porter who acted as a sounding board for many of my ideas, both good and bad, throughout the project and Jim Bybee who developed the instrumentation package so critical to this effort. The entire AGAS team, including Richard Benney, Glen Brown, Roy Haggard, and Rich Almassy, was a tremendous inspiration. Thanks to Dr. Isaac Kaminer and Dr. Richard Howard who, while at NPS, taught me how to think logically again. Most importantly, to the three people who gave me the motivation to keep pressing on, my wonderful wife Kathy and two terrific children, C.J. and Katie. You all sacrificed so much for me and I am forever grateful. Thanks for everything!

## LIST OF SYMBOLS, ACRONYMS AND ABBREVIATION

**Symbols:**

| | |
|---|---|
| $\{B\}$ | name of the coordinate system, $B$ denotes body-axis, $W$ denotes wind-axis, $A$ denotes air-mass axis, and $U$ denotes inertial-axis |
| ${}^{C}_{A}R$ | rotation matrix from coordinate system $\{A\}$ to coordinate system $\{C\}$ |
| $S()$ | skew symmetric matrix |
| ${}^{C}F$ | forces in $\{C\}$ |
| ${}^{C}N$ | moments in $\{C\}$ |
| ${}^{C}P_{D}$ | position of point D, measured in $\{C\}$ and expressed in $\{C\}$ |
| ${}^{A}({}^{C}P_{D})$ | position of point D, measured in $\{C\}$ and expressed in $\{A\}$ where<br>${}^{A}({}^{C}P_{D}) = {}^{A}_{C}R({}^{C}P_{D}) \neq {}^{C}P_{D}$ |
| $P_e$ | position error |
| ${}^{C}V_{D}$ | velocity of point D, measured in $\{C\}$ and expressed in $\{C\}$ |
| ${}^{C}\Omega_{D}$ | angular velocity of point D, measured in $\{C\}$ and expressed in $\{C\}$ |
| $\frac{d}{dt}$ | time derivatives in the body-axis $\{B\}$ |
| $(\dot{\ })$ | time derivatives in the inertial-axis $\{U\}$ |
| $d$ | distance |
| $l_{ii}$ | length |
| $\rho$ | atmospheric density |
| $\overline{q}$ | dynamic pressure |
| $W_i$ | weight of $i$ |
| $m$ | mass |
| $M$ | mass matrix |
| $\alpha_{ii}$ | apparent mass coefficient |
| $A$ | apparent mass matrix |
| $I_{ii}$ | moment of inertia |
| $D$ | drag |
| $S_o$ | reference area |
| $C_D S$ | drag area |
| $\phi$ | roll |
| $\theta$ | pitch |
| $\psi$ | yaw |
| $p$ | roll rate |
| $q$ | pitch rate |
| $r$ | yaw rate |
| $\gamma$ | glide ratio |
| $\delta$ | control deflection |
| $X, Y, Z$ | forces in the x-, y-, z-axis, respectively |
| $L, M, N$ | moments in the x-, y-, z-axis, respectively |
| $X_i, Y_i, Z_i$ | change in force with respect to $i$ |
| $L_i, M_i, N_i$ | change in moment with respect to $i$ |
| *NOTES:* | Capital letters/symbols denote vectors or matrices<br>Small letters/symbols denote scalars<br>If coordinate axis symbol is omitted, $\{U\}$ is assumed |

**Subscripts**:

| | |
|---|---|
| c.g. | center of gravity |
| l | suspension lines |
| c | canopy |
| p | payload |
| a | actuator |
| ss | steady state |
| xx or 1 | x-axis |
| yy or 2 | y-axis |
| zz or 3 | z-axis |
| e | error |
| $AERO$ | aerodynamic |
| $AM$ | apparent mass |
| $GRAV$ | gravity |

**Abbreviations**:

| | |
|---|---|
| A-D | Analog to Digital |
| AGAS | Affordable Guided Air Delivery System |
| AHRS | Attitude Heading Reference System |
| C/A-Code | Course Acquisition Code |
| CARP | Computed Air Release Point |
| CEP | Circular Error Probable |
| DOF | Degree of Freedom |
| GNC | Guidance, Navigation, and Control |
| P-code | Precision Code |
| PMA | Pneumatic Muscle Actuator |
| PPS | Pulse Per Second |
| RAWIN | Radiosonde Wind Measuring System |
| RMS | Root Mean Square |

# I. INTRODUCTION

The United States Air Force Science Advisory board was tasked to develop a forecast of the requirements for the most advanced air and space ideas to project the Air Force into the next century. The study, encompassing all aspects of Air Force operations, assessed a variety of technology developments critical to the Air Force mission. This study culminated in a report titled "New World Vistas, Air and Space Power for the 21st Century."[1] The study identified a critical need to improve the Point-of-Use Delivery; that is, getting the materiel where it needs to be, when it needs to be there. Airdrop is an important aspect of Point-of-Use Delivery. The report indicated that immediate improvements are needed with emphasis provided by the statement: "In the future, the problem of airdrop should be treated as seriously as the problem of bomb drop."

To date, significant emphasis has been placed on the development of large-scale parafoil systems. These systems provide the accuracy required with delivery from high altitude and large offset distances. The drawback is prohibitive cost for each pound of payload delivered. Alternate approaches were required to reduce system cost. The team of the United States Army and Air Force, The Boeing Company, and Vertigo, Incorporated is evaluating alternative airdrop technologies. These efforts include the design and development of the Affordable Guided Airdrop System, which incorporates a low-cost guidance, navigation, and control system into fielded cargo air delivery systems. This study focused on evaluating the feasibility of the AGAS concept and encompassed the design and execution of a flight test program to assess dynamic response of a flat circular parachute, to the design of initial guidance and control techniques, and to evaluate the feasibility of the AGAS concept.

# II. SYSTEM DESCRIPTION

## A. AFFORDABLE GUIDED AIRDROP SYSTEM (AGAS)

The Affordable Guided Airdrop System[2] (AGAS) is being evaluated as a low-cost alternative for meeting the military's requirements for precision airdrop. Designed to bridge the gap between expensive high glide ratio parafoil systems and uncontrolled (ballistic) round parachutes, the AGAS concept offers the benefits of high altitude parachute releases but cannot provide the same level of offset from the desired impact point (IP) as high-glide systems. The design goal of the AGAS development is to provide a Guidance, Navigation, and Control (GNC) system that can be placed in-line with existing fielded cargo parachute systems (G-12 and G-11) and standard delivery containers (A-22). The system is required to provide an accuracy of 100 meters, Circular Error Probable (CEP), with a desired goal of 50 meters CEP. No changes to the parachute or cargo system are allowed.

The current design concept includes implementation of a commercial Global Positioning System (GPS) receiver and a heading reference as the navigation sensors, a guidance computer to determine and activate the desired control input, and the application of Pneumatic Muscle Actuators (PMAs) to effect the control. The navigation system and guidance computer would be secured to the existing container delivery system while the PMAs would be attached to each of four parachute risers and to the container. Figure 1 illustrates the concept. Control is affected by lengthening a single or two adjacent actuators. The parachute deforms creating an asymmetrical shape, essentially shifting the center of pressure, and providing a drive or slip condition. Upon deployment of the system from the aircraft, the guidance computer would steer the system to a pre-planned trajectory. This concept relies on the ability of sufficient drive to be produced to overcome errors in wind estimation and the point of release of the system from the aircraft.

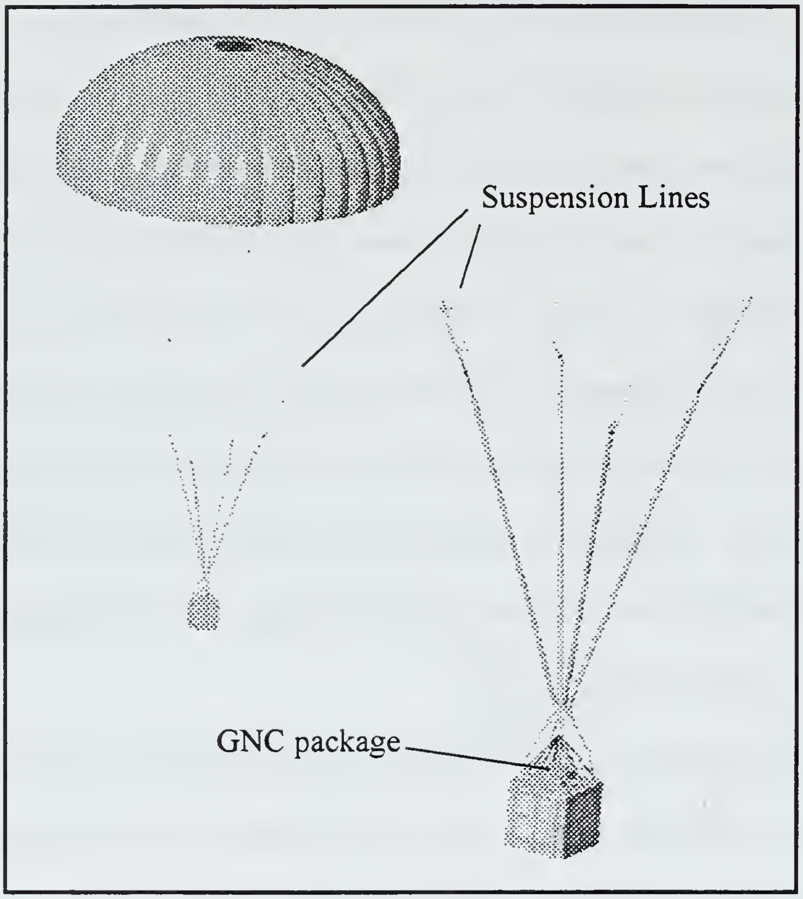

Figure 1. Affordable Guided Airdrop System[3]

## B. PARACHUTE

The C-9 parachute was selected for this feasibility demonstration due to its availability and representation of the larger cargo-type parachutes (G-11 and G-12) on which this system will ultimately be used. Although the C-9 was initially designed as an ejection seat parachute, it is a standard flat circular parachute as are the larger G-11 and

G-12 cargo parachutes. A flat circular parachute is one that when laid out on the ground forms a circle.

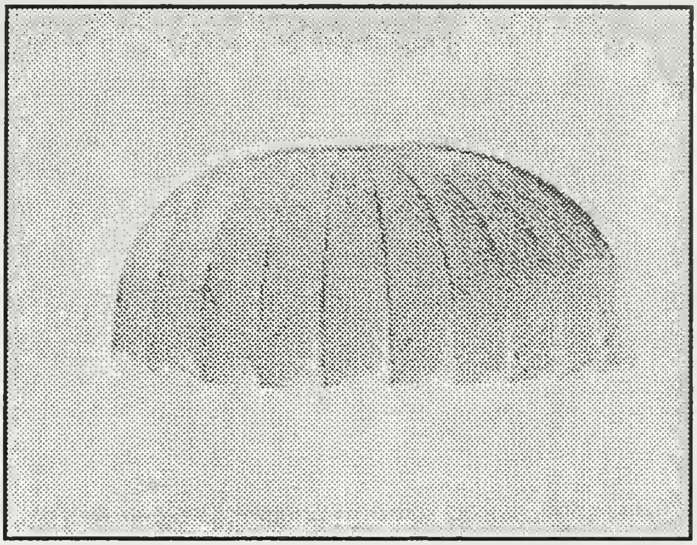

Figure 2. C-9 Parachute

The reference diameters of these chutes are 28 feet (C-9), 64 feet (G-12), and 100 feet (G-11). The reference area of the C-9 parachute is taken to be the total surface area of the canopy (a circle of 28 foot diameter) and is 615.8 square feet. The C-9 is static-line deployed and utilizes 28 suspension lines connecting to four risers.

A cargo box was suspended from the system and housed the remote control system, control actuators, and instrumentation system.

## C. ACTUATORS

Vertigo, Incorporated developed Pneumatic Muscle Actuators[3] (PMAs) to effect the control inputs for this system. The PMAs are braided fiber tubes with neoprene inner sleeves that can be pressurized. Uninflated PMAs as installed on a scaled system are shown in Figure 3. Upon pressurization, the PMAs contract in length and expand in diameter.

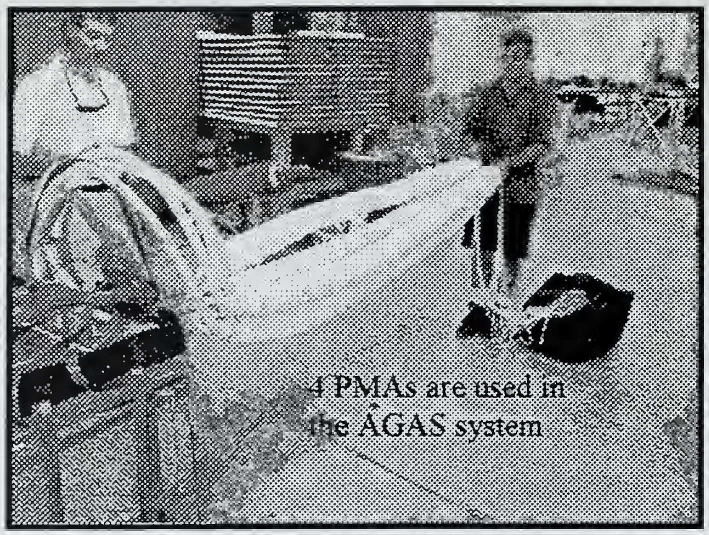

Figure 3. Pneumatic Muscle Actuators (PMAs)

With four independently controlled actuators, two of which can be activated simultaneously, eight different control inputs can be affected. For this demonstration, a throw of approximately 3 feet was selected [measured to be 3.25 feet during ground testing]. When depressurized, the PMAs are completely flexible allowing for efficient packing of the actuators with the parachute.

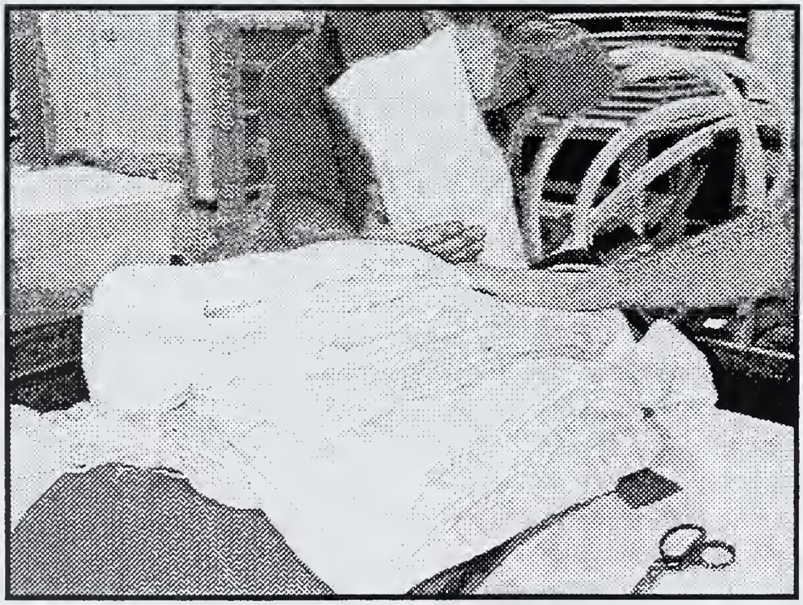

Figure 4. Packing the Parachute and Actuators

The concept employed for the AGAS is to fully pressurize all actuators upon successful deployment of the parachute. To affect control of the system, one or two actuators are depressurized. This action "deforms" the parachute creating drive in the opposite direction of the control action. Figure 5 illustrates this action while the Figure 6 illustrates the parachute deformation upon control actuation.

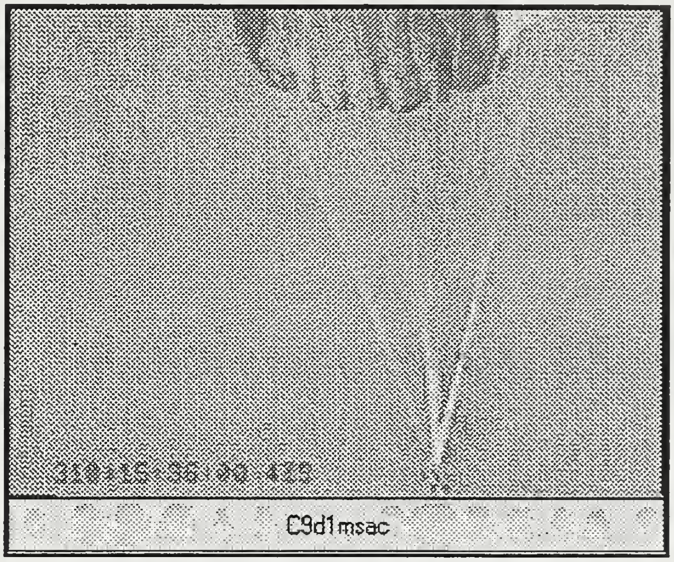

Figure 5. PMA Actuation (video clip)

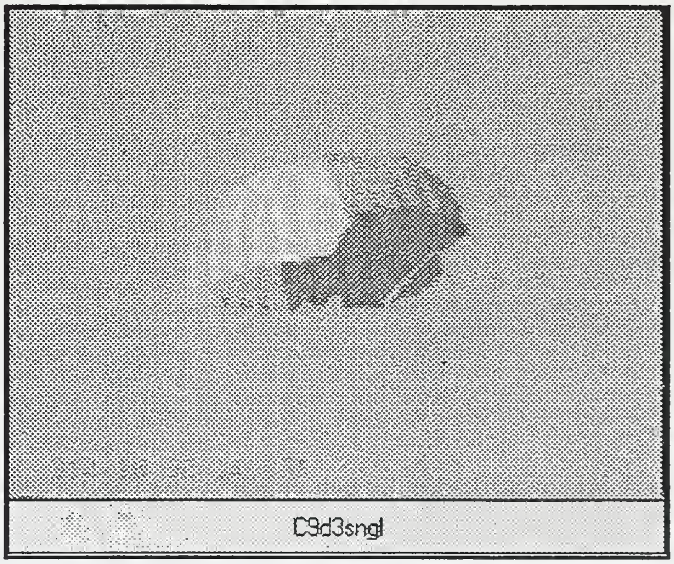

Figure 6. Parachute Response to Control Input (video clip)

## D. MASS AND CENTER OF GRAVITY

The weights of the major system components were determined through direct measurement or calculation using known material weights (e.g. parachute canopy fabric weight of 1.1 ounces per square yard). The major system component weights are summarized in Table 1.

The theoretical center of gravity of the system was found to be 11.4 feet vertically upward from the center of the payload for a standard sea-level atmosphere. This calculation includes the mass of the trapped air in the canopy and as such is dependent on the air density. The relationship of center of gravity to air density is as follows:

$$l_{cg} = [l_p(\rho V g + W_p) + l_a W_a + l_l W_l + l_c W_c] / W_{system} \tag{1}$$

Substituting known parameters equation 1 reduces to:

$$l_{cg} = 4323\rho + 0.5 \text{ feet and } P_o = \begin{bmatrix} 0 \\ 0 \\ l_{cg} \end{bmatrix} = \begin{bmatrix} 0 \\ 0 \\ 4323\rho + .5 \end{bmatrix}$$

| Component | Weight (pounds) sea level - standard atmosphere |
|---|---:|
| Parachute | 7.5 |
| Suspension Lines | 4.5 |
| Actuators (total for four) | 13.3 |
| Payload<br>cargo box<br>instrumentation<br>actuator valves/nitrogen tanks | 320.7 |
| ***Total System*** | ***346.0*** |

Table 1. System Weight

## E. MOMENTS OF INERTIA

The moments of inertia of the parachute (including trapped air mass), payload, suspension lines, and actuators were determined as shown below. A summary of these values is shown in Table 2. Due to symmetry of the parachute and payload system, all cross products of inertia where assumed to be zero.

| **Component** | **Moment of Inertia (slugs·ft$^2$)<br>sea level - standard atmosphere** | | |
|---|---|---|---|
| | $I_{XX}$ | $I_{YY}$ | $I_{ZZ}$ |
| Parachute | 1865.9 | 1865.9 | 211.3 |
| Suspension Lines | neglected | | |
| Actuators (total for four) | neglected | | |
| Payload<br>cargo box<br>instrumentation<br>actuator valves/nitrogen tanks | 1328.3 | 1328.3 | 39.9 |
| ***Total System*** | ***3194.2*** | ***3194.2*** | ***251.2*** |

Table 2. Moments of Inertia

### 1. Parachute

When inflated, a flat circular parachute approximates a hemisphere with a radius (r). The moments of inertia can be found as follows:

$$I_{XX} = I_{YY} = I_{ZZ} = \frac{2}{3} m r^2 . \tag{2}$$

These values then must be translated to the principal axis located at the center of gravity at the system. The parallel axis theorem[4] is applied as follows:

$$I_{XX'} = I_{YY'} = I_{XX} + m d_x^{\,2} \text{ and } I_{ZZ'} = I_{ZZ} . \tag{3}$$

$$I_{XX'} = I_{YY'} = \frac{2}{3} m r^2 + m d_x^{\,2} \text{ where: } d_x = d_p - l_{cg} . \tag{4}$$

The moment of inertia, like the center of gravity, varies with air density as the trapped air mass is a significant contributer to this term. Substituting $m = m_p + \rho V g$ (where $m_p$ is the mass of the parachute material and all known parameters:

$$I_{XX'} = I_{YY'} = 734436\rho + 1449.0$$

$$I_{ZZ} = 83152\rho + 53.5$$

### 2. Payload

The cargo box dimensions were 2 feet by 2 feet by 2 feet. It is assumed that the center of gravity of this box was located at the center of the box. The moments of inertia can be found as follows:

$$I_{XX} = I_{YY} = I_{ZZ} = \frac{1}{2}m(a^2 + l^2);\ \text{where } \boldsymbol{a = l}. \tag{5}$$

Again applying the parallel axis theorem, the moments of inertia about the principal axis were found. The parallel axis theorem is applied as follows:

$$I_{XX'} = I_{YY'} = I_{XX} + md_x^{\,2} \text{ and } I_{ZZ'} = I_{ZZ}. \tag{6}$$

### 3. Actuators and Suspension Lines

The actuators and suspension lines were treated as slender rods with the body axis located at the end of the rod. The moments of inertia were found as follows:

$$I_{XX} = I_{YY} = \frac{1}{3}ml^2 \text{ and } I_{ZZ} = 0. \tag{7}$$

These values for this system were found to be extremely small as compared to the values for the parachute and payload and therefore were considered negligible.

# III. CONTROL SYSTEM

For an airdrop mission, the aircrew will determine the Computed Air Release Point (CARP) based on the best wind estimate available at that time. The aircraft will then be navigated to that point for air delivery of the materiel. Should the wind estimate and calculation of the predicted release point be perfect and the aircrew gets the aircraft to the precise release point, then the parachute would fly precisely to the target without control inputs. However, wind estimation is far from a precise science. The calculation of the CARP relies on less than perfect estimates of parachute aerodynamics and the flight crews cannot possibly precisely hit the predicted release point for each airdrop mission. Therefore, the AGAS control system design must help overcome these potential errors.

A glide ratio (ratio of horizontal to vertical velocity) demonstrated in flight test was approximately 0.4-0.5. Considering this relatively low glide ratio and a descent rate of approximately 25 feet per second, the AGAS can overcome only a twelve foot per second (approximately 7 knots) wind. It is therefore imperative to implement the system to overcome poor estimates in the wind and not try to steer the system against the entire wind. In other words, the drive of the system is insufficient to attempt to fly straight to the target but is sufficient to overcome up to a twelve foot per second error in the wind estimate. For this reason, a trajectory control approach was selected.

A pre-planned trajectory, based on the best wind estimate available, must be determined and provided to the guidance computer. The GPS navigation system will provide a continuous position of the system. The guidance computer will compare the actual horizontal position, at the system's current altitude, to the planned trajectory at that altitude. This represents the position error ($P_e$) at the current time.

A tolerance cone is established about the planned trajectory (Figure 7) starting at 600 feet at the beginning of the trajectory and gradually decreasing to 60 feet at ground level. Should the position error be outside this tolerance, a control is activated to slip the system back to the planned trajectory. When the system is within 30 feet of the planned trajectory the control is disabled and the parachute drifts with the wind. Thirty feet was selected to encompass approximately 1-sigma of the GPS errors (Selective Availability off).

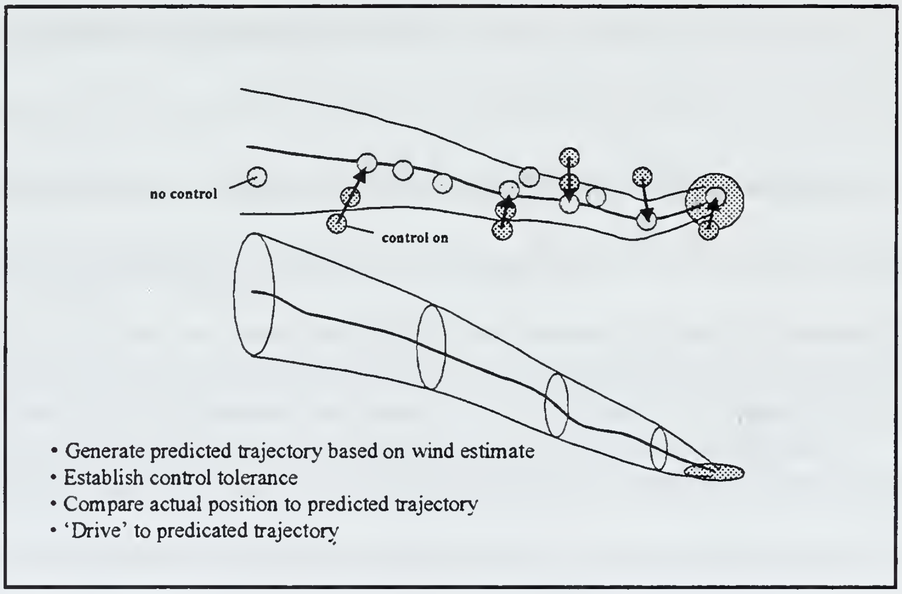

- Generate predicted trajectory based on wind estimate
- Establish control tolerance
- Compare actual position to predicted trajectory
- 'Drive' to predicated trajectory

Figure 7. Control Concept (double click to see animation)

As outlined above, the control system relies on the current horizontal position error to determine if control input is required. This position error ($P_e$) is determined in inertial space and is then rotated to the body axis using an Euler angle rotation with heading only. The resultant body-axis error ($P_b$) is then used to identify which control input must be activated as shown in Equation 8. Two components are returned, a + or -

for the x-axis and a + or - for the y-axis. It was assumed for this simulation that a +x would activate control A, a -x activates control C, a +y activates control B, while a -y activates control D. The actual rigging of the operational system must align these control actuators to the compass reference line to ensure proper control. Control A is assumed to be aligned with the compass zero reference line.

$$(8) \qquad input = sign\left(\frac{P_b}{\|P_b\|}\right);$$

The magnitude of this calculation is used to determine if the selected control input will be activated. If the magnitude is greater than 0.3, then that control is activated. This will allow the activation of a single control input or two simultaneous control inputs. Preventing activation of control when this value is less than 0.3 will ensure that unnecessary control inputs are not activated when the predominate error is in a single direction. Figure 8 illustrates the region of active control.

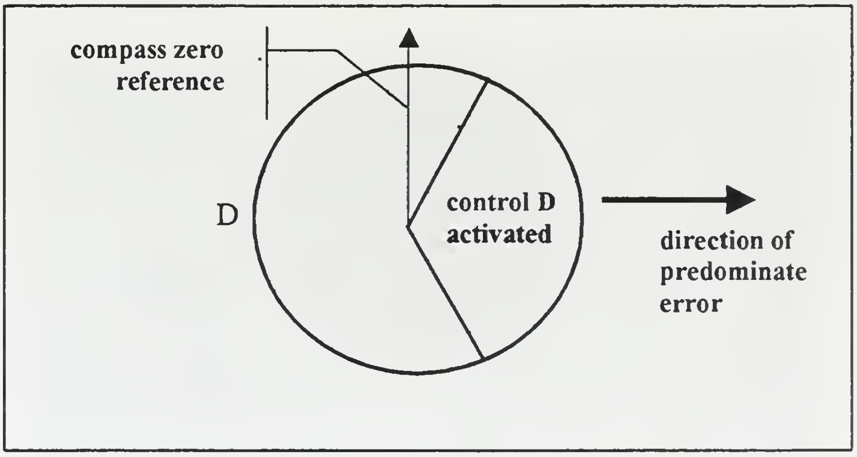

Figure 8. Control Activation

# IV. TESTING

The objectives of the test program were to investigate the apparent mass effects on flat circular parachutes and to obtain sufficient data to assess the feasibility of the AGAS concept. To meet these objectives, ground testing of the C-9 parachute and flight testing of the prototype AGAS, using remotely controlled activation of the actuators, were conducted.

## A. INVESTIGATION OF APPARENT MASS EFFECTS

To illustrate the effects of apparent mass on the dynamics of a parachute, a test program was established to collect the forces along the z-axis of the parachute during acceleration. The concept defined by Vertigo, Incorporated[5] to evaluate the apparent mass terms was implemented. The C-9 parachute was attached to a tower installed on the vehicle with two attaching risers and towed behind a ground vehicle (Figure 9).

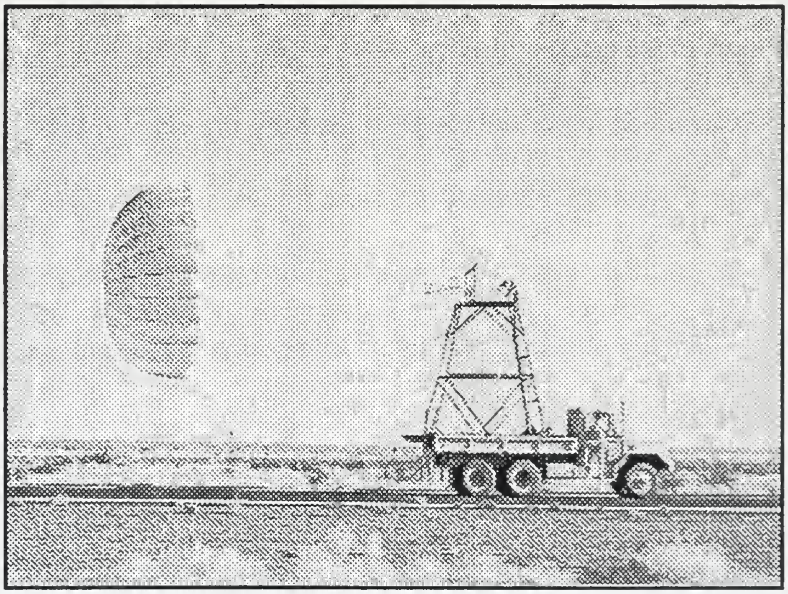

Figure 9. Tow Test

The vehicle first accelerated to a speed of approximately 10 feet per second. After a brief period of constant velocity, the vehicle then accelerated at a near constant acceleration. Figure 10 shows a typical velocity profile for these tests.

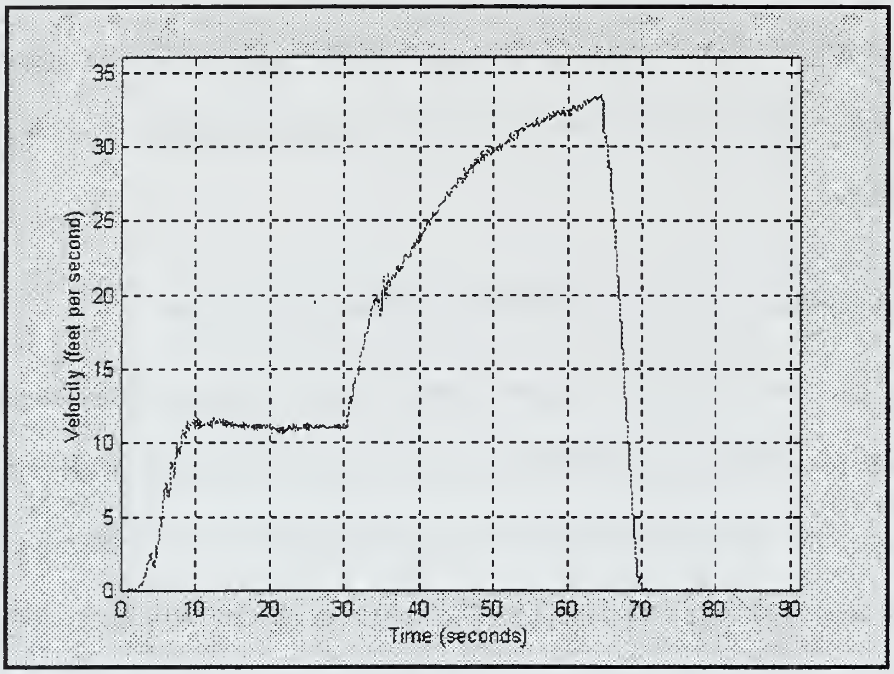

Figure 10. Tow Test Velocity Profile

The forces in the attaching risers were measured with strain gauges. In addition, a "box" was constructed on top of the tower to measure the vertical and lateral forces on the riser attachment points. By measuring these forces, an estimate of the parachute angle of incidence could be derived. Figure 11 illustrates the instrumentation configuration at one riser attachment point. The velocity was measured with differential GPS and an anemometer.

To estimate the actual apparent mass parameters, the motion of the parachute would be ideally fixed in one direction. In the Vertigo test, the parachute used was very stable. Therefore, the assumption of motion in only one axis was very reasonable. With the C-9 parachute significant oscillations were observed.

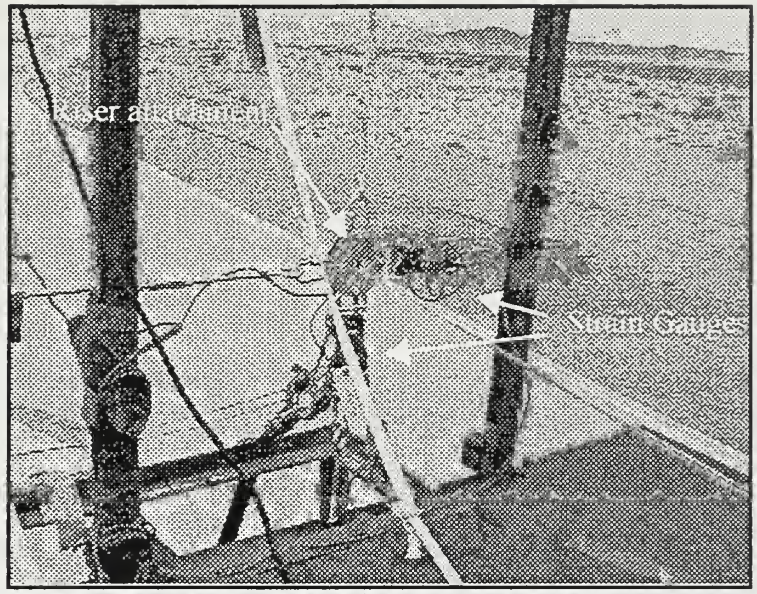

Figure 11. Instrumentation Configuration: Riser Attachment

A plot of the calculated incidence angle (ϕ) demonstrates the oscillatory nature of this parachute. Therefore, estimation of the apparent mass coefficients using these techniques was not possible.

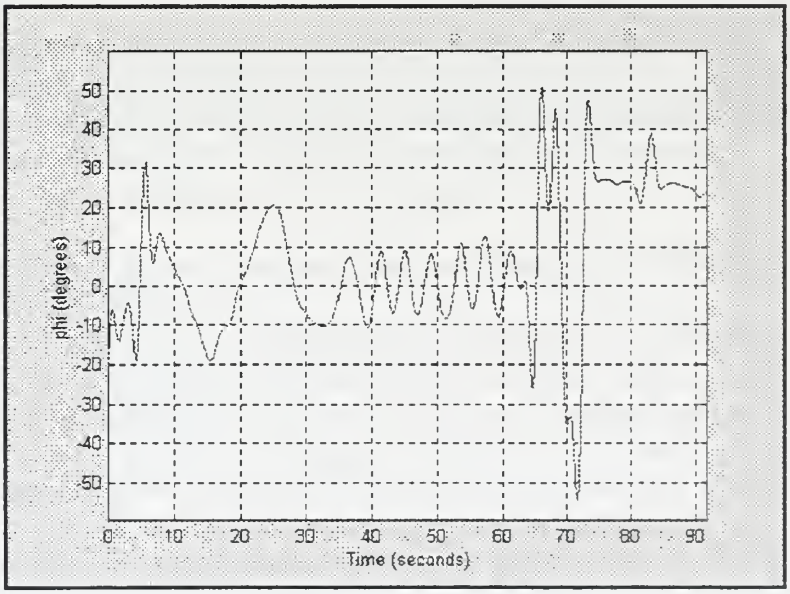

Figure 12. Incidence Angle (ϕ)

Even though precise apparent mass coefficients cannot be found, insight to the apparent mass contributions can be gained by analyzing these data. Figure 13 demonstrates the influence of apparent mass on parachute dynamics. The total force along the parachutes z-axis, as measured in the risers, is plotted along with the steady state drag calculations as found by:

*(9)* $D_{ss} = \frac{1}{2}\rho V^2 \cdot S_o \cdot C_D$; *where $S_o$ is the reference area of the parachute and $C_D$ is the steady-state drag coefficient (0.68).*

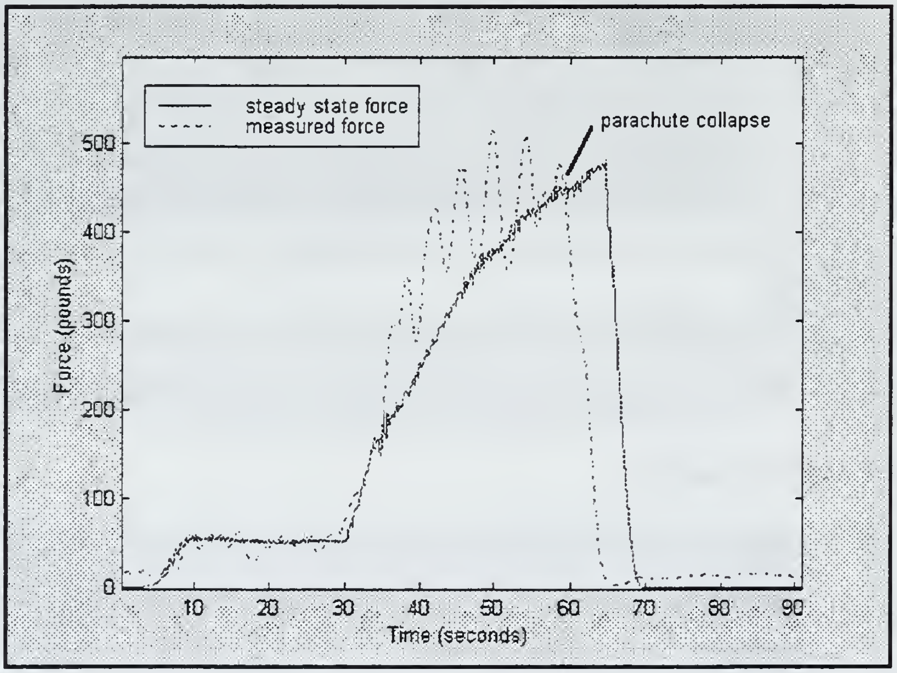

Figure 13. Apparent Mass Effects on Parachute Dynamics

The figure shows increased measured force above the predicted steady-state drag along the parachute when the parachute is accelerating. Note during the first accelerations that the measured force did not rise above the steady state drag estimate. This is likely due to the parachute inflation and the greatly changing angle of incidence during this inflation. Concentrating on the area where the parachute has settled into pure oscillations, the apparent mass effects can be observed. Figure 14 presents an excerpt of data for this time:

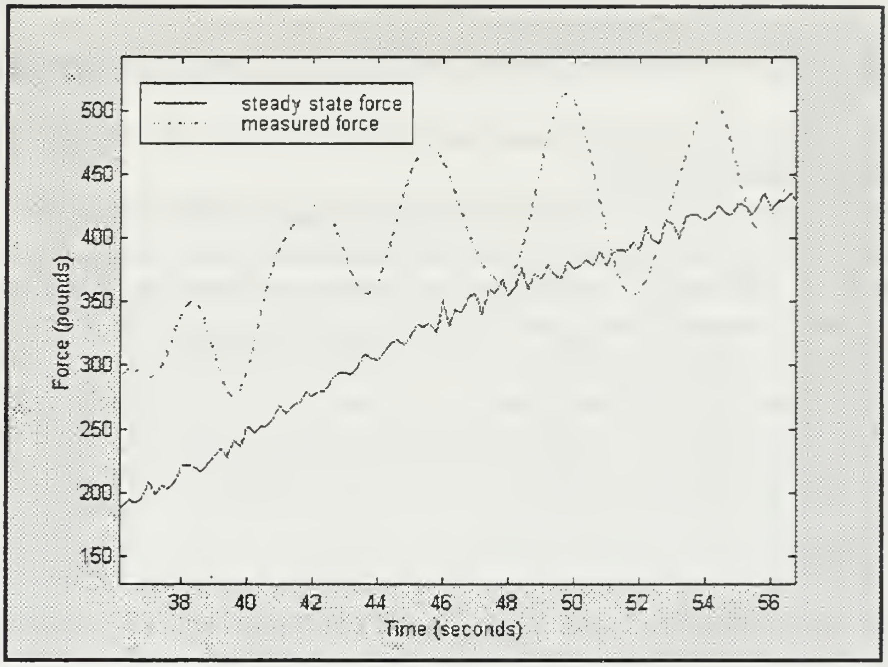

Figure 14. Apparent Mass Effects

These data demonstrate that the apparent mass effects must be considered in flight dynamic modeling. Even with the relatively small accelerations experienced here, the effect is very large and varies greatly with acceleration of the parachute (as observed with the oscillating parachute). Techniques for estimating apparent mass coefficients are presented in the system modeling section of this report.

## B. FLIGHT TESTING

The flight test effort focused on the collection of flight dynamic data to support modeling of the AGAS concept. The flight test effort was conducted with four actuators in-line with a C-9 parachute and a one-half scale container delivery system. The actuators were activated using a manual radio control system. Flight dynamic data were obtained including the position, velocity, acceleration, attitude, and attitude rates of the system. It was necessary to correlate these data with control inputs. Therefore, the state of control activation was monitored. Parachute performance is significantly influenced by the winds. It was critical to this effort to measure the winds as precisely as possible.

## C. INSTRUMENTATION

Ideally, both the parachute and payload would have been instrumented to collect all necessary data. However, the state-of-the-art in instrumentation is not yet sufficient to adequately instrument the parachute itself. As a result, only the payload could be instrumented. A custom instrumentation system was developed and it included a differential GPS system for precise position and velocity, 3-axis accelerometers for acceleration, and an Attitude Heading Reference System (AHRS) for 3-axis attitudes and attitude rates. Pressure transducers were put in line with the pneumatic actuators to monitor their action. Figure 15 illustrates the instrumentation design. A summary of the major instrumentation components is provided in Appendix D.

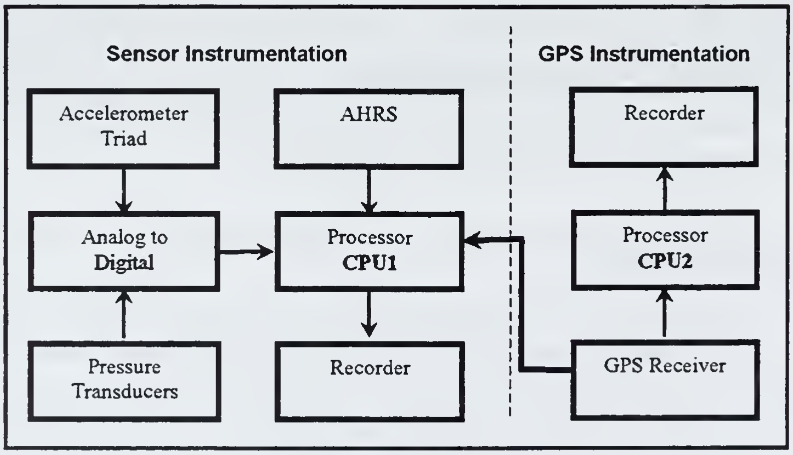

Figure 15. Instrumentation Block Diagram

The critical part of this design is the time synchronization of data from all sources. To achieve this, the IRIG time generator was synchronized with GPS time using the Havequick Time Interface and the 1-Pulse Per Second time sync. The AHRS data were available at its interface approximately 71 times per second. This is the fastest rate for all the sensors. Therefore, these data were used as the key for capturing data from all sensors. When an AHRS message was first detected by CPU1, the first record was time-tagged and the entire message was sent to the recorder. At that time, the Analog-Digital (A-D) converter was polled for its data. The first record from the A-D converter was time-tagged and the message sent to the data recorder. The GPS data from the differential receiver were independently captured (with an embedded time-tagging using GPS time) and recorded on a separate PC-Card. The synchronization of the data was validated in two ways. First, it was desired to have a discrete event that would effect all data sensors. The obvious event was ground impact, which resulted in immediate changes in the data from each sensor. This discrete event showed that the data from the independent sensors were time synchronized to less than 200 milliseconds (the rate of GPS data). Next, the acceleration data were integrated to estimate velocity. This estimated velocity was then compared to the GPS velocity (after rotation from the body reference frame to the inertial reference frame using the AHRS attitude data). These results also showed the data were time-tagged to within 200 milliseconds.

## D. WIND ESTIMATION

Two methods of wind estimation are presented. The first includes the accepted standard of the Radiosonde Wind Measuring System (RAWIN) system used throughout the test community. A RAWIN balloon was launched at approximately one-hour intervals near the release time in the vicinity of the Drop Zone. This system provided a direct measurement of the winds as a function of altitude. Although an accepted standard, the RAWIN system has limitations in airdrop operations. The largest problem is that real-time winds are not available. The balloon must be launched and data processed resulting in approximately a one-hour delay. Figure 16 illustrates the magnitude of wind changes over time. Data from three RAWIN launches are presented as a function of altitude. It is clear that as the parachute gets close to the ground, the wind changes can be significant.

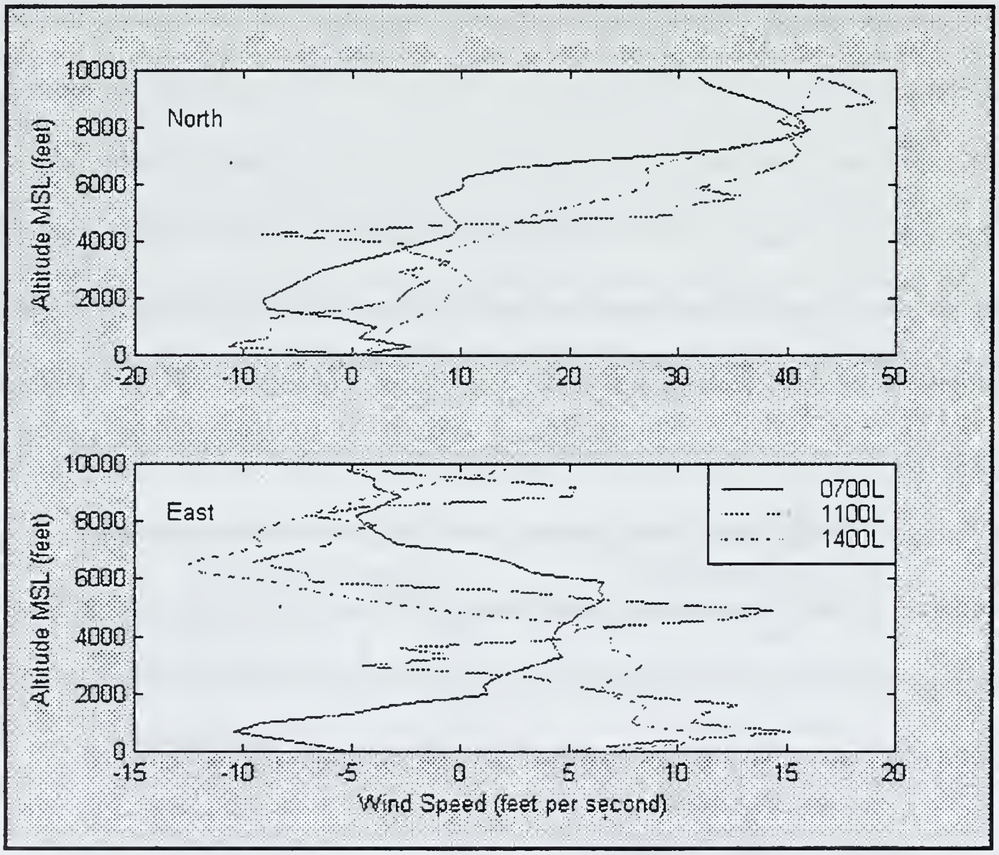

Figure 16. Wind Changes Over Time

A second method of deploying a "calibration system" just prior to release of the test payload was implemented. A tri-lobe parachute was used with a reference drag area

($C_DS$) of 90.88. Oscillations of this parachute were observed to be very small. The system was weighted at 58 pounds to provide approximately the same descent rate as the C-9 system. The calibration system was instrumented with differential GPS on the payload. Initially, the wind estimate was simply taken as the ground velocity as measured by the GPS. This approach effectively considers the calibration system massless and therefore does not account for changes in momentum.

To validate the ability to simply use the measured ground track velocity as the wind estimate, a model of the calibration parachute system was developed. A point-mass system was assumed with the only forces on the system being drag and weight. The applicable equations of motion are:

$$X = (m + \alpha_{11})\dot{u} = -D\cos\gamma\cos\psi \tag{10}$$

$$Y = (m + \alpha_{22})\dot{v} = -D\cos\gamma\sin\psi \tag{11}$$

$$Z = (m + \alpha_{33})\dot{w} = -D\sin\gamma + W \tag{12}$$

where: W is the calibration system weight, D is drag ($D = qC_DS$), $\gamma$ and $\psi$ are the flight path angle and yaw angle respectfully. The reference angles are:

$$\sin\gamma = \frac{w}{V_T}; \quad \cos\gamma = \frac{\sqrt{V_T^2 - w^2}}{V_T}; \quad \sin\psi = \frac{v}{\sqrt{V_T^2 - w^2}}; \quad \cos\psi = \frac{u}{\sqrt{V_T^2 - w^2}} \tag{13}$$

Substituting, rearranging terms, and putting in state space form:

$$\begin{bmatrix} \dot{u} \\ \dot{v} \\ \dot{w} \end{bmatrix} = \begin{bmatrix} m + \alpha_{11} & 0 & 0 \\ 0 & m + \alpha_{22} & 0 \\ 0 & 0 & m + \alpha_{33} \end{bmatrix}^{-1} \left\{ \frac{-qC_DS}{V_T} \begin{bmatrix} u \\ v \\ w \end{bmatrix} + \begin{bmatrix} 0 \\ 0 \\ W \end{bmatrix} \right\} \tag{14}$$

where: $\alpha_{xx}$ are the apparent mass terms, here assumed to be constant

Assuming no rotation between the fixed earth reference and the system's body axis, the ground velocity can be determined.

$V_G = V_A + V_W$; where $V_G$, $V_A$, and $V_W$ are the ground velocity, parachute velocity relative to the local air mass (airspeed), and wind velocity, respectively.

$$\dot{V}_G = \dot{V}_A + \dot{V}_W \tag{15}$$

Applying 15 to 14:

$$\dot{V}_G = \begin{bmatrix} \dot{u} \\ \dot{v} \\ \dot{w} \end{bmatrix}_G = \begin{bmatrix} m+\alpha_{11} & 0 & 0 \\ 0 & m+\alpha_{22} & 0 \\ 0 & 0 & m+\alpha_{33} \end{bmatrix}^{-1} \left\{ \frac{-qC_D S}{V_T} \begin{bmatrix} u \\ v \\ w \end{bmatrix} + \begin{bmatrix} 0 \\ 0 \\ W \end{bmatrix} \right\} + \dot{V}_W \tag{16}$$

Equation 16 can be solved numerically to estimate the system response to the estimated winds. This estimate can then be compared to the measured velocity of the system. Using the measured ground track velocity as the initial wind estimate, the modeled ground track was determined. The difference between this modeled ground track and the actual measured ground track reflects the errors in the wind estimate. The magnitude of these errors indicates the significance of accounting for momentum changes caused by changes in the wind. A Simulink® model was implemented (Figure 17).

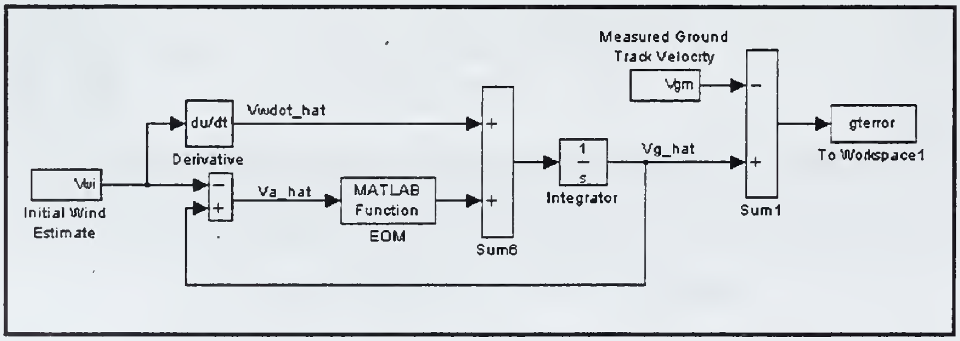

Figure 17. Simulink® Realization for Wind Estimation

---

® Registered trademark of Mathworks, Inc., Natick, MA

Figure 18 presents the results of this validation. Use of the measured ground track velocity as the wind estimate resulted in errors of less than 0.3 feet per second.

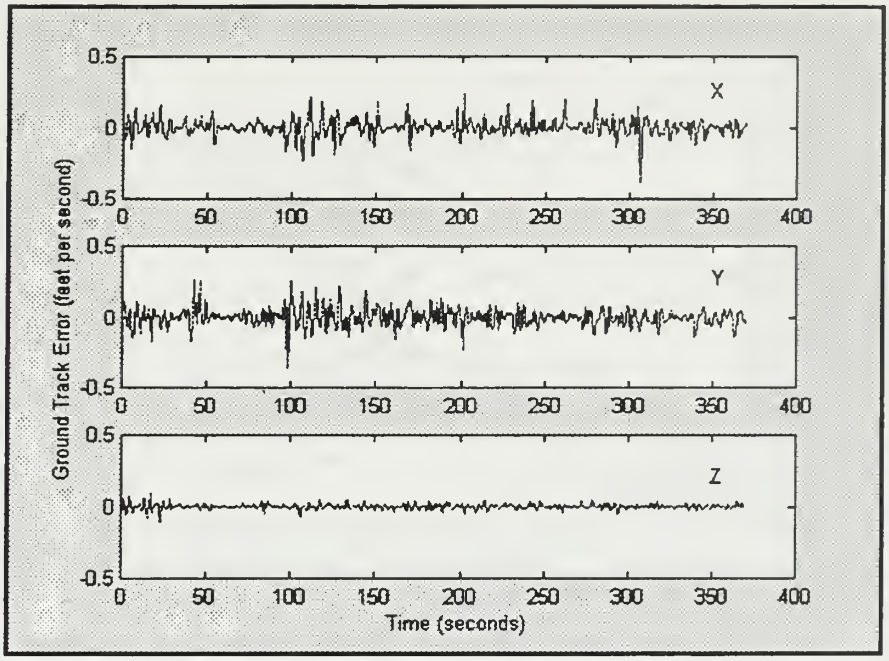

Figure 18. Wind Estimation Results

To further assess this technique, the equations for wind estimation utilized with hurricane dropsondes[6] was applied. In this application, the 3-dimensional velocity of a dropsonde is determined. The horizontal velocity components of the air mass are then found as follows:

$$(17) \qquad x_W \approx \dot{x} - \frac{\ddot{x}\dot{z}}{g} \text{ and } y_W \approx \dot{y} - \frac{\ddot{y}\dot{z}}{g};$$

To apply equation 17, a Simulink® model was implemented (Figure 19). The correction that would be applied to the horizontal velocity is presented in Figure 20. These data show that the corrected wind estimate, using the hurricane approach, differs from the measured ground track by less than 0.3 feet per second. More errors are seen close to ground impact where additional shears are present. This is not of consequence for this study as the flight dynamic data of interest is at much higher altitude.

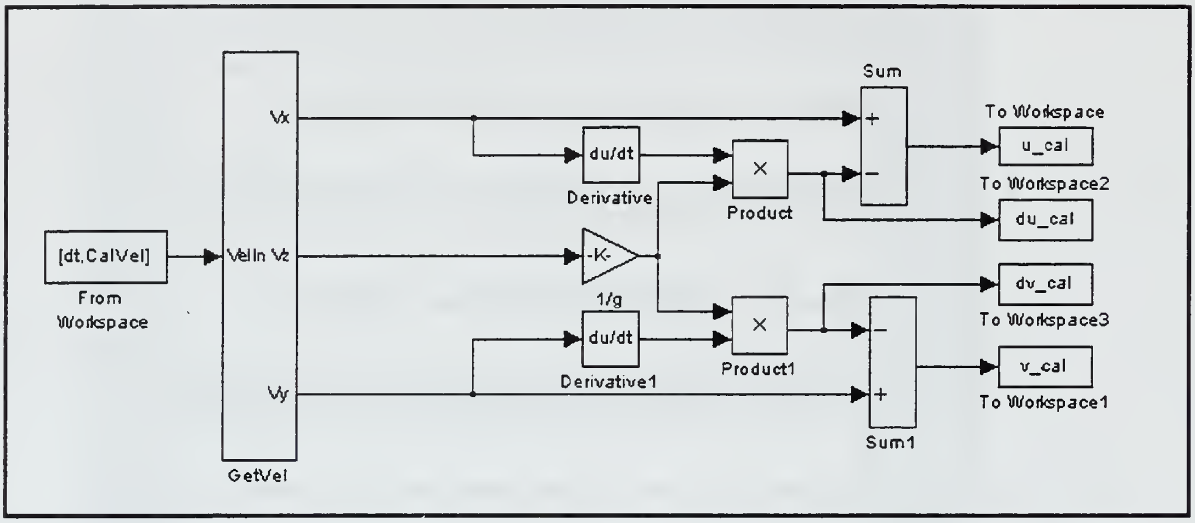

Figure 19. Hurricane Wind Estimation Implementation

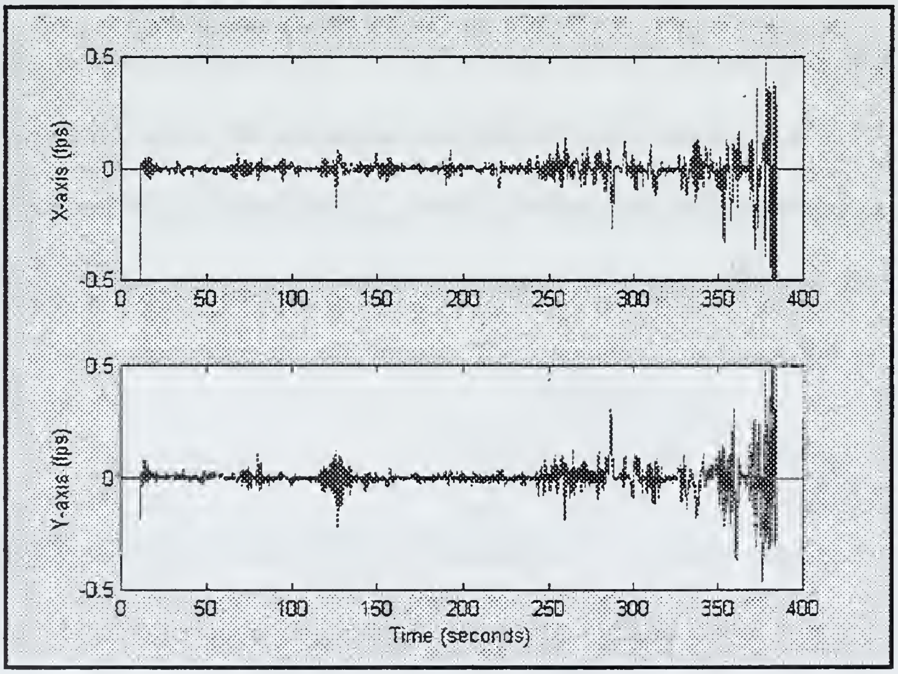

Figure 20. Hurricane Wind Estimation Results

These results indicate that the momentum effects can be ignored for wind estimation for the selected parachute system. Figure 21 illustrates the comparison of the wind estimate to the winds measured by the RAWIN. Recall that the RAWIN balloon was launched only every hour. The closest RAWIN data were used for this comparison.

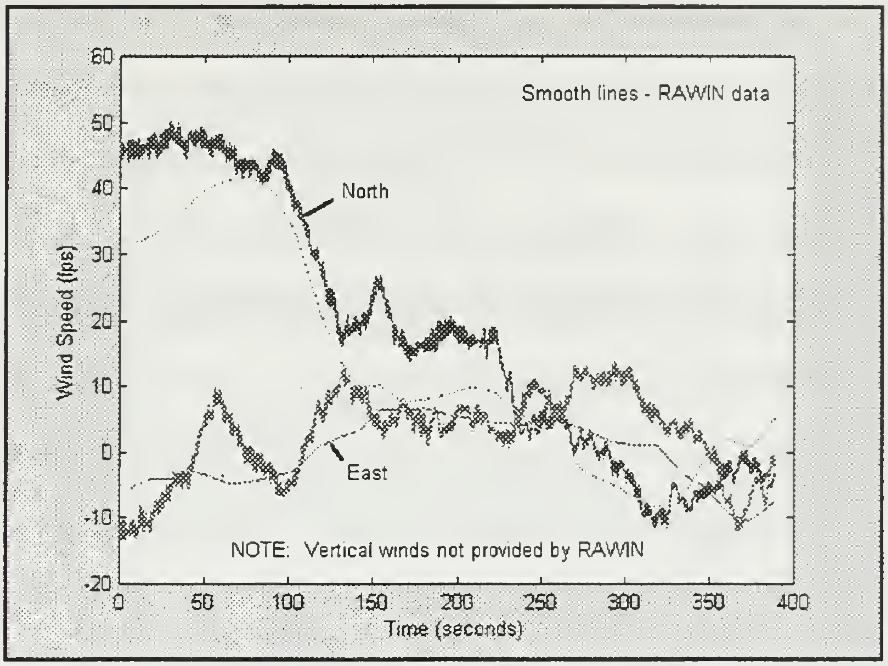

Figure 21. Wind Estimation Compared to RAWIN

These results demonstrate this technique will provide significantly better estimates of winds than using the RAWIN system. By adjusting the weight of the calibration system to match the descent rate of the test item, the two parachutes will be subjected to the same (as close as possible) atmospheric conditions. Using the measured GPS ground track velocities is an adequate approximation for wind estimation. Other techniques, such as that presented above, may provide some refinement on the wind estimates, but the difference is likely to be insignificant for most testing. The key to application of this technique is the use of a very stable parachute due to the reductions in apparent mass effects resulting from oscillations.

## E. DATA REDUCTION

Data from all sources were time correlated using the AHRS time tag. As these data were recorded at the fastest rate, all other data parameters were correlated with this time field. A linear interpolation was used to estimate the acceleration, actuator movement, and trajectory of the AGAS system at the time of the AHRS measurement. The data recorded on the calibration parachute (differential GPS only) were correlated to the system data again using linear interpolation. Instead of time correlating, the calibration data were correlated to the AGAS trajectory data with the AGAS altitude. As previously discussed, the velocity data from the calibration parachute were taken as the wind without any processing (excluding the vertical). For the vertical winds, the mean and density effects were removed from the calibration parachute vertical velocity.

The performance of the C-9 parachute is characterized by significant oscillations (Figure 22) in both pitch and roll. Due to the increased mass of the trapped air, the larger G-12 parachute system is not expected to oscillate as severely as this parachute.

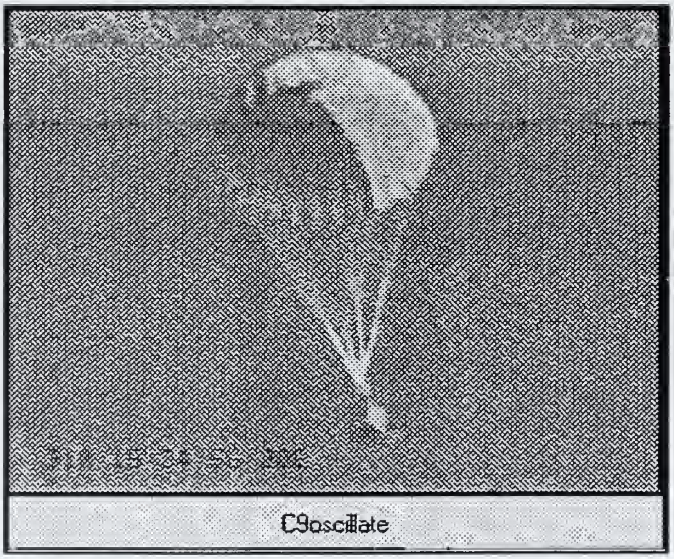

Figure 22. Parachute Oscillations (video clip)

The system instrumentation was all located in the payload and therefore measured the movement of the payload induced from the oscillations. The velocity data best demonstrates this character (Figure 23).

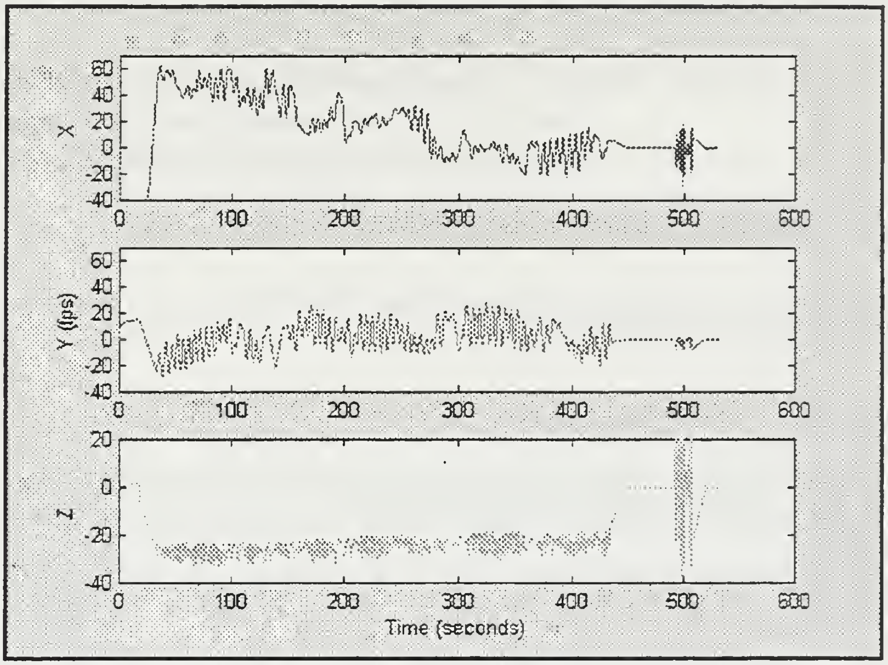

Figure 23. Data Characteristics Due to Oscillations

To better represent the operational system during this feasibility test, attempts were made to modify the C-9 parachute to minimize the oscillations by cutting large symmetrical slots in the canopy. This modification proved very stable during tow testing as well as the initial test drop. The system was then dropped with one riser extended representing a single control input. The objective of this drop was to qualitatively assess the amount of drive that could be obtained with this modified parachute. There was insufficient indication that this modification allowed enough drive for the guided system. Had the results been favorable, additional instrumented drops with the actuator/control system would have been accomplished.

Since the trials with the modified parachute did not present the desired results, the oscillation in the data needed to be dealt with prior to parameter estimation. These data must be corrected to the location of the system's center-of-gravity.

Starting with the position corrections:

(18) $P_{CG} = P_L + {}^U_B RL$; where $P_L$ is the measured position of the payload and L is the lever-arm from the location of the instrumentation to the center of gravity in body-axis coordinates {B}.

The velocity correction is then given by:

(19) $$V_{CG} = \dot{P}_{CG} = \dot{P}_L + {}^U_B\dot{R}L + {}^U_B R \frac{d}{dt} L$$

Noting: $${}^U_B\dot{R} = {}^U_B RS(\omega)$$

(20) $${}^U_B\dot{R}L = {}^U_B RS(\omega)L = {}^U_B R(\omega x L)$$

Substituting (20) into (19):

(21) $$V_{CG} = \dot{P}_L + {}^U_B R(\omega x L) + {}^U_B R \frac{d}{dt} L$$

For rigid bodies, L is assumed constant and therefore $\frac{d}{dt}L = 0$.

Applying this condition to a parachute did not yield adequate results, as the oscillations were still apparent in the velocity data. It is presumed that in an oscillating parachute, the forces on the parachute are changing due to the linear acceleration induced by the oscillations (apparent mass effects) while the forces on the payload are not varying. With this imbalance of forces in the parachute and payload, an effective change in center-of-gravity of the system results.

To illustrate this situation, the lever-arm correction is determined by rearranging Equation 21.

(22) $L = {}^{B}_{U}R(P_{CG} - P_{L})$

**$P_L$** is measured. **$P_{CG}$** is estimated using the measured velocity at the payload (**$V_L$**). A low-pass filter is applied to **$V_L$** to remove the effect of the oscillations. Using this filtered velocity (**$V_{LF}$**) and removing the wind velocity (**$V_W$**), an estimate of the velocity at the center-of-gravity is obtained (**$V_{CG}$**).

(23) $V_{CG} \approx V_{LF} - V_{W}$

This velocity is then integrated from the parachute release point. The estimated location of the center-of-gravity was then determined using Equation 22. Figure 24 presents these results.

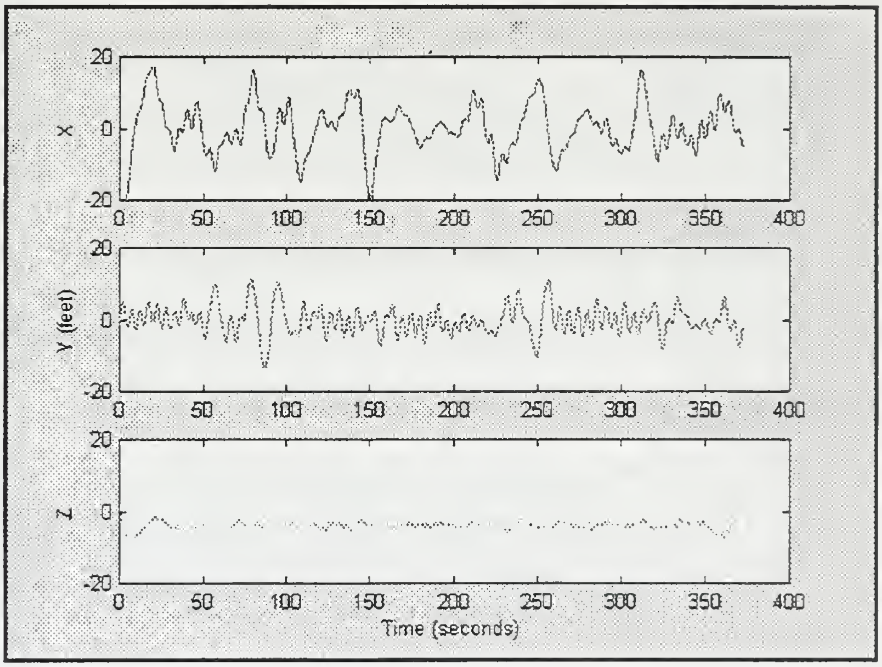

Figure 24. Movement of Lever Arm Correction

The mean lever arm corrections are $L_x$=0.0, $L_y$=-0.1, and $L_z$=-3.94 feet. Yavus and Cockrell[7] demonstrated that acceleration of the air mass and angle of attack of the parachute significantly affects the apparent mass coefficients. Attempts were made to correlate these data to linear and angular acceleration of the payload. However, no direct correlation could be found. Ideally, acceleration of the parachute should be measured in future work. With the existing instrumentation suite, it appears the flight test data must be filtered to remove the effects of oscillations prior to parameter estimation. Using the data obtained from the uncontrolled test drop (311drop1), a filter was derived using the MATLAB® System Identification Tools. A 5th-order low-pass filter with a cut-off frequency of 0.009 (in fractions of the Nyquist frequency) was selected. Figure 25 compares the measured data to the filtered data for velocity.

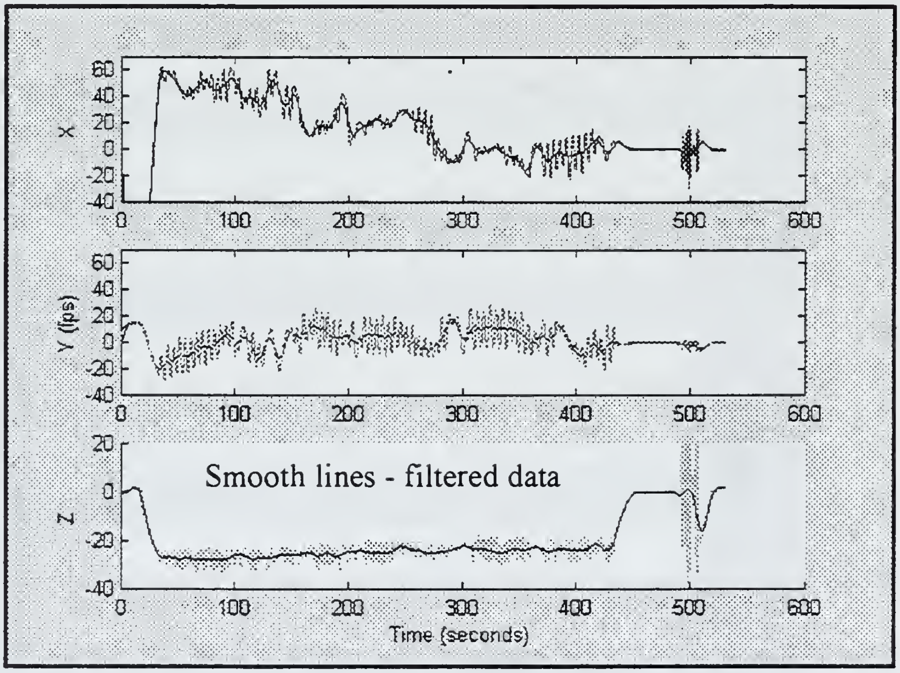

Figure 25. Comparison of Measured and Filtered Velocities

This filter was applied to the position and velocity data for all drops to estimate the motion of the system at the center-of-gravity. The obvious concern about filtering is

---

® Registered trademark of Mathworks, Inc, Natick, MA.

the potential of eliminating true system motion while removing "noise." Figure 26 compares the glide ratio filtered and unfiltered response to a single control input.

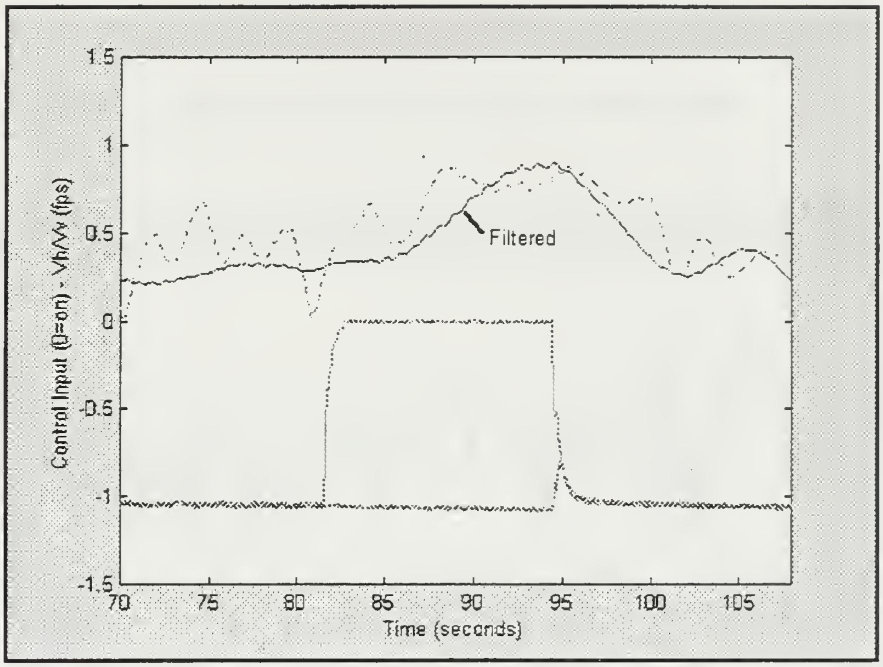

Figure 26. Assessment of Filtering

Implementation of the designed filter appears to have the potential of eliminating desired response data. The character of the response (magnitude) remains in the filtered data but the response time appears to be adversely affected. A filter of this magnitude is not desired but may be necessary for parameter estimation.

# V. FLIGHT TEST RESULTS

The control system is intended to affect a change in horizontal velocity. This is best demonstrated by assessing the glide ratio of the system with the winds removed. Figure 27 presents the glide ratio with the measured control inputs.

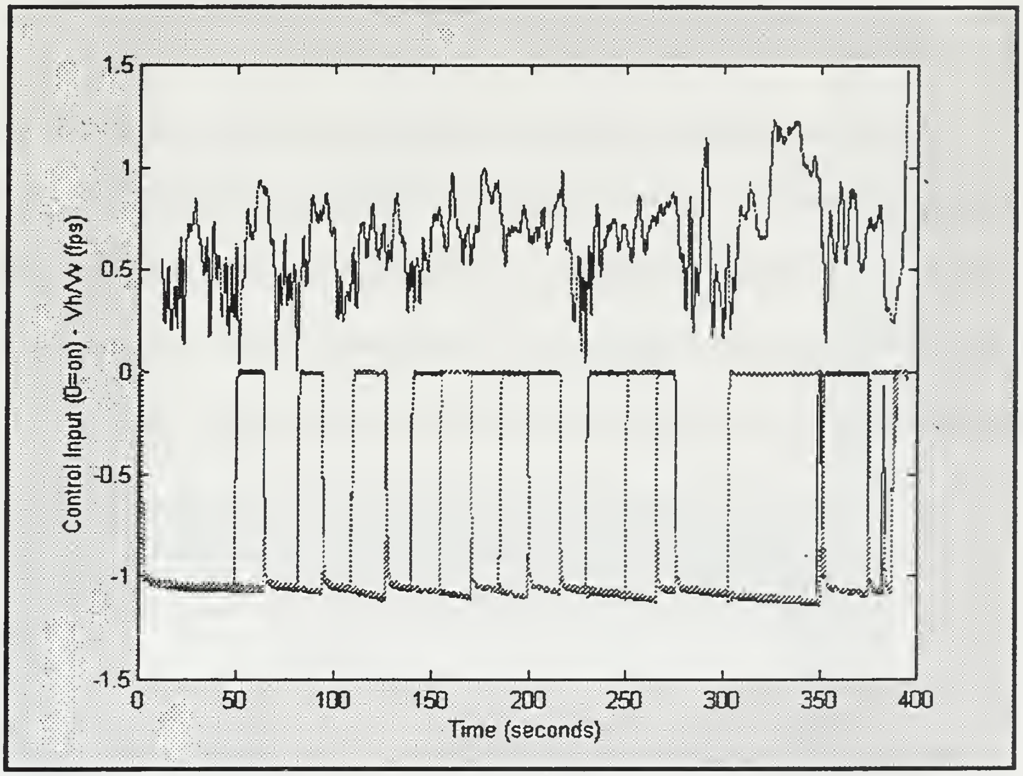

Figure 27. System Response - Glide Ratio

The results show that a nominal glide ratio of 0.4 to 0.5 exists with no control inputs. Potential causes of this induced glide are motion induced by the oscillations, imperfections in length of the pressurized actuators, the mathematics of creating a horizontal glide ratio which eliminates direction of motion, or errors in the wind estimate. This nominal glide ratio does not limit the assessment of the response due to control input, as we are interested in the change of glide ratio at the time of control activation. At time zero, all PMAs were pressurized. The system was then allowed to stabilize to a 'trim' condition. A change in glide ratio is apparent at approximately 20 seconds with no change in the state of the controls. The first incident of change in glide ratio can be attributed to the parachute stabilization/inflation process. The remaining data clearly show a correlation of glide ratio changes to the activation of the controls.

## A. SINGLE CONTROL INPUT

Figure 28 isolates the response of a single control input. An increase in glide ratio from approximately 0.5 to approximately 1.0 with a time constant of about 4 to 5 seconds is observed. The system returns to its oscillatory trim state after about 5 seconds following removal of the control input. The reduced magnitude of oscillation or coning angle contributes to a reduced rate of descent and increased glide ratio.

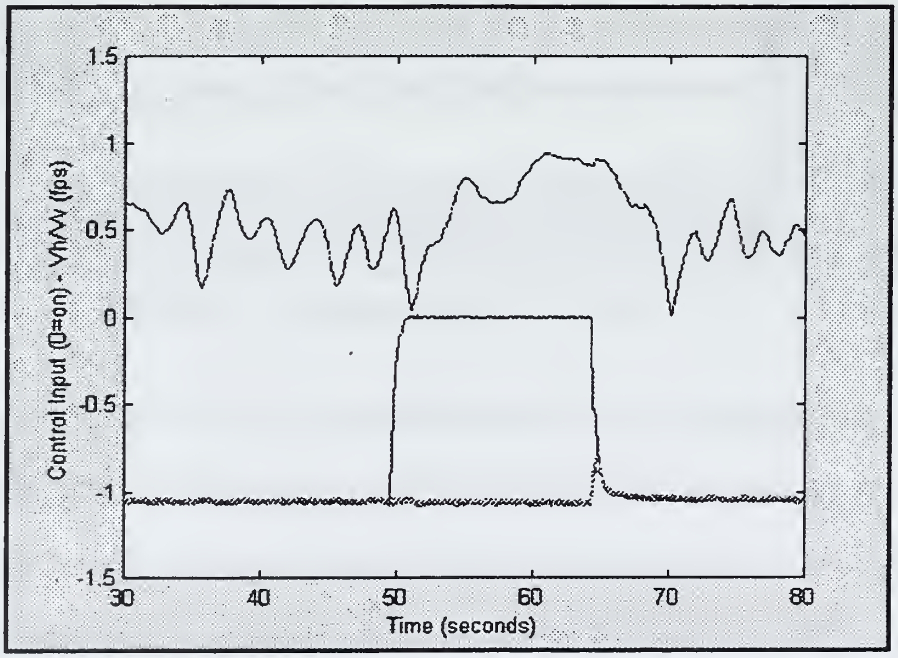

Figure 28. Single Control Response

## B. TWO SIMULTANEOUS CONTROL INPUTS

Recall that the two control inputs can be activated simultaneously. The intent is to provide additional resolution (every 45 degrees) in controlling the system. Figure 29 presents the response with two simultaneous inputs.

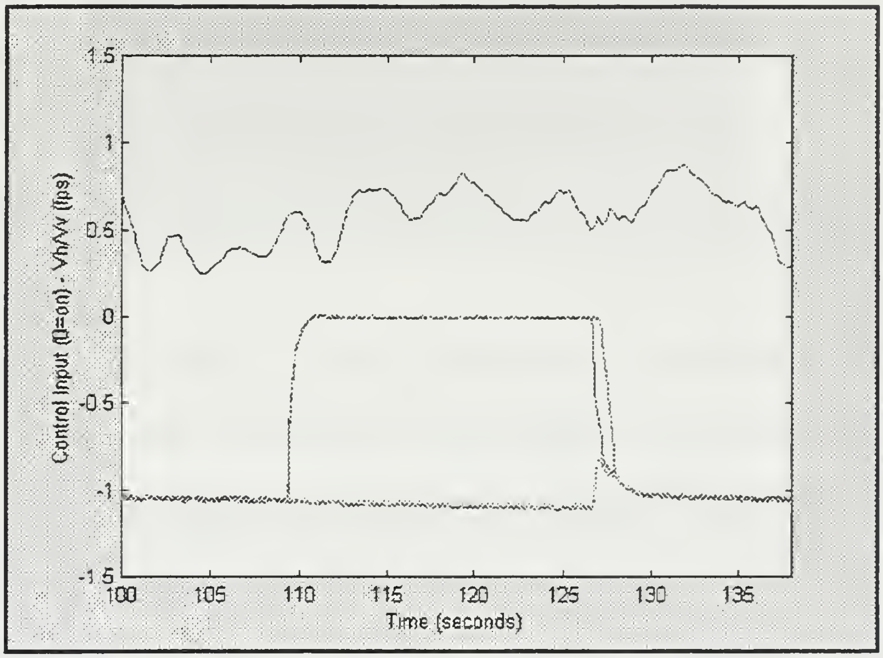

Figure 29. Two Control Response

As exemplified by this figure, there is no increase in performance with two control inputs over that achieved with one. In fact, the data indicates reduced response results from the simultaneous activation of two PMAs. This reduced performance is likely due to leading edge collapse (as observed in the ground-to-air video, Figure 30) of the parachute with two control inputs. The magnitude of the oscillations is not reduced as dramatically as with a single control input.

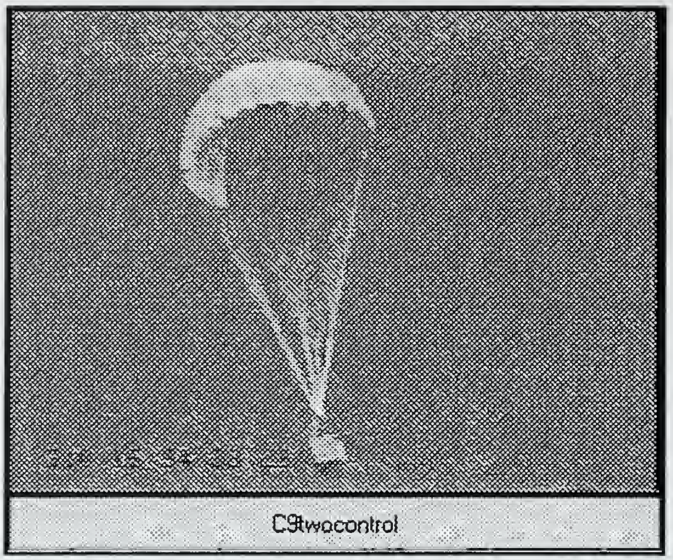

Figure 30. Parachute Collapse from Two Control Inputs (video clip)

The vertical velocity of the system was observed to decrease with a single control input but remained essentially constant with two simultaneous control inputs. This reduction is likely due to the reduced "coning" angle from the oscillation damping effect of the control system. Figure 31 presents the vertical velocity with control actuation from a single and a double input.

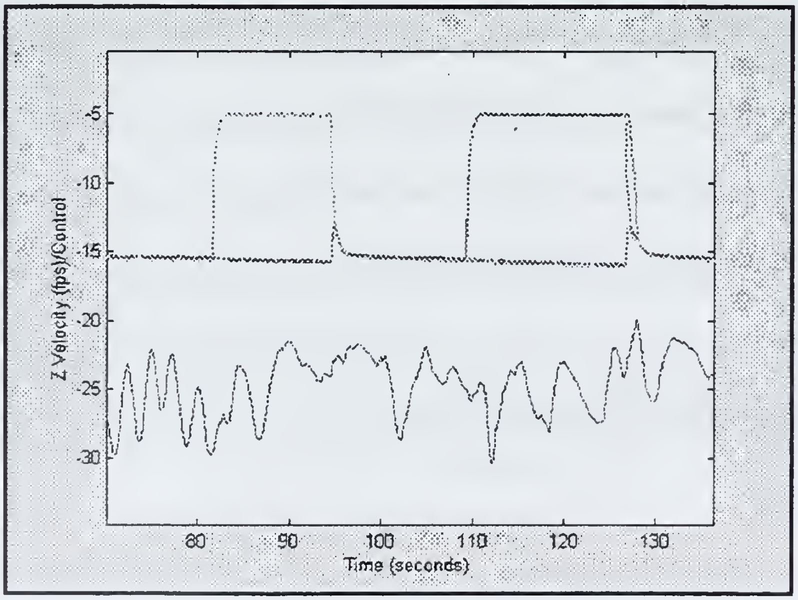

Figure 31. Vertical Velocity Response to Control Input

## C. ATTITUDE RESPONSE

For control system design, understanding the heading and yaw rate responses of the system is critical. The heading and attitude rates, as measured by the AHRS, were correlated to the control inputs for analysis. Actuation of the control system resulted in significantly decreased parachute oscillations. Figure 32 illustrates the roll rate data collected from the AHRS. Whenever a control was activated, the attitude rates were significantly reduced.

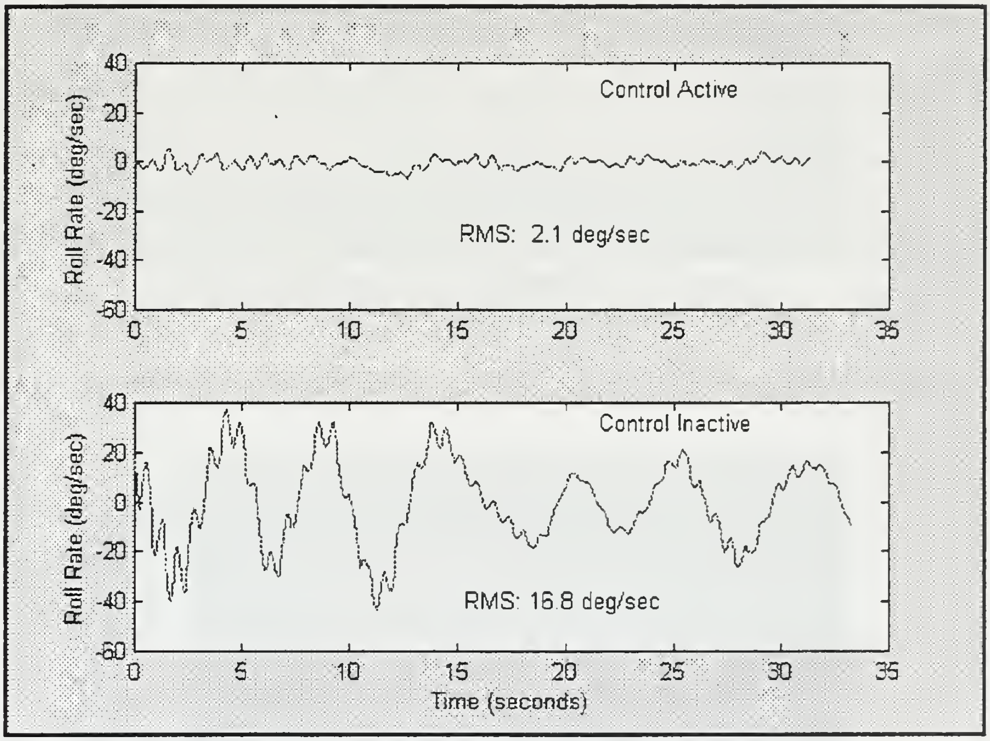

Figure 32. Roll Rate Response

The root mean square (RMS) of the roll rate reduced from 16.8 degrees per second down to 2.1 degrees per second with control activation. This behavior was observed each time a control was activated.

A plot of the total displacement (or coning) angle from vertical also demonstrates the reduction in oscillations.

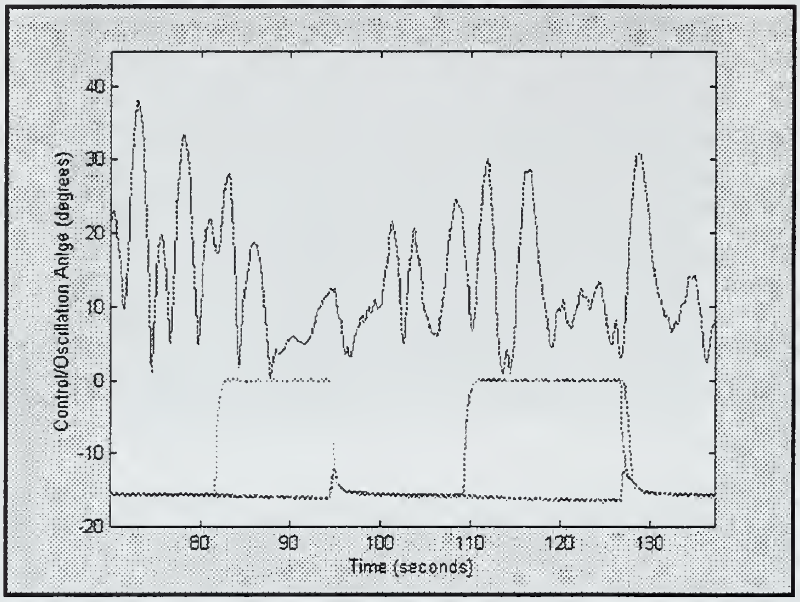

Figure 33. Oscillation Angle with Control Input

Figure 34 presents heading, measured by AHRS, and the control activation.

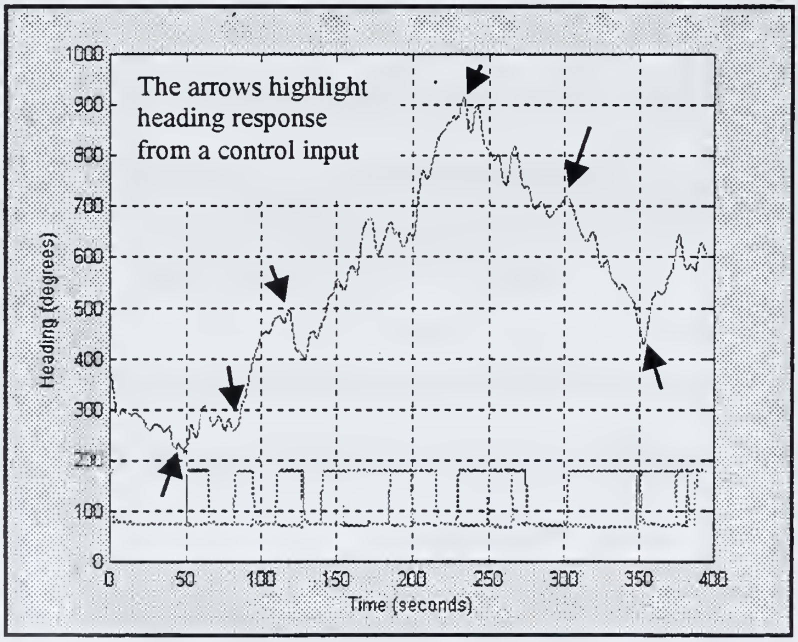

Figure 34. Heading Response

With careful examination of these data, one can correlate changes in heading with control inputs as indicated with the arrows on the graph. However, the response appears to vary greatly. The magnitude and direction of heading changes vary with the activation of the same control. The cause of this variation in heading response has not yet been identified. Factors such as the coning angle at the time of control input must be evaluated.

During initial modeling efforts, it was apparent that the rotation rate of the C-9 parachute severely limited the efficiency of this control concept. Excessive control inputs would be needed to affect control in a single cardinal direction. Therefore, it was crucial to this study to determine if the operational G-12 system exhibited similar characteristics. The results from this demonstration clearly show a significantly reduced rotation in the larger G-12 parachute as compared to the C-9 parachute. The C-9 rotations can be observed in Figure 35.

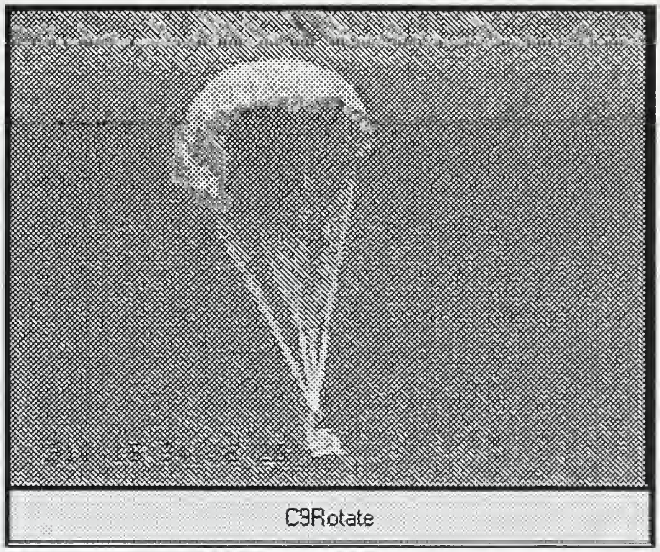

Figure 35. C-9 Rotation Rate (video clip)

Figure 36 presents a video from a camera installed on the payload. With the sun as a reference, the very low rotation rate of this system can be observed. A ground based video (Figure 37) also demonstrates a low rotation rate for the G-12 parachute.

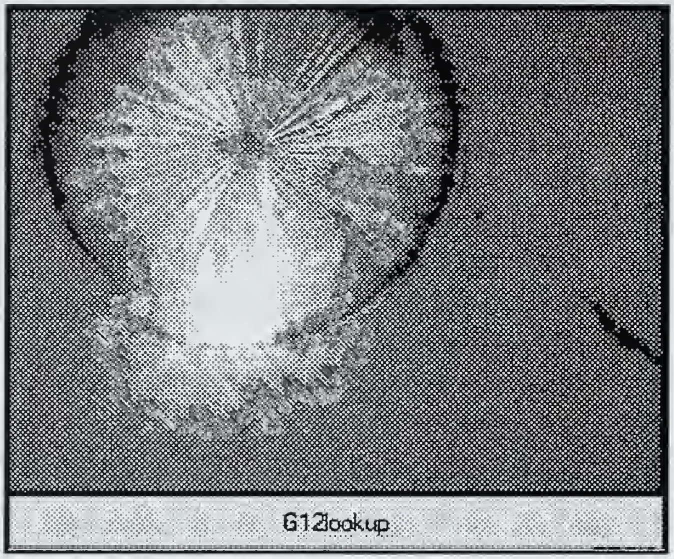

Figure 36. G-12 Rotation Rate (video clip)

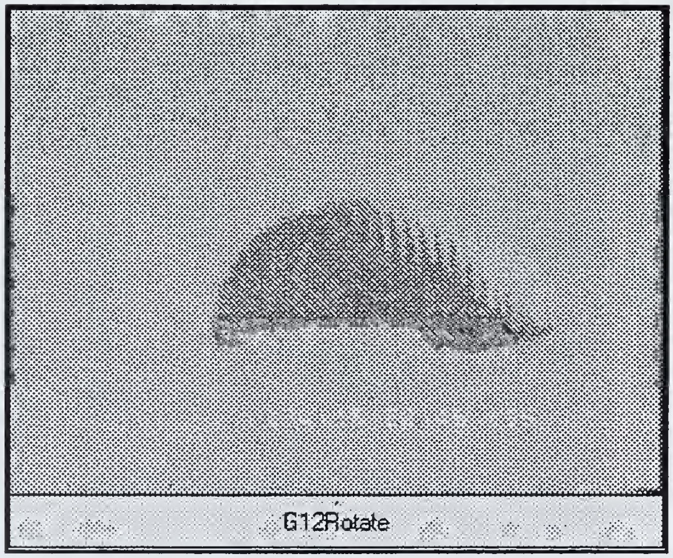

Figure 37. G-12 Rotation Rate (video clip)

# VI. NAVIGATION SENSOR MODELS

The AGAS is expected to include two navigation sensors: 1) a commercial Global Positioning System (GPS) receiver for position determination and 2) a heading reference assumed to be a magnetic compass for this study. To assess the effects of navigation sensor errors, models for each sensor must be incorporated into the simulation.

## A. GLOBAL POSITIONING SYSTEM (GPS)

GPS error sources include errors induced by the atmosphere (ionospheric and tropospheric), multi-path, receiver noise, satellite clock noise, and Selective Availability. Modeling techniques for GPS range errors resulting from these sources have been developed and validated[8] to model range errors and not errors in a Cartesian reference as desired here. Cartesian (x, y, z) errors would therefore have to be formed from the range errors for implementation in this simulation. This necessitates application of a numerical solution like maximum likelihood techniques.[9] Although this implementation is relatively trivial, the computation resources required severely limit the simulation speed on a Personal Computer (PC). Therefore, a variation of this approach was implemented.

### 1. Selective Availability

Selective Availability is a means of intentionally inducing errors into the GPS satellite signal. The DoD induces these errors to restrict use of the full precision of GPS to unauthorized users. Authorized users must apply a receiver capable of processing the cryptographic codes to remove these induced errors. Although the AGAS concept could incorporate an authorized receiver, it is desired to utilize a commercial GPS receiver for cost savings. Also, with airdrop the loads may not be fully recoverable and loss of the authorized receivers would not be desirable.

The errors resulting from Selective Availability are not stochastic in nature. Therefore system identification methods were employed to obtain a reasonable error model. Data were collected at the Yuma Proving Ground Satellite Reference Station. An unauthorized GPS receiver was placed on a known survey point. GPS position data were collected for over two hours. The position data in the three Cartesian axes were differenced with the surveyed coordinates resulting in the Cartesian errors. These errors represent all GPS error sources identified above. Figure 38 illustrates the apparent random nature of these data.

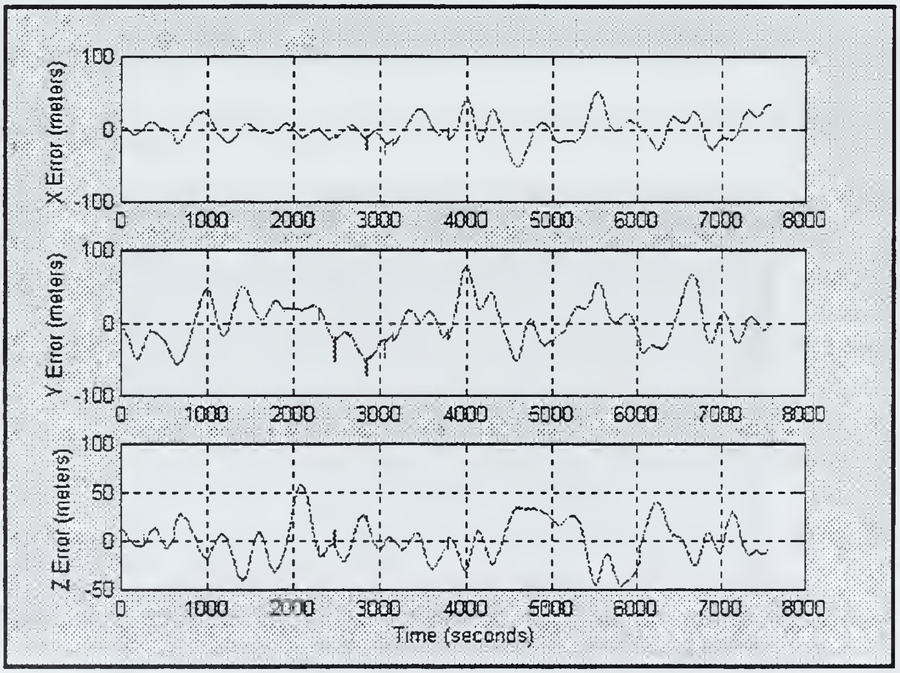

Figure 38. Measured Unauthorized GPS Errors

To obtain a model of these data, the MATLAB® system identification toolbox was utilized. An ARMAX[10] model was utilized with the input being white noise and the output being the position errors shown above. The ARMAX model incorporates a prediction error method with a model represented by a set of difference equations of the form:

(24) $A(q)y(t) = B(q)u(t - nk) + C(q)e(t)$; *where y and u are the outputs and inputs of the system, respectively.*

The coefficients A, B, and C are polynomials that describe the model's difference equations. The prediction error is minimized using an iterative Gauss-Newton algorithm. The ARMAX function returns a matrix of the polynomial coefficients. This matrix, referred to as THETA format, can then be transformed into a transfer function using the MATLAB® command TH2TF. This technique resulted in the following transfer function that was utilized in the overall system model to obtain GPS errors:

$$\frac{z^4 - 1.5302z^3 + 0.2608z^2 + 0.2566z + 0.0192}{z^4 - 2.6500z^3 + 1.9582z^2 + 0.0337z - 0.3420} \tag{25}$$

Figure 39 presents the output of the GPS error model including Selective Availability Errors.

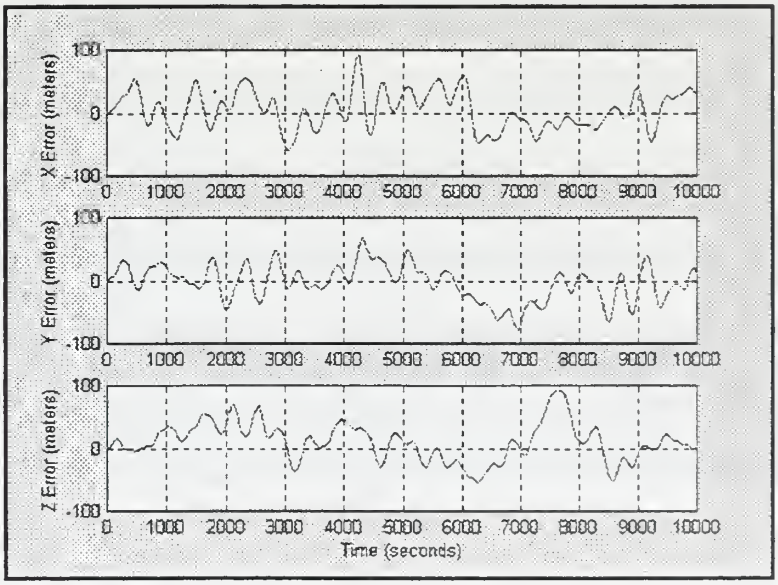

Figure 39. Modeled GPS (Unauthorized) Errors

The transfer function input is white noise initiated with a random seed ensuring variable errors are introduced from simulation to simulation. To assess the adequacy of this model, the mean, standard deviation, and root mean square were calculated for the measured and modeled GPS errors. The sample of measured errors presented above has a mean value of approximately zero meters in each axis and a standard deviation of 17.2, 28.8, and 21.1 meters in the x-, y-, and z-axes, respectively. The modeled results demonstrated mean errors of three to six meters with standard deviations ranging from 25 to 35 meters. The root mean square errors for the model were found to range from 26 to 37 meters for three independent simulations. The model produces a reasonable representation of the measured GPS data.

### 2. Model Without Selective Availability Errors

With Selective Availability turned off, that is no induced errors, a commercial GPS receiver is capable of navigating with greater accuracy. A GPS Error Model was derived considering a noise structure proposed by Draper Laboratory.[11] This report models a P-code GPS receiver incorporated into the Honeywell Embedded GPS/Inertial Navigation System. The noise model incorporates two components, accuracy and jitter. The accuracy noise component is considered exponentially correlated noise. The jitter component consists of two elements: an exponentially correlated noise component with a faster time constant than the accuracy component and a uniform uncorrelated noise component. The GPS position noise model, suggested for GPS-only operations (no inertial aiding), was adapted for a commercial grade (C/A-code) receiver by adjusting the accuracy and jitter standard deviation specification. Table 3 presents the original and adapted models.

| | Draper P-code Model | C/A-code Model |
|---|---|---|
| Accuracy Standard Deviation | 30 | 45 |
| Accuracy Correlation Time Constant (seconds) | 0.1 | 0.1 |
| Jitter Standard Deviation (feet) | 5 | 8 |
| Jitter Correlation Time Constant (seconds) | 0.05 | 0.05 |
| Uniform Uncorrelated Noise Standard Deviation | q/(2*sqrt(3)) | q/(2*sqrt(3)) |
| Note: q is the quantization interval | | |

Table 3. GPS Position Error Model

This model was incorporated into the Simulink® simulation. Figures 40 and 41 illustrate the results obtained from this model for a 400-second simulation and 50-second simulation, respectively. The standard deviation of the 3-axis error for this simulation was 56.3 feet (17.2 meters) which is close to the specifications for an commercial receiver with Selective Availability off.

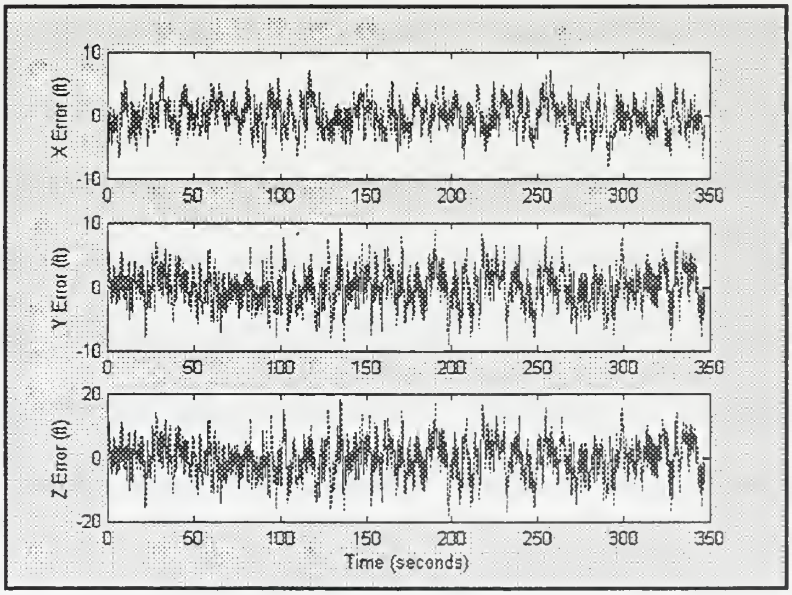

Figure 40. GPS Error Model - SA Off

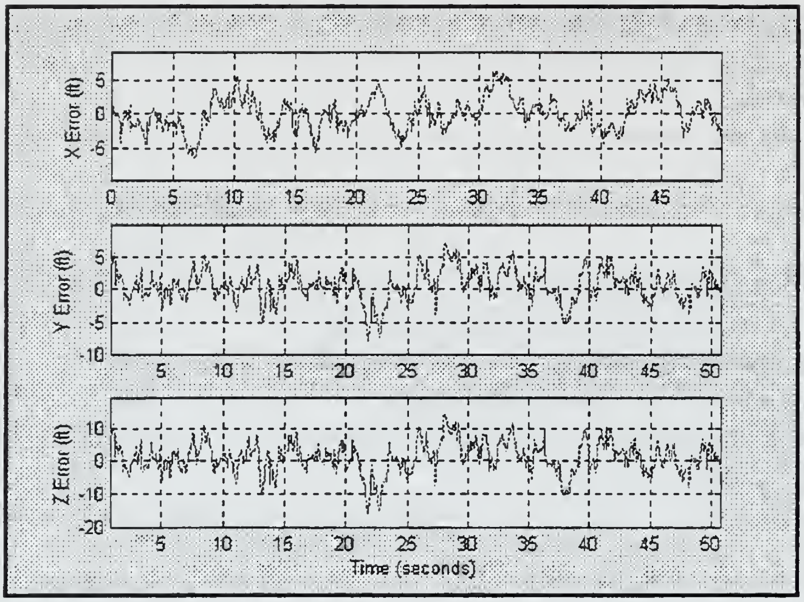

Figure 41. GPS Error Model - SA Off (50-second Simulation)

## B. HEADING SENSOR

The heading sensor is assumed to be a magnetic compass for this study. Two components of errors are considered here, a static error or bias and a dynamic (noise) component. System specifications for the Attitude Heading Reference System (AHRS) provide a static error of ±2 degrees (± 1 degree with velocity aiding) and a dynamic component of ±2 percent. The AHRS incorporates rate-gyros to obtain 3-axis attitude rates and attitude data. Specification sheets of a low-cost digital magnetic compass produced by KVH Industries presented similar accuracy statements. The static error is incorporated as a bias element in the Simulink® model and is set as a uniform random variable at the start of each simulation. The dynamic component is found by adding 2% of the current heading reading. Figure 42 presents a 400-second simulation of the heading error.

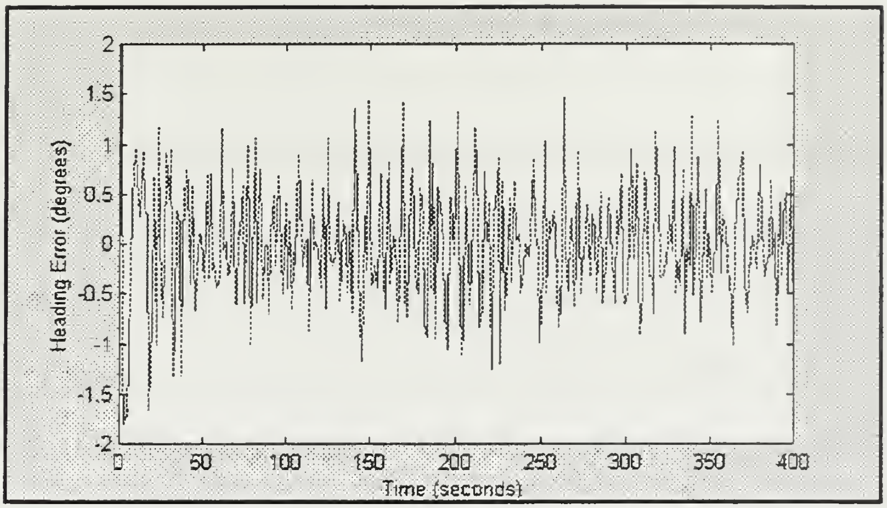

Figure 42. Modeled Heading Error

# VII. EQUATIONS OF MOTION

The kinematic equations of motion are determined assuming the parachute and payload system are a rigid body. A six-degree of freedom model is considered with the motion about the center of gravity. The notation and derivation follow the convention presented by Isaac Kaminer[12] as well as by Antonio Pascoal and Carlos Silvestre[13]. The derivation first considers an origin displaced from the system's center of gravity by a distance $P_o$. In the implementation of these equations to this problem, the origin is moved to the center of gravity of the system.

## A. NOTATION

The following illustrates the reference system used for this effort:

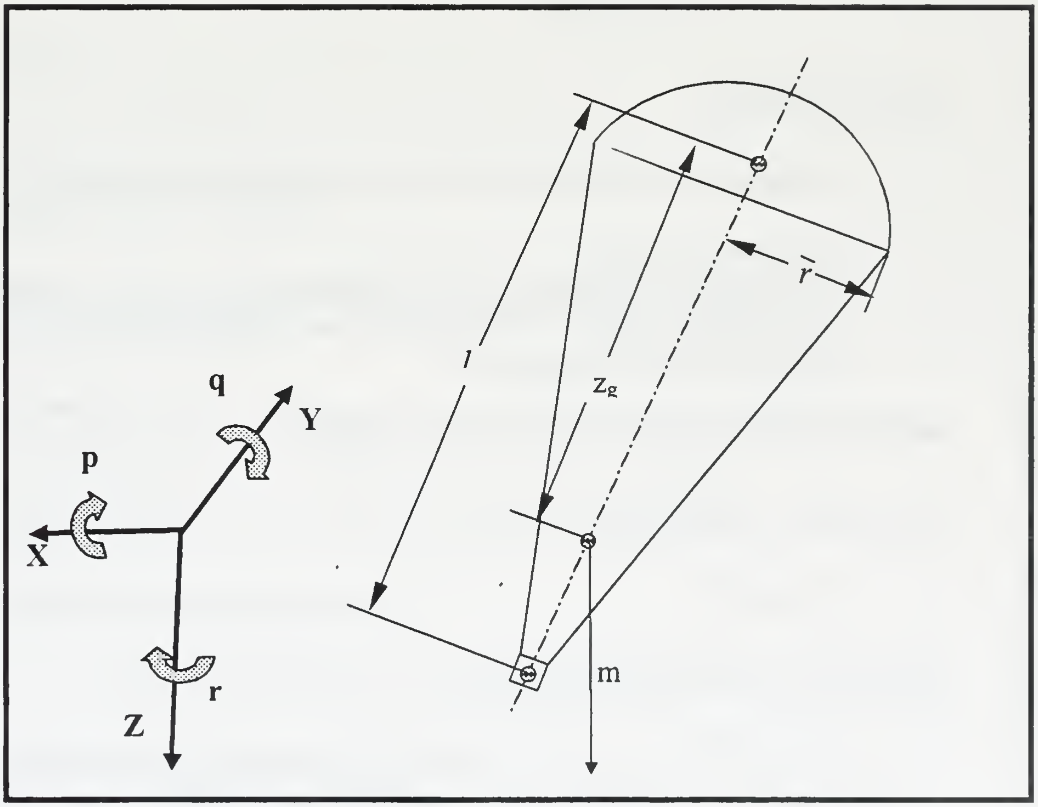

Figure 43. Coordinate Convention

The following notations are used in the development of the equations of motion.

- Capital letters/symbols denote vectors or matrices
- Small letters/symbols denote scalars
- *{B}*: name of the coordinate system, *B* denotes body-axis, *W* denotes wind-axis, and *U* denotes inertial axis.
- ${}^{C}_{A}R$: rotation matrix from coordinate system *{A}* to coordinate system *{C}*
- ${}^{C}P_{D}$ : position of point D, measured in *{C}* and expressed in *{C}*
- ${}^{A}({}^{C}P_{D})$: position of point D, measured in *{C}* and expressed in *{A}* where ${}^{A}({}^{C}P_{D}) = {}^{A}_{C}R({}^{C}P_{D}) \neq {}^{C}P_{D}$.
- ${}^{C}V_{D}$ : velocity of point D, measured in *{C}* and expressed in *{C}*
- ${}^{C}\Omega_{D}$ : angular velocity of point D, measured in *{C}* and expressed in *{C}*
- $\frac{d}{dt}$ : time derivatives in the body-axis *{B}*
- $(\dot{\ })$: time derivatives in the inertial-axis *{U}*

**NOTE**: if the symbol for the coordinate axis is omitted, the inertial-axis *{U}* is assumed.

## B. ASSUMPTIONS

Throughout this effort, the following assumptions were considered:

- Rigid-body system
- Only the motion after complete parachute deployment is considered.
- Non-rotating earth, i.e. ECEF coordinate equals inertial coordinate
- Wind axis equals inertial axis

## C. DERIVATION OF EQUATIONS OF MOTION

Starting with Newton's Law, $F = ma$

$$^{U}F = m\,{}^{U}\dot{V}_{B}$$

The inertial velocity of the body is:

$${}^{U}V_{B} = {}^{U}_{B}R\left\{{}^{B}V_{B} + \Omega \times P_{O}\right\}$$ ; where $P_O$ is the position of the parachute reference to the origin (center-of-gravity).

Taking the derivative:

(26) $${}^{U}\dot{V}_{B}={}^{U}_{B}R\left\{\frac{d}{dt}{}^{B}V_{B}+\dot{\Omega}\times P_{O}+\Omega\times\dot{P}_{O}\right\}+{}^{U}_{B}\dot{R}\left({}^{B}V_{B}+\Omega\times P_{O}\right);$$ *where* $\dot{P}_{O}=0$ *due to rigid body assumption*

recall:

(27) $${}^{U}_{B}\dot{R}={}^{U}_{B}R\cdot S({}^{B}\Omega_{B}),\quad {}^{B}\Omega_{B}=\begin{bmatrix}p\\q\\r\end{bmatrix}$$

and $S({}^{B}\Omega_{B})=\begin{bmatrix}0&-r&q\\r&0&-p\\-q&p&0\end{bmatrix}$ (skew symmetric matrix)

Substituting (27) into (26):

(28) $${}^{U}\dot{V}_{B}={}^{U}_{B}R\left\{\frac{d}{dt}{}^{B}V_{B}+\dot{\Omega}\times P_{O}\right\}+{}^{U}_{B}R\cdot S({}^{B}\Omega_{B})\left({}^{B}V_{B}+\Omega\times P_{O}\right)$$

Noting:

(29) $$S({}^{B}\Omega_{B}){}^{B}V_{B}={}^{B}\Omega_{B}x{}^{B}V_{B}$$

Substituting (29) into (28):

$${}^{U}\dot{V}_{B}={}^{U}_{B}R\left\{\frac{d}{dt}{}^{B}V_{B}+\dot{\Omega}\times P_{O}\right\}+{}^{U}_{B}R\,{}^{B}\Omega_{B}x\left({}^{B}V_{B}+\Omega\times P_{O}\right)$$

Rearranging Terms:

$${}^{U}\dot{V}_{B}={}^{U}_{B}R\left\{\frac{d}{dt}{}^{B}V_{B}-P_{O}\times\dot{\Omega}\right\}+{}^{U}_{B}R\,{}^{B}\Omega_{B}x\left(-P_{O}\times\Omega+{}^{B}V_{B}\right)$$

Consider forces in the body axis:

$${}^{B}F={}^{B}_{U}R\cdot{}^{U}F={}^{B}_{U}R\cdot M_{T}\,{}^{U}\dot{V}_{B};\ \text{where: } M_{T}=mI_{3}$$

$$=M_{T}\,{}^{B}_{U}R\left\{{}^{U}_{B}R\left\{\frac{d}{dt}{}^{B}V_{B}-P_{O}\times\dot{\Omega}\right\}+{}^{U}_{B}R\,{}^{B}\Omega_{B}x\left\{-P_{O}\times\Omega+{}^{B}V_{B}\right\}\right\}$$

$$= M_T\left\{\frac{d}{dt}{}^{B}V_B - P_O \times \dot{\Omega}\right\} + M_T\,{}^{B}\Omega_B x\left(-P_O \times \Omega + {}^{B}V_B\right)$$

$$(30) \qquad = M_T\frac{d}{dt}{}^{B}V_B - M_T P_O \times \dot{\Omega} + {}^{B}\Omega_B x\left(-M_T P_O \times \Omega + M_T\,{}^{B}V_B\right)$$

Again applying the notation used by Pascoal by defining the general mass matrix:

$$(31) \qquad M = \begin{bmatrix} M_T & M_{TR} \\ M_{RT} & M_R \end{bmatrix} = \begin{bmatrix} mI_3 & -m^{B}P_O \times \\ m^{B}P_O \times & I_B \end{bmatrix}$$

Equation (30) reduces to:

$$F_B = M_T\frac{d}{dt}{}^{B}V_B + M_{TR}\dot{\Omega} + {}^{B}\Omega_B \times \left(M_{TR}\Omega + M_T\,{}^{B}V_B\right)$$

Solving for velocity in the body axis:

$$(32) \qquad \frac{d}{dt}{}^{B}V_B = M_T^{-1}\left\{M_{TR}\dot{\Omega} + {}^{B}\Omega_B \times \left\{M_{TR}\Omega + M_T\,{}^{B}V_B\right\}\right\} + M_T^{-1}F_B$$

Now applying Euler's Law:

(33) $\quad {}^{U}\dot{L}_B = {}^{U}N_B - M_T P_O \times {}^{U}\dot{V}_B$; *angular momentum equals total applied moment;*

where: $M = mI_3$; $I_3$ is a 3x3 identity matrix and m is the system's mass

Recall:

$${}^{U}V_B = {}^{U}_{B}R\,{}^{B}V_B$$

$${}^{U}\dot{V}_B = {}^{U}_{B}R\frac{d}{dt}{}^{B}V_B + {}^{U}_{B}\dot{R}\,{}^{B}V_B$$

$${}^{U}_{B}\dot{R}\,{}^{B}V_B = {}^{U}_{B}R\left(\Omega \times {}^{B}V_B\right)$$

$$(34) \qquad {}^{U}\dot{V}_B = {}^{U}_{B}R\frac{d}{dt}{}^{B}V_B + {}^{U}_{B}R\left(\Omega \times {}^{B}V_B\right)$$

Substituting (34) into (33):

$${}^{U}\dot{L}_B = {}^{U}N_B - M_T P_O \times \left({}^{U}_{B}R\frac{d}{dt}{}^{B}V_B + {}^{U}_{B}R\left(\Omega \times {}^{B}V_B\right)\right)$$

$$ {}^{U}L_B = {}^{U}_{B}R\,{}^{B}L\,; \quad {}^{U}\dot{L}_B = {}^{U}_{B}R\frac{d}{dt}{}^{B}L + {}^{U}_{B}\dot{R}\,{}^{B}L = {}^{U}_{B}R\frac{d}{dt}{}^{B}L + {}^{U}_{B}R\left(\Omega\times{}^{B}L\right) $$

$$ {}^{U}_{B}R\frac{d}{dt}{}^{B}L + {}^{U}_{B}R\left(\Omega\times{}^{B}L\right) = {}^{U}N_B - M_T P_O \times \left( {}^{U}_{B}R\frac{d}{dt}{}^{B}V_B + {}^{U}_{B}R\left(\Omega\times{}^{B}V_B\right) \right) \tag{35} $$

By definition:

${}^{B}L = I_B\Omega$; where $I_B$ is the system's moment of inertia matrix

$$ {}^{B}\dot{L} = I_B\dot{\Omega} \tag{36} $$

Substituting (36) into (35)

$$ {}^{U}_{B}RI_B\dot{\Omega} + {}^{U}_{B}R\left(\Omega\times I_B\Omega\right) = {}^{U}N_B - M_T P_O \times \left( {}^{U}_{B}R\frac{d}{dt}{}^{B}V_B + {}^{U}_{B}R\left(\Omega\times{}^{B}V_B\right) \right) $$

Rearranging Terms:

$$ {}^{U}N_B = {}^{U}_{B}RI_B\dot{\Omega} + {}^{U}_{B}R\left(\Omega\times I_B\Omega\right) + M_T P_O \times \left( {}^{U}_{B}R\frac{d}{dt}{}^{B}V_B + {}^{U}_{B}R\left(\Omega\times{}^{B}V_B\right) \right) $$

Transforming into the body axis {B}:

$$ {}^{B}N_B = {}^{B}_{U}R\,{}^{U}N_B = I_B\frac{d}{dt}\Omega + \left(\Omega\times I_B\Omega\right) + M_T P_O \times \left( \frac{d}{dt}{}^{B}V_B + \left(\Omega\times{}^{B}V_B\right) \right) $$

$$ {}^{B}N_B = I_B\frac{d}{dt}\Omega + \left(\Omega\times I_B\Omega\right) + M_T P_O \times \left(\Omega\times{}^{B}V_B\right) + M_T P_O \times \left( \frac{d}{dt}{}^{B}V_B \right) \tag{37} $$

Applying (31) to (37):

$$ {}^{B}N_B = M_R\frac{d}{dt}\Omega + M_{RT}\left( \frac{d}{dt}{}^{B}V_B \right) + \Omega\times M_R\Omega + M_{RT}\left(\Omega\times{}^{B}V_B\right) $$

Rearranging:

$$ \frac{d}{dt}\Omega = M_R^{-1}\left\{ M_{RT}\left( \frac{d}{dt}{}^{B}V_B \right) + \Omega\times M_R\Omega + M_{RT}\left(\Omega\times{}^{B}V_B\right) \right\} + M_R^{-1}\,{}^{B}N_B \tag{38} $$

Combining (38) and (32) in state space form:

$$\begin{bmatrix} {}^{B}F \\ {}^{B}N_{B} \end{bmatrix} = \begin{bmatrix} M_{T}\frac{d}{dt}{}^{B}V_{B} + M_{TR}\dot{\Omega} + {}^{B}\Omega_{B} \times \left\{ M_{TR}\Omega + M_{T}\,{}^{B}V_{B} \right\} \\ M_{R}\frac{d}{dt}\Omega + M_{RT}\left(\frac{d}{dt}{}^{B}V_{B}\right) + \Omega \times M_{R}\Omega + M_{RT}\left(\Omega \times {}^{B}V_{B}\right) \end{bmatrix}$$

$$\begin{bmatrix} \frac{d}{dt}{}^{B}V_{B} \\ \frac{d}{dt}\Omega \end{bmatrix} = \begin{bmatrix} M_{T}^{-1}\left\{ M_{TR}\dot{\Omega} + {}^{B}\Omega_{B} \times \left\{ M_{TR}\Omega + M_{T}\,{}^{B}V_{B} \right\}\right\} \\ M_{R}^{-1}\left\{ M_{RT}\left(\frac{d}{dt}{}^{B}V_{B}\right) + \Omega \times M_{R}\Omega + M_{RT}\left(\Omega \times {}^{B}V_{B}\right)\right\} \end{bmatrix} + \begin{bmatrix} M_{T}^{-1} & 0 \\ 0 & M_{R}^{-1} \end{bmatrix} \begin{bmatrix} {}^{B}F_{B} \\ {}^{B}N_{B} \end{bmatrix} \tag{39}$$

## D. APPARENT MASS

As a body accelerates through a fluid, the fluid itself must accelerate to accommodate the motion of the body. Resultant forces and moments are applied to the body. A common method for accounting for these forces is to include added or apparent mass terms in the equations of motion. Sir Horace Lamb performed the original work on the effects of accelerating fluid on a body.[14] Lamb derives the apparent mass effects and identifies 15 independent terms. Cockrell and Doherr[15] showed that for a revolution of the body about a plane of symmetry, the number of independent terms reduces to the following:

$\alpha_{11}$ - motion along the x-axis
$\alpha_{22}$ - motion along the y-axis
$\alpha_{33}$ - motion along the z-axis
$\alpha_{44}$ - motion about the x-axis
$\alpha_{55}$ - motion about the y-axis
$\alpha_{15}$ - coupling between motion along the x-axis and about the y-axis.
$\alpha_{24}$ - coupling between motion along the y-axis and about the x-axis

These terms have been demonstrated to change significantly with acceleration of the body.[16] However, estimation of these changes is very difficult and beyond the scope of this research. Therefore, only the scalar values of apparent mass and moment of inertia terms are considered.

### 1. Estimation of Apparent Mass Terms

Doherr and Saliaris[17] demonstrated that for an equivalent parachute, four independent apparent mass terms exist:

$$\alpha_{33} = \{\frac{4}{3}\pi(\frac{D_P}{2})^3\} \text{ ; } D_p \textit{ is the profile diameter of the parachute} \quad (40)$$

$$\alpha_{11} = \alpha_{22} = \frac{1}{2}\alpha_{33} \quad (41)$$

$$\alpha_{15} = -\alpha_{24} = 0.2\alpha_{11} l_b \quad (42)$$

$$\alpha_{44} = \alpha_{55} = 0.048 D_P^{\,2} \alpha_{11} \quad (43)$$

### 2. Effects on the Equations of Motion

The force imparted on the body by the air mass can be determined by starting with the equations of motion for the body itself (Equation 39) and replacing the mass matrices with apparent mass matrices as shown here:

$$M_T \rightarrow A_T;\ M_{TR} \rightarrow A_{TR};\ M_{RT} \rightarrow -A_{TR};\ M_R \rightarrow A_R$$

$$\begin{bmatrix} {}^{B}F \\ {}^{B}N_B \end{bmatrix} = \begin{bmatrix} M_T \frac{d}{dt} {}^{B}V_B + M_{TR}\dot{\Omega} + {}^{B}\Omega_B \times \left\{ M_{TR}\Omega + M_T\, {}^{B}V_B \right\} \\ M_R \frac{d}{dt}\Omega + M_{RT}\left(\frac{d}{dt} {}^{B}V_B\right) + \Omega \times M_R \Omega + M_{RT}\left(\Omega \times {}^{B}V_B\right) \end{bmatrix} \quad (44)$$

$$A_T = \begin{bmatrix} \alpha_{11} & 0 & 0 \\ 0 & \alpha_{22} & 0 \\ 0 & 0 & \alpha_{33} \end{bmatrix};\quad A_R = \begin{bmatrix} \alpha_{44} & 0 & 0 \\ 0 & \alpha_{55} & 0 \\ 0 & 0 & 0 \end{bmatrix}; \quad (45)$$

$$(46)\qquad A_{TR}=\begin{bmatrix}0&\alpha_{15}&0\\\alpha_{24}&0&0\\0&0&0\end{bmatrix}\; A_{RT}=\begin{bmatrix}0&\alpha_{24}&0\\\alpha_{15}&0&0\\0&0&0\end{bmatrix}=\begin{bmatrix}0&-\alpha_{15}&0\\-\alpha_{24}&0&0\\0&0&0\end{bmatrix}$$

$$(47)\qquad A_{RT}=-A_{TR}$$

Substituting (46 and 45) into (44):

$$(48)\qquad \begin{bmatrix}{}^{B}F_{A}\\{}^{B}N_{A}\end{bmatrix}=\begin{bmatrix}A_{T}\dfrac{d}{dt}{}^{B}V_{B}+A_{TR}\dot{\Omega}+{}^{B}\Omega_{B}\times\left\{A_{TR}\Omega+A_{T}\,{}^{B}V_{B}\right\}\\ A_{R}\dfrac{d}{dt}\Omega+A_{RT}\left(\dfrac{d}{dt}{}^{B}V_{B}\right)+\Omega\times A_{R}\Omega+A_{RT}\left(\Omega\times{}^{B}V_{B}\right)\end{bmatrix}$$

In addition to those forces and moments presented here, an additional term is required in the moment equation to account for the additional moments generated by changes in momentum due to air acting on the parachute. The term ${}^{B}V\times A_{T}\,{}^{B}V$ is added to (48).

$$(49)\qquad \begin{bmatrix}{}^{B}F_{A}\\{}^{B}N_{A}\end{bmatrix}=\begin{bmatrix}A_{T}\dfrac{d}{dt}{}^{B}V_{B}+A_{TR}\dot{\Omega}+{}^{B}\Omega_{B}\times\left\{A_{TR}\Omega+A_{T}\,{}^{B}V_{B}\right\}\\ A_{R}\dfrac{d}{dt}\Omega+A_{RT}\left(\dfrac{d}{dt}{}^{B}V_{B}\right)+\Omega\times A_{R}\Omega+A_{RT}\left(\Omega\times{}^{B}V_{B}\right)+{}^{B}V\times A_{T}\,{}^{B}V\end{bmatrix}$$

Combining (49) and (39) and rearranging terms:

$$\begin{bmatrix}\dfrac{d}{dt}{}^{B}V_{B}\\ \dfrac{d}{dt}\Omega\end{bmatrix}=\begin{bmatrix}M_{T}'^{-1}\left\{M_{TR}'\dot{\Omega}+{}^{B}\Omega_{B}\times\left\{M_{TR}'\Omega+M_{T}'\,{}^{B}V_{B}\right\}\right\}\\ M_{R}'^{-1}\left\{M_{RT}'\left(\dfrac{d}{dt}{}^{B}V_{B}\right)+\Omega\times M_{R}'\Omega+M_{RT}'\left(\Omega\times{}^{B}V_{B}\right)\right\}+{}^{B}V\times A_{T}\,{}^{B}V\end{bmatrix}+\begin{bmatrix}M_{T}'^{-1}&0\\0&M_{R}'^{-1}\end{bmatrix}\begin{bmatrix}{}^{B}F_{B}\\{}^{B}N_{B}\end{bmatrix}$$

where:

$$M'=\begin{bmatrix}M_{T}'&M_{TR}'\\M_{RT}'&M_{R}'\end{bmatrix}=\begin{bmatrix}M_{T}+A_{T}&M_{TR}+A_{TR}\\M_{RT}+A_{RT}&M_{R}+A_{R}\end{bmatrix}$$

## E. EXTERNAL FORCES AND MOMENTS

The external forces and moments on the body include the effects of aerodynamics (including actuation of the control surfaces) and gravity.

$$^{B}F_{B} = F_{AERO} + F_{AM} + F_{GRAV}$$

$$^{B}N_{B} = N_{AERO} + N_{AM} + N_{GRAV}$$

Buoyancy terms as discussed by Gockel[18] are not included as the convention used herein does not include the mass of the trapped air in the overall systems mass. As Gockel demonstrates, if one is to include the mass of the trapped air a compensating "buoyancy" term must be added to the equations of motion.

### 1. Aerodynamic Forces and Moments

Using a first order Taylor series expansion about a nominal trim condition and following Kaminer's[19] notation, the aerodynamic effects are found to be:

$$F_{AERO} = F_{o} + \delta F_{x} + \delta F_{\dot{x}}\dot{x} + \delta F_{\Delta}\Delta$$

$$N_{AERO} = N_{o} + \delta N_{x} + \delta N_{\dot{x}}\dot{x} + \delta N_{\Delta}\Delta$$

where x and $\dot{x}$ are the state vector and first derivative of the state vector and $\Delta$ is the control vector. δF and δM are the partial derivatives of the forces and moments with respect to each parameter in the state vector and their first time derivative.

**Non-dimensionalizing and putting in state space form**:

$$F_{AERO} = qS_{o}\left\{C_{F_o} + \delta C_{F_x} + \delta C_{F_{\dot{x}}}\dot{x} + \delta C_{F_\Delta}\Delta\right\}$$

$$N_{AERO} = \bar{q}S_{o}d_{o}\left\{C_{N_o} + \delta C_{N_x} + \delta C_{N_{\dot{x}}}\dot{x} + \delta C_{N_\Delta}\Delta\right\}$$

where:

$$C_{Fo} = \begin{bmatrix} C_{Xo} & C_{Yo} & C_{Zo} & C_{Lo} & C_{Mo} & C_{No} \end{bmatrix}^T$$

$$C_{Fo} = \begin{bmatrix} C_{Xo} & C_{Yo} & C_{Zo} & C_{Lo} & C_{Mo} & C_{No} \end{bmatrix}^T$$

$$\delta C_{Fx} = \begin{bmatrix} C_{Xu} & C_{Xv} & C_{Xw} & C_{Xp} & C_{Xq} & C_{Xr} \\ C_{Yu} & C_{Yv} & C_{Yw} & C_{Yp} & C_{Yq} & C_{Yr} \\ C_{Zu} & C_{Zv} & C_{Zw} & C_{Zp} & C_{Zq} & C_{Zr} \end{bmatrix}$$

$$\delta C_{Nx} = \begin{bmatrix} C_{Lu} & C_{Lv} & C_{Lw} & C_{Lp} & C_{Lq} & C_{Lr} \\ C_{Mu} & C_{Mv} & C_{Mw} & C_{Mp} & C_{Mq} & C_{Mr} \\ C_{Nu} & C_{Nv} & C_{Nw} & C_{Np} & C_{Nq} & C_{Nr} \end{bmatrix}$$

$$\delta C_{F\dot{x}} = \begin{bmatrix} C_{X\dot{u}} & C_{X\dot{v}} & C_{X\dot{w}} & C_{X\dot{p}} & C_{X\dot{q}} & C_{X\dot{r}} \\ C_{Y\dot{u}} & C_{Y\dot{v}} & C_{Y\dot{w}} & C_{Y\dot{p}} & C_{Y\dot{q}} & C_{Y\dot{r}} \\ C_{Z\dot{u}} & C_{Z\dot{v}} & C_{Z\dot{w}} & C_{Z\dot{p}} & C_{Z\dot{q}} & C_{Z\dot{r}} \end{bmatrix}$$

$$\delta C_{N\dot{x}} = \begin{bmatrix} C_{L\dot{u}} & C_{L\dot{v}} & C_{L\dot{w}} & C_{L\dot{p}} & C_{L\dot{q}} & C_{L\dot{r}} \\ C_{M\dot{u}} & C_{M\dot{v}} & C_{M\dot{w}} & C_{M\dot{p}} & C_{M\dot{q}} & C_{M\dot{r}} \\ C_{N\dot{u}} & C_{N\dot{v}} & C_{N\dot{w}} & C_{N\dot{p}} & C_{N\dot{q}} & C_{N\dot{r}} \end{bmatrix}$$

$$\delta C_{F\Delta} = \begin{bmatrix} C_{X\Delta} & C_{Y\Delta} & C_{Z\Delta} \end{bmatrix}^t; \quad \delta C_{N\Delta} = \begin{bmatrix} C_{L\Delta} & C_{M\Delta} & C_{N\Delta} \end{bmatrix}^t$$

## 2. Gravity

The gravitational force acting on the body in the inertial reference frame is given by:

$$^{U}F_{GRAV} = \begin{bmatrix} 0 \\ 0 \\ mg \end{bmatrix}$$

The force in the body axis is found using an Euler angle transformation:

$$^{B}F_{GRAV} = {}^{B}_{U}R\, {}^{U}F_{GRAV} = {}^{B}_{U}R \begin{bmatrix} 0 \\ 0 \\ mg \end{bmatrix};$$

$$\text{where } {}^{B}_{U}R = \begin{bmatrix} \cos\psi\cos\theta & \sin\psi\cos\theta & -\sin\theta \\ \cos\psi\sin\theta\sin\phi - \sin\psi\cos\phi & \sin\psi\sin\theta\sin\phi + \cos\psi\cos\phi & \cos\theta\sin\phi \\ \cos\psi\sin\theta\cos\phi + \sin\psi\sin\theta & \sin\psi\sin\theta\cos\phi - \cos\psi\sin\phi & \cos\theta\cos\phi \end{bmatrix}$$

Recall that $P_o$ is defined as the distance from the origin to the center of gravity. The gravitational force creates a moment about the defined origin.

$$^{B}N_{GRAV} = P_o\,{}^{B}F_{GRAV} = P_o\,{}^{B}_{U}R\begin{bmatrix} 0 \\ 0 \\ mg \end{bmatrix}; \text{ later } P_o \text{ will be defined.}$$

### 3. Total External Forces and Moments

The total external forces and moments are now given as:

$$^{B}F_{B} = qS_o\{\delta C_{F_o} + \delta C_{F_x} + \delta C_{F_{\dot{x}}}\dot{x} + \delta C_{F_\Delta}\Delta\} + {}^{B}_{U}R\begin{bmatrix} 0 \\ 0 \\ mg \end{bmatrix}$$

$$N_B = \bar{q}S_o d_o\{\delta C_{N_o} + \delta C_{N_x} + \delta C_{N_{\dot{x}}}\dot{x} + \delta C_{N_\Delta}\Delta\} + P_o\,{}^{B}_{U}R\begin{bmatrix} 0 \\ 0 \\ mg \end{bmatrix}$$

In matrix form:

$$\begin{bmatrix} ^{B}F_{B} \\ ^{B}N_{B} \end{bmatrix} = \begin{bmatrix} \bar{q}S_o I_3 & 0 \\ 0 & \bar{q}S_o d_o I_3 \end{bmatrix}\begin{bmatrix} \{\delta C_{F_o} + \delta C_{F_x} + \delta C_{F_{\dot{x}}}\dot{x} + \delta C_{F_\Delta}\Delta\} \\ \{\delta C_{N_o} + \delta C_{N_x} + \delta C_{N_{\dot{x}}}\dot{x} + \delta C_{N_\Delta}\Delta\} \end{bmatrix} + \begin{bmatrix} {}^{B}_{U}R \\ P_o\,{}^{B}_{U}R \end{bmatrix}\begin{bmatrix} 0 \\ 0 \\ mg \end{bmatrix}$$

## F. COMPLETE EQUATIONS OF MOTION

This derivation assumes that the system is a single rigid body and resulted in a general set of equations of motion. These equations could then be applied to the parachute and payload separately. For example, to fully capture the oscillations of the parachute system, it may be beneficial to establish a coordinate system at the parachute aerodynamic center. The model would then incorporate the applicable components of these equations for both the parachute and payload. The general equations of motion are completely defined as:

$$\begin{bmatrix} \frac{d}{dt}{}^{B}V_{B} \\ \frac{d}{dt}\Omega \end{bmatrix} = \begin{bmatrix} M_T'^{-1}\left\{M_{TR}'\dot{\Omega}+{}^{B}\Omega_{B}\times\left\{M_{TR}'\Omega+M_T'{}^{B}V_{B}\right\}\right\} \\ M_R'^{-1}\left\{M_{RT}'\left(\frac{d}{dt}{}^{B}V_{B}\right)+\Omega\times M_R'\Omega+M_{RT}'\left(\Omega\times{}^{B}V_{B}\right)\right\}+{}^{B}V\times A_T{}^{B}V \end{bmatrix}+\cdots$$

$$+\begin{bmatrix} M_T'^{-1} & 0 \\ 0 & M_R'^{-1} \end{bmatrix}\begin{bmatrix} \bar{q}S_oI_3 & 0 \\ 0 & \bar{q}S_od_oI_3 \end{bmatrix}\begin{bmatrix} \left\{\delta C_{F_o}+\delta C_{F_x}+\delta C_{F_{\dot{x}}}\dot{x}+\delta C_{F_\Delta}\Delta\right\} \\ \left\{\delta C_{N_o}+\delta C_{N_x}+\delta C_{N_{\dot{x}}}\dot{x}+\delta C_{N_\Delta}\Delta\right\} \end{bmatrix}+\begin{bmatrix} {}_{U}^{B}R \\ P_o{}_{U}^{B}R \end{bmatrix}\begin{bmatrix} 0 \\ 0 \\ mg \end{bmatrix}$$

where:

$$M' = \begin{bmatrix} M_T' & M_{TR}' \\ M_{RT}' & M_R' \end{bmatrix} = \begin{bmatrix} M_T + A_T & M_{TR} + A_{TR} \\ M_{RT} + A_{RT} & M_R + A_R \end{bmatrix}$$

# VIII. ANALYSIS OF EQUATIONS OF MOTIONS

## A. EQUATIONS OF MOTION EXPANSION

Expansion of the equations of motion is necessary for parameter estimation. This expansion also serves to validate the derivation of these equations against existing works in the field. First, the coordinate system axis is selected aligned with the parachute body axis but displaced from the center of gravity by a distance z. Expanding the equations of motion:

$$
\begin{aligned}
X &= (m+\alpha_{11})\dot{u} + (mz+\alpha_{15})\dot{q} + (m-\alpha_{24})pr - (m+\alpha_{22})rv + (m+\alpha_{33})qw \\
Y &= (m+\alpha_{22})\dot{v} - (mz-\alpha_{24})\dot{p} + (m+\alpha_{11})ru + (mz+\alpha_{15})qr - (m+\alpha_{33})pw \\
Z &= (m+\alpha_{33})\dot{w} - (mz+\alpha_{15})q^2 - (m+\alpha_{11})qu - (m-\alpha_{24})p^2 + (m+\alpha_{22})pv \\
L &= (I_x+\alpha_{44})\dot{p} - (mz-\alpha_{24})\dot{v} + (I_z-I_y-\alpha_{55})qr - (mz+\alpha_{15})ru - (mz-\alpha_{24})pw + (\alpha_{11}-\alpha_{33})uw \\
M &= (I_y+\alpha_{55})\dot{q} + (mz+\alpha_{15})\dot{u} + (I_x-I_z+\alpha_{44})pr - (mz+\alpha_{15})(qw-rv) - (\alpha_{11}-\alpha_{33})uw \\
N &= I_z\dot{r}
\end{aligned}
$$

These equations are validated by the work of Cockrell and Doherr[20].

Taking terms like rv, qw, etc. to be small and eliminating non-linear terms like $p^2$:

$$
\begin{aligned}
X &= (m+\alpha_{11})\dot{u} + (mz+\alpha_{15})\dot{q} \\
Y &= (m+\alpha_{22})\dot{v} - (mz-\alpha_{24})\dot{p} \\
Z &= (m+\alpha_{33})\dot{w} \\
L &= (I_x+\alpha_{44})\dot{p} - (mz-\alpha_{24})\dot{v} \\
M &= (I_y+\alpha_{55})\dot{q} + (mz+\alpha_{15})\dot{u} \\
N &= I_z\dot{r}
\end{aligned}
$$

Forming forces and moments as an initial (trim) value plus a perturbation and applying gravitational forces and moments.

$$
\begin{aligned}
X &= \Delta X - mg\sin(\theta) = (m+\alpha_{11})\dot{u} + (mz+\alpha_{15})\dot{q} \\
Y &= \Delta Y - mg\cos(\theta)\sin(\phi) = (m+\alpha_{22})\dot{v} - (mz-\alpha_{24})\dot{p}
\end{aligned}
$$

$$
\begin{aligned}
&Z = Z_0 + \Delta Z + mg\cos(\theta)\cos(\phi) = (m + \alpha_{33})\dot{w} \\
&L = \Delta L + mgz\sin(\phi) = (I_x + \alpha_{44})\dot{p} - (mz - \alpha_{24})\dot{v} \\
&M = \Delta M - mgz\sin(\theta) = (I_y + \alpha_{55})\dot{q} + (mz + \alpha_{15})\dot{u} \\
&N = \Delta N = I_z\dot{r}
\end{aligned}
$$

Subtracting initial conditions as defined as $X_0$=0, $Z_0$=-mg, Y0=0, $L_0$=0, $M_0$=0, $N_0$=0, $\theta_0$=0, $\Phi_0$=0 and applying small angle assumption (e.g. $\cos\theta \approx 1, \sin\theta \approx \theta$) two sets (Longitudinal and Lateral-Directional) of uncoupled equations are formed.

## B. LONGITUDINAL EQUATIONS

$$
\begin{aligned}
&(m + \alpha_{11})\dot{u} + (mz + \alpha_{15})\dot{q} = \Delta X - mg\theta \\
&(m + \alpha_{33})\dot{w} = \Delta Z \\
&(mz + \alpha_{15})\dot{u} + (I_y + \alpha_{55})\dot{q} = \Delta M - mgz\theta
\end{aligned}
$$

The external forces and moments are approximated with a Taylor-Series expansion:

$$\Delta X = \Delta X_u \frac{u}{W_0} + \Delta X_{\dot{u}} \frac{\dot{u}}{W_0} + \Delta X_w \frac{w}{W_0} + \Delta X_{\dot{w}} \frac{\dot{w}}{W_0} + \Delta X_q q + \Delta X_{\dot{q}} \dot{q} + \Delta X_\delta \delta$$

$$\Delta Y = \Delta Z_u \frac{u}{W_0} + \Delta Z_{\dot{u}} \frac{\dot{u}}{W_0} + \Delta Z_w \frac{w}{W_0} + \Delta Z_{\dot{w}} \frac{\dot{w}}{W_0} + \Delta Y_q q + \Delta Z_{\dot{q}} \dot{q} + \Delta Z_\delta \delta$$

$$\Delta M = \Delta M_u \frac{u}{W_0} + \Delta M_{\dot{u}} \frac{\dot{u}}{W_0} + \Delta M_w \frac{w}{W_0} + \Delta M_{\dot{w}} \frac{\dot{w}}{W_0} + \Delta M_q q + \Delta M_{\dot{q}} \dot{q} + \Delta M_\delta \delta$$

Reducing terms that have no apparent effect on forces or moments in a particular direction (e.g. $\Delta X_w w, \Delta Z_{\dot{u}}\dot{u}$) and substituting:

$$
\begin{aligned}
&W_0(m + \alpha_{11})\frac{\dot{u}}{W_0} + (mz + \alpha_{15})\dot{q} = \Delta X_u \frac{u}{W_0} + \Delta X_{\dot{u}} \frac{\dot{u}}{W_0} - mg\theta + \Delta X_\delta \delta \\
&W_0(m + \alpha_{33})\frac{\dot{w}}{W_0} = \Delta Z_w \frac{w}{W_0} + \Delta Z_{\dot{w}} \frac{\dot{w}}{W_0} + \Delta Z_q q + \Delta Z_\delta \delta
\end{aligned}
$$

$$W_0(mz+\alpha_{15})\frac{\dot{u}}{W_0}+(I_y+\alpha_{55})\dot{q}=\Delta M_u\frac{u}{W_0}+\Delta M_{\dot{u}}\frac{\dot{u}}{W_0}+\Delta M_w\frac{w}{W_0}+\Delta M_{\dot{w}}\frac{\dot{w}}{W_0}+\Delta M_q q-mgz\theta+\Delta M_\delta\delta$$

Defining the stability derivatives:

$$X_i=\frac{\Delta X_i}{W_o(m+\alpha_{11})};\quad Z_i=\frac{\Delta Z_i}{W_o(m+\alpha_{33})};\quad M_i=\frac{\Delta M_i}{W_o(I_y+\alpha_{55})}$$

where: $i=u,\dot{u},w,\dot{w}$

$$X_j=\frac{\Delta X_j}{(m+\alpha_{11})};\quad Z_j=\frac{\Delta Z_j}{(m+\alpha_{33})};\quad M_j=\frac{\Delta M_j}{(I_y+\alpha_{55})}$$

where: $j=q,\dot{q},\delta$

Establishing the coordinate system now at the center of mass of the system, substituting the stability derivatives and rearranging terms:

$$(1-X_{\dot{u}})\frac{\dot{u}}{W_0}+\frac{\alpha_{15}}{W_0(m+\alpha_{11})}\dot{q}=X_u\frac{u}{W_0}-\frac{mg\theta}{W_0(m+\alpha_{11})}+\frac{X_\delta\delta}{W_o}$$

$$(1-Z_{\dot{w}})\frac{\dot{w}}{W_0}=Z_w\frac{w}{W_0}+\frac{Z_q q}{W_0}+\frac{Z_\delta\delta}{W_0}$$

$$W_0\left(\frac{\alpha_{15}}{(I_y+\alpha_{55})}-M_{\dot{u}}\right)\frac{\dot{u}}{W_0}-W_oM_{\dot{w}}\frac{\dot{w}}{W_0}+\dot{q}=W_0M_u\frac{u}{W_0}+W_0M_w\frac{w}{W_0}+M_q q+M_\delta\delta$$

In state space form with $\dot{\theta}=q$:

$$\begin{bmatrix} (1-X_{\dot{u}}) & 0 & \frac{\alpha_{15}}{W_o(m+\alpha_{11})} & 0 \\ 0 & (1-Z_{\dot{w}}) & 0 & 0 \\ W_o\left(\frac{\alpha_{15}}{(I_y+\alpha_{55})}-M_{\dot{u}}\right) & -W_0M_{\dot{w}} & 1 & 0 \\ 0 & 0 & 0 & 1 \end{bmatrix}\begin{bmatrix} \frac{\dot{u}}{W_0} \\ \frac{\dot{w}}{W_0} \\ \dot{q} \\ \dot{\theta} \end{bmatrix}=\begin{bmatrix} X_u & 0 & 0 & \frac{-mg}{W_o(m+\alpha_{11})} \\ 0 & Z_w & \frac{Z_q}{W_o} & 0 \\ W_0M_u & W_0M_w & M_q & 0 \\ 0 & 0 & 1 & 0 \end{bmatrix}\begin{bmatrix} \frac{u}{W_0} \\ \frac{w}{W_0} \\ q \\ \theta \end{bmatrix}+\begin{bmatrix} \frac{X_\delta}{W_o} \\ \frac{Z_\delta}{W_o} \\ M_\delta \\ 0 \end{bmatrix}\delta$$

## C. LATERAL-DIRECTIONAL EQUATIONS

$$(m+\alpha_{22})\dot{u}-(mz-\alpha_{24})\dot{p}=\Delta Y-mg\phi$$
$$-(mz-\alpha_{24})\dot{v}+(I_x+\alpha_{44})\dot{p}=\Delta L+mgz\phi$$
$$I_z\dot{r}=\Delta N$$

The external forces and moments are approximated with a Taylor-Series expansion:

$$\Delta Y = \Delta Y_v \frac{v}{W_0} + \Delta Y_{\dot{v}} \frac{\dot{v}}{W_0} + \Delta Y_p p + \Delta Y_{\dot{p}} \dot{p} + \Delta Y_r r + \Delta Y_{\dot{r}} \dot{r} + \Delta Y_\delta \delta$$

$$\Delta L = \Delta L_v \frac{v}{W_0} + \Delta L_{\dot{v}} \frac{\dot{v}}{W_0} + \Delta L_p p + \Delta L_{\dot{p}} \dot{p} + \Delta L_r r + \Delta L_{\dot{r}} \dot{r} + \Delta L_\delta \delta$$

$$\Delta N = \Delta N_v \frac{v}{W_0} + \Delta N_{\dot{v}} \frac{\dot{v}}{W_0} + \Delta N_p p + \Delta N_{\dot{p}} \dot{p} + \Delta N_r r + \Delta N_{\dot{r}} \dot{r} + \Delta N_\delta \delta$$

Reducing terms that have no apparent effect on forces or moments in a particular direction (e.g. $\Delta Y_p p; \Delta N_{\dot{v}} \dot{v}$) and substituting:

$$W_o(m + \alpha_{22}) \frac{\dot{v}}{W_o} - (mz - \alpha_{24})\dot{p} = \Delta Y_v \frac{v}{W_0} + \Delta Y_{\dot{v}} \frac{\dot{v}}{W_0} + \Delta Y_r r + \Delta Y_\delta \delta - mg\phi$$

$$-W_o(mz - \alpha_{24}) \frac{\dot{v}}{W_o} + (I_x + \alpha_{44})\dot{p} = \Delta L_v \frac{v}{W_0} + \Delta L_{\dot{v}} \frac{\dot{v}}{W_0} + \Delta L_p p + \Delta L_r r + \Delta L_\delta \delta + mgz\phi$$

$$I_z \dot{r} = \Delta N_v \frac{v}{W_0} + \Delta N_p p + \Delta N_r r + \Delta N_\delta \delta$$

Defining the stability derivatives:

$$Y_i = \frac{\Delta Y_i}{W_o(m + \alpha_{22})}; \quad L_i = \frac{\Delta L_i}{W_o(I_x + \alpha_{44})}; \quad N_i = \frac{\Delta N_i}{W_o I_z}$$

where: $i = v, \dot{v}$

$$Y_i = \frac{\Delta Y_i}{(m + \alpha_{22})}; \quad L_i = \frac{\Delta L_i}{(I_x + \alpha_{44})}; \quad N_i = \frac{\Delta N_i}{I_z}$$

where: $j = p, \dot{p}, r, \dot{r}, \delta$

Establishing the coordinate system now at the center of mass of the system, substituting the stability derivatives and rearranging terms:

$$(1-Y_{\dot{v}})\frac{\dot{v}}{W_o}+\frac{\alpha_{24}}{W_o(m+\alpha_{22})}\dot{p}=Y_v\frac{v}{W_0}+\frac{Y_r}{W_0}r+\frac{Y_\delta}{W_0}\delta-\frac{mg\phi}{W_o(m+\alpha_{22})}$$

$$W_o(\frac{\alpha_{24}}{I_x+\alpha_{44}}-L_{\dot{v}})\frac{\dot{v}}{W_o}+\dot{p}=W_oL_v\frac{v}{W_0}+L_pp+L_rr+L_\delta\delta$$

$$\dot{r}=W_oN_v\frac{v}{W_0}+N_pp+N_rr+\Delta N_\delta\delta$$

In state space form with $\dot{\phi}=p$:

$$\begin{bmatrix} (1-Y_{\dot{v}}) & \dfrac{\alpha_{24}}{W_o(m+\alpha_{22})} & 0 & 0 \\ W_o(\dfrac{\alpha_{24}}{I_x+\alpha_{44}}-L_{\dot{v}}) & 1 & 0 & 0 \\ 0 & 0 & 1 & 0 \\ 0 & 0 & 0 & 1 \end{bmatrix} \begin{bmatrix} \dfrac{\dot{v}}{W_o} \\ \dot{p} \\ \dot{r} \\ \dot{\phi} \end{bmatrix} = \begin{bmatrix} Y_v & 0 & \dfrac{Y_r}{W_0} & -\dfrac{mg}{W_o(m+\alpha_{22})} \\ W_oL_v & L_p & L_r & 0 \\ W_oN_v & N_p & N_r & 0 \\ 0 & 1 & 0 & 0 \end{bmatrix} \begin{bmatrix} \dfrac{v}{W_0} \\ p \\ r \\ \phi \end{bmatrix} + \begin{bmatrix} \dfrac{Y_\delta}{W_0} \\ L_\delta \\ N_\delta \\ 0 \end{bmatrix} \delta$$

## D. SUMMARY OF EQUATIONS

In summary, two sets of independent equations have been derived for the longitudinal and the lateral-directional motion. These equations form the models to be used for parameter estimation.

Longitudinal:

$$\begin{bmatrix} 1-X_{\dot{u}} & 0 & \dfrac{\alpha_{15}}{W_o(m+\alpha_{11})} & 0 \\ 0 & 1-Z_{\dot{w}} & 0 & 0 \\ W_o\left(\dfrac{\alpha_{15}}{(I_y+\alpha_{55})}-M_{\dot{u}}\right) & -W_0M_{\dot{w}} & 1 & 0 \\ 0 & 0 & 0 & 1 \end{bmatrix} \begin{bmatrix} \dfrac{\dot{u}}{W_0} \\ \dfrac{\dot{w}}{W_0} \\ \dot{q} \\ \dot{\theta} \end{bmatrix} = \begin{bmatrix} X_u & 0 & \dfrac{X_q}{W_o} & \dfrac{-mg}{W_o(m+\alpha_{11})} \\ 0 & Z_w & \dfrac{Z_q}{W_o} & 0 \\ W_0M_u & W_0M_w & M_q & 0 \\ 0 & 0 & 1 & 0 \end{bmatrix} \begin{bmatrix} \dfrac{u}{W_0} \\ \dfrac{w}{W_0} \\ q \\ \theta \end{bmatrix} + \begin{bmatrix} \dfrac{X_\delta}{W_o} \\ \dfrac{Z_\delta}{W_o} \\ M_\delta \\ 0 \end{bmatrix} \delta$$

Lateral-Directional:

$$\begin{bmatrix} (1-Y_v) & \dfrac{\alpha_{24}}{W_o(m+\alpha_{22})} & 0 & 0 \\ W_o(\dfrac{\alpha_{24}}{I_x+\alpha_{44}}-L_{\dot{v}}) & 1 & 0 & 0 \\ 0 & 0 & 1 & 0 \\ 0 & 0 & 0 & 1 \end{bmatrix} \begin{bmatrix} \dfrac{\dot{v}}{W_o} \\ \dot{p} \\ \dot{r} \\ \dot{\phi} \end{bmatrix} = \begin{bmatrix} Y_v & \dfrac{Y_p}{W_0} & \dfrac{Y_r}{W_0} & -\dfrac{mg}{W_o(m+\alpha_{22})} \\ W_oL_v & L_p & L_r & 0 \\ W_oN_v & N_p & N_r & 0 \\ 0 & 1 & 0 & 0 \end{bmatrix} \begin{bmatrix} \dfrac{v}{W_0} \\ p \\ r \\ \phi \end{bmatrix} + \begin{bmatrix} \dfrac{Y_\delta}{W_0} \\ L_\delta \\ N_\delta \\ 0 \end{bmatrix} \delta$$

Non-dimensionalizing:

$F = \bar{q} S_o C_F$ and $M = \bar{q} S_o d_o C_M$; where: $\bar{q}$, $S_o$, and $d_o$ are the dynamic pressure, parachute reference area, and the parachute reference diameter, respectively.

Longitudinal:

$$\begin{bmatrix} 1-\frac{\bar{q}S_o}{(m+\alpha_{11})}C_{X_{\dot u}} & 0 & \frac{\alpha_{15}}{W_o(m+\alpha_{11})} & 0 \\ 0 & 1-\frac{\bar{q}S_o}{(m+\alpha_{33})}C_{Z_{\dot w}} & 0 & 0 \\ W_o\left(\frac{\alpha_{15}-\bar{q}S_o d_o C_{M_u}}{(I_y+\alpha_{55})}\right) & -\frac{W_0\bar{q}S_o d_o}{(I_y+\alpha_{55})}C_{M_{\dot w}} & 1 & 0 \\ 0 & 0 & 0 & 1 \end{bmatrix} \begin{bmatrix} \frac{\dot u}{W_0} \\ \frac{\dot w}{W_0} \\ \dot q \\ \dot\theta \end{bmatrix} = \cdots$$

$$= \begin{bmatrix} \frac{\bar{q}S_o}{(m+\alpha_{11})} & 0 & 0 & 0 \\ 0 & \frac{\bar{q}S_o}{(m+\alpha_{33})} & 0 & 0 \\ 0 & 0 & \frac{\bar{q}S_o d_o}{(I_y+\alpha_{55})} & 0 \\ 0 & 0 & 0 & 1 \end{bmatrix} \left\{ \begin{bmatrix} C_{X_u} & 0 & 0 & \frac{-mg}{\bar{q}S_o W_o} \\ 0 & C_{Z_w} & \left(\frac{d_o}{2W_o}\right)\frac{C_{Z_q}}{W_o} & 0 \\ W_0 C_{M_u} & W_0 C_{M_w} & \left(\frac{d_o}{2W_o}\right)C_{M_q} & 0 \\ 0 & 0 & 1 & 0 \end{bmatrix} \begin{bmatrix} \frac{u}{W_0} \\ \frac{w}{W_0} \\ q \\ \theta \end{bmatrix} + \begin{bmatrix} \frac{C_{X\delta}}{W_o} \\ \frac{C_{Z\delta}}{W_o} \\ C_{M\delta} \\ 0 \end{bmatrix} \delta \right\}$$

Lateral-Directional:

$$\begin{bmatrix} \left(1-\frac{\bar{q}S_o}{(m+\alpha_{22})}C_{Y_{\dot v}}\right) & \frac{\alpha_{24}}{\bar{q}S_o W_o} & 0 & 0 \\ W_o\left(\frac{\alpha_{24}-\bar{q}S_o d_o C_{L_{\dot v}}}{I_x+\alpha_{44}}\right) & 1 & 0 & 0 \\ 0 & 0 & 1 & 0 \\ 0 & 0 & 0 & 1 \end{bmatrix} \begin{bmatrix} \frac{\dot v}{W_o} \\ \dot p \\ \dot r \\ \dot\phi \end{bmatrix} = \cdots$$

$$= \begin{bmatrix} \frac{\bar{q}S_o}{(m+\alpha_{22})} & 0 & 0 & 0 \\ 0 & \frac{\bar{q}S_o d_o}{(I_x+\alpha_{44})} & 0 & 0 \\ 0 & 0 & \frac{\bar{q}S_o d_o}{I_z} & 0 \\ 0 & 0 & 0 & 1 \end{bmatrix} \left\{ \begin{bmatrix} C_{Y_v} & \left(\frac{d_o}{2W_o}\right)\frac{C_{Y_p}}{W_0} & \left(\frac{d_o}{2W_o}\right)\frac{C_{Y_r}}{W_0} & -\frac{mg}{\bar{q}S_o W_o} \\ W_o C_{L_v} & \left(\frac{d_o}{2W_o}\right)C_{L_p} & \left(\frac{d_o}{2W_o}\right)C_{L_r} & 0 \\ W_o C_{N_v} & \left(\frac{d_o}{2W_o}\right)C_{N_p} & \left(\frac{d_o}{2W_o}\right)C_{N_r} & 0 \\ 0 & 1 & 0 & 0 \end{bmatrix} \begin{bmatrix} \frac{v}{W_0} \\ p \\ r \\ \phi \end{bmatrix} + \begin{bmatrix} \frac{C_{Y\delta}}{W_0} \\ C_{L\delta} \\ C_{N\delta} \\ 0 \end{bmatrix} \delta \right\}$$

Which are in the form $I_n \dot x = A_n x + B_n u$; define: $A = I_n^{-1} A_n$ and $B = I_n^{-1} B_n$ to get in the form: $\dot x = Ax + Bu$

# IX. PARAMETER ESTIMATION

## A. OVERVIEW

Parameter estimation is the process of determining aerodynamic stability and control derivatives from flight test data. A large number of techniques have been employed for parameter estimation in aircraft research. This study investigated the application of Maximum Likelihood Estimation methods described by Richard Maine and Kenneth Iliff of NASA[21].

Wind tunnel data on the stability and control derivatives for this system are not available. This effort encompassed an initial start at tackling this problem. Parachute aerodynamics are truly non-linear and significantly coupled across axes. The maximum likelihood techniques implement linear models with no cross-coupling.

## B. MODIFIED MAXIMUM LIKELIHOOD ESTIMATION

Once the system is modeled, the system's equations of motion, expressed in state space form, are utilized to model the dynamic response due to a simulated input with an initial "guess" of the aerodynamic parameters. The modeled output is compared to the flight test results; the unknown parameters are adjusted as to minimize the output error. Detailed descriptions of the **MMLE3** algorithm as implemented in the MATLAB® are provided in the user's guide[22]. A block diagram of this concept is provided in Figure 44.

A coning motion characterizes the dynamics of a flat circular parachute. This motion will likely not be identified during the estimation process due to the averaging

---

® MATLAB is a registered trademark of Mathworks, Inc., Natick, MA techniques implemented. Karl Doherr suggests[23] the addition of noise to the average normal force or pitching moment coefficients to compensate for this.

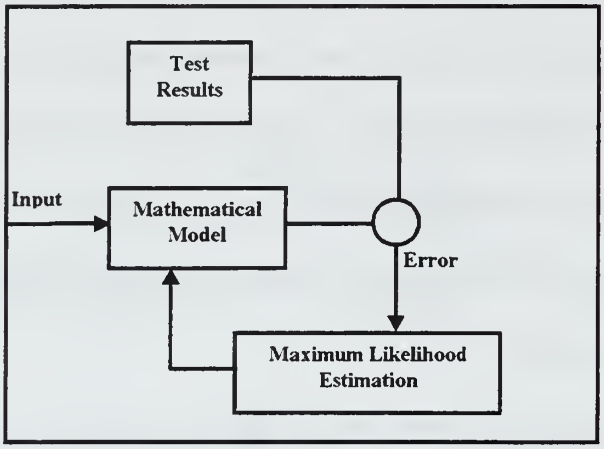

Figure 44. Parameter Estimation Concept

## C. RESULTS

The **MMLE3** algorithm as implemented in MATLAB386 (an obsolete version of MATLAB®) was successfully run for several test cases. First, **MATLAB386** was hosted on a Windows 95® on a PC. The program needed to be run in the DOS mode and could not be run in a Windows shell. In addition, several memory management conflicts had to be resolved before being able to run the program. After successfully launching the program, the Naval Postgraduate School's (NPS) **MMLE3** implementation for parameter estimation was executed. Several test cases were executed including the T37 and F14 aircraft simulations. In all cases, duplicate results to those obtained by Graham[24] were obtained.

---

® Registered Trademark of the Microsoft Corporation

The NPS implementation was then modified to incorporate the equations of motion for the parachute (identified above). Simulated data (using estimates for the stability derivatives) were generated and qualitatively observed to have the same general character of the flight test data. However when utilizing the simulated data to estimate the applicable stability derivatives, the algorithms failed to predict the stability derivatives utilized to generate the simulated data. The program's execution would halt after receiving errors indicating the **HES** matrix was near singular. This matrix rotates and scales the gradient to provide a single step convergence for the quadratic cost function.[25] Initially, it was believed that this error resulted from the model being overparameterized. After significant investigation and numerous trials using simulated and flight-test data, no results could be obtained using these algorithms.

The implementation of the F-14 models was then analyzed again. The F-14 equations of motion were utilized and the F-14 parameters were modified to reflect a slower aircraft (approximately the speed of the descent rate of the parachute). Simulated data were successfully generated but when applying the **MMLE3** algorithm, the HES matrix again went singular. It was concluded that the **MMLE3** algorithm, as implemented in **MATLAB386**, could not provide estimates of parachute stability derivatives. There appears to be a numerical sensitivity in the algorithms to the relatively low numbers representing the parachute system. Further work may result in the successful application of this algorithm to the parachute problem. However, this is beyond the scope of this study. It is also recognized that the utility of results, should they be achieved, may not be sufficient. This implementation requires linearization of the equations of motion. The parachute dynamic behavior is clearly not linear. In addition, other research[26] has demonstrated that the stability derivatives themselves are functions of angle of attack, and may even vary with time. Figure 45 shows how the drag, lift, and moment coefficients change for a typical flat-circular parachute.

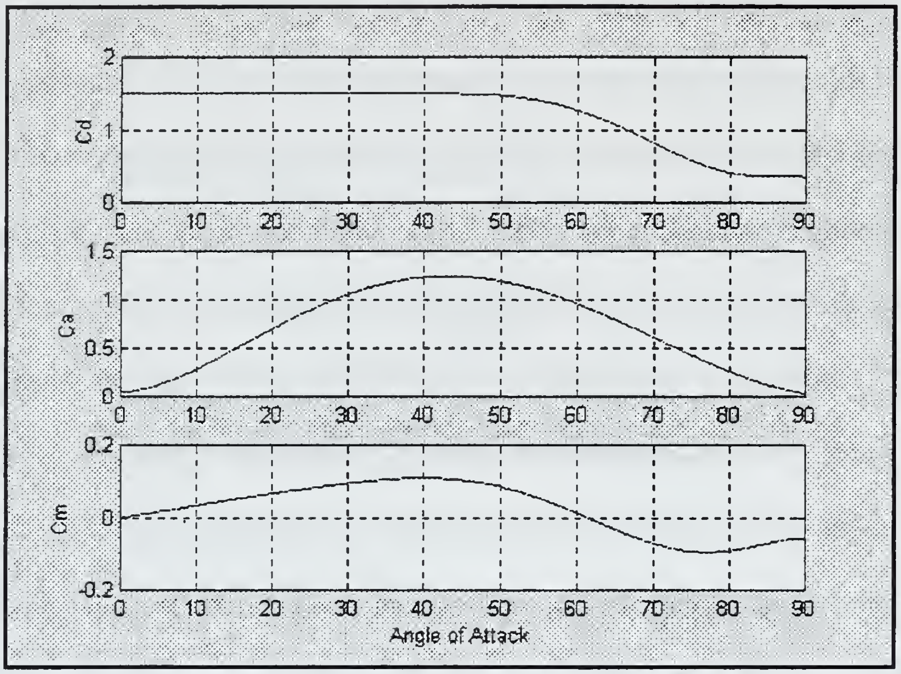

Figure 45. Flat Circular Aerodynamic Coefficients

# X. SYSTEM MODEL

Without successful MMLE results and in the absence of sufficient wind tunnel data for the C-9 parachute, a point-mass system was assumed with the only forces on the system being drag and weight. The applicable equations of motion are:

*(50)* $$X = (m+\alpha_{11})\dot{u} = -D\cos\gamma\cos\psi$$

*(51)* $$Y = (m+\alpha_{22})\dot{v} = -D\cos\gamma\sin\psi$$

*(52)* $$Z = (m+\alpha_{33})\dot{w} = -D\sin\gamma + W$$

where: W is the calibration system weight, $\gamma$ and $\psi$ are the flight path angle and yaw angle respectfully. $D = \bar{q}C_D S$ D is drag.

The reference angles are

*(53)* $$\sin\gamma = \frac{w}{V_T};\quad \cos\gamma = \frac{\sqrt{V_T^2 - w^2}}{V_T};\quad \sin\psi = \frac{v}{\sqrt{V_T^2 - w^2}};\quad \cos\psi = \frac{u}{\sqrt{V_T^2 - w^2}}$$

Substituting, rearranging terms, and putting in state space form:

*(54)* $$\begin{bmatrix}\dot{u}\\ \dot{v}\\ \dot{w}\end{bmatrix} = \begin{bmatrix} m+\alpha_{11} & 0 & 0 \\ 0 & m+\alpha_{22} & 0 \\ 0 & 0 & m+\alpha_{33}\end{bmatrix}^{-1} \left\{ \frac{-qC_D S}{V_T}\begin{bmatrix}u\\ v\\ w\end{bmatrix} + \begin{bmatrix}0\\ 0\\ W\end{bmatrix}\right\}$$

*(55)* *where: $\alpha_{xx}$ are the apparent mass terms, here assumed to be constant.*

Noting that:

$V_G = V_A + V_W$; where VG = ground velocity, VA=velocity relative to the local air mass (airspeed), VW=wind velocity. Assumes no rotation between the fixed earth reference and the system's body axis.

$$\dot{V}_G = \dot{V}_A + \dot{V}_W$$

Equation (54) presents the equation for $\dot{V}_A$. Substituting, the EOM for estimating ground speed results.

$$(56)\qquad \dot{V}_G = \begin{bmatrix} \dot{u} \\ \dot{v} \\ \dot{w} \end{bmatrix}_G = \begin{bmatrix} m+\alpha_{11} & 0 & 0 \\ 0 & m+\alpha_{22} & 0 \\ 0 & 0 & m+\alpha_{33} \end{bmatrix}^{-1} \left\{ \frac{-qC_D S}{V_T} \begin{bmatrix} u \\ v \\ w \end{bmatrix} + \begin{bmatrix} 0 \\ 0 \\ W \end{bmatrix} \right\} + \dot{V}_W$$

Equation (56) can be solved numerically to estimate the system response. To estimate heading, a constant rate of rotation was assumed. The flight test results for the C-9 parachute showed significant rotations and changes in rotation rate with control activation. Flight testing of the larger G-12 parachute showed a mean rotation rate of approximately 1.8 degrees per second. A standard deviation of 1.0 degree per second was assumed based on qualitative observations during flight test. An insufficient sample size was available to accurately determine a standard deviation for rotation rate. A normal random number generator at the start of each simulation determines the rotation rate. That rate is then integrated to provide heading. This model was incorporated into Simulink®. Multiple wind profiles were incorporated into the simulation using a lookup table based on the current system altitude. The equations of motion are contained in a MATLAB® function block which calls a script file titled DOF3. This script file (Appendix E) also incorporates the parachute system parameters and apparent mass terms.

Figure 47 presents the measured velocity data from flight test as compared to the modeled velocity data for an uncontrolled drop. The 'noise' in the measured data results from the velocity being measured at the payload which is experiencing significant oscillations. Since the point mass model does not incorporate these oscillations, no 'noise' is apparent in the modeled data. As is demonstrated in the graph, the velocity data agree very well for this uncontrolled condition. For this run, atmospheric density measurements were not available. Therefore, the modeled descent rate does not match precisely with the measured descent rate but the differences appear negligible.

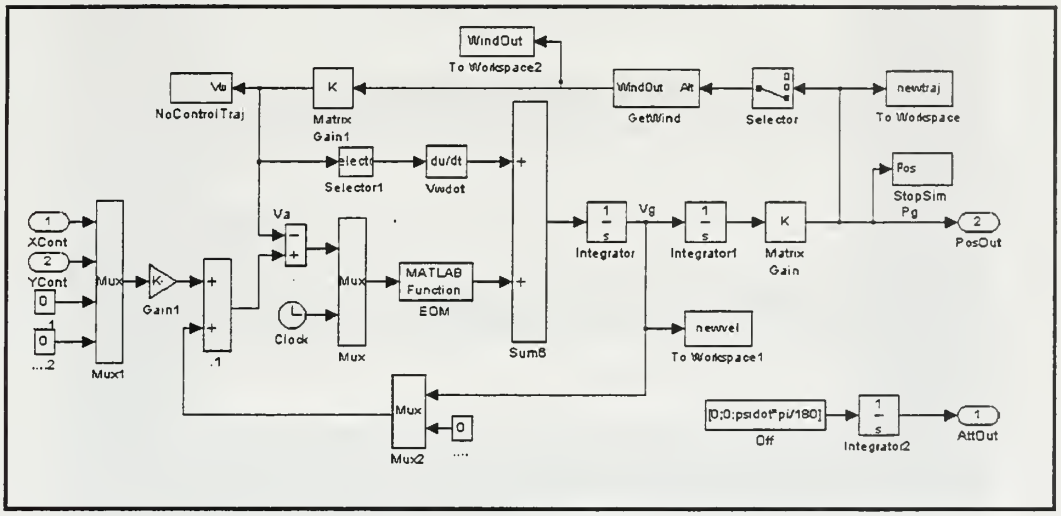

Figure 46. Simulink Realization of System Model

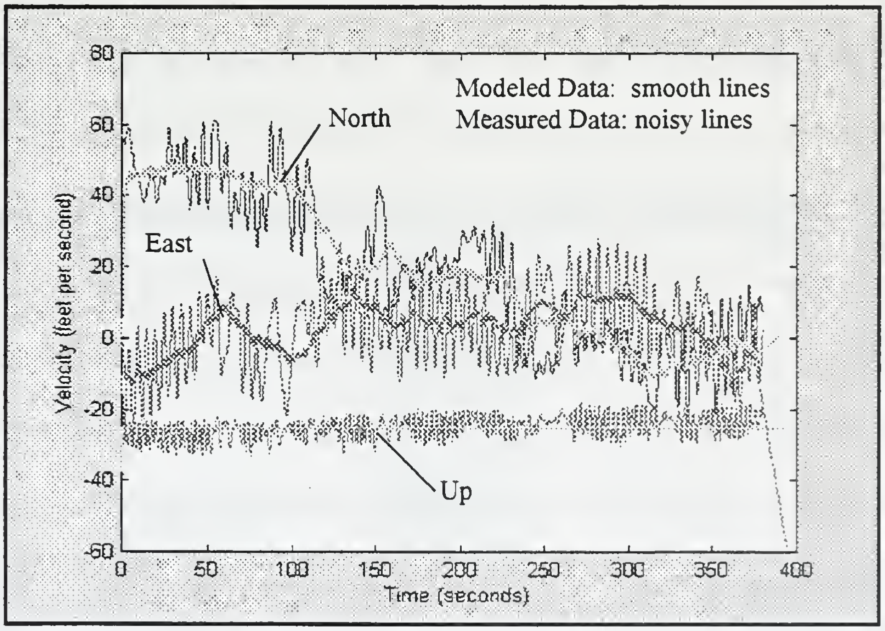

Figure 47. Measured vs. Modeled Velocity

Initializing the model at the start position of the flight test, the model's ability to estimate position of the system was evaluated. Figure 48 shows the model very accurately predicts the flight path of the system under the given wind conditions.

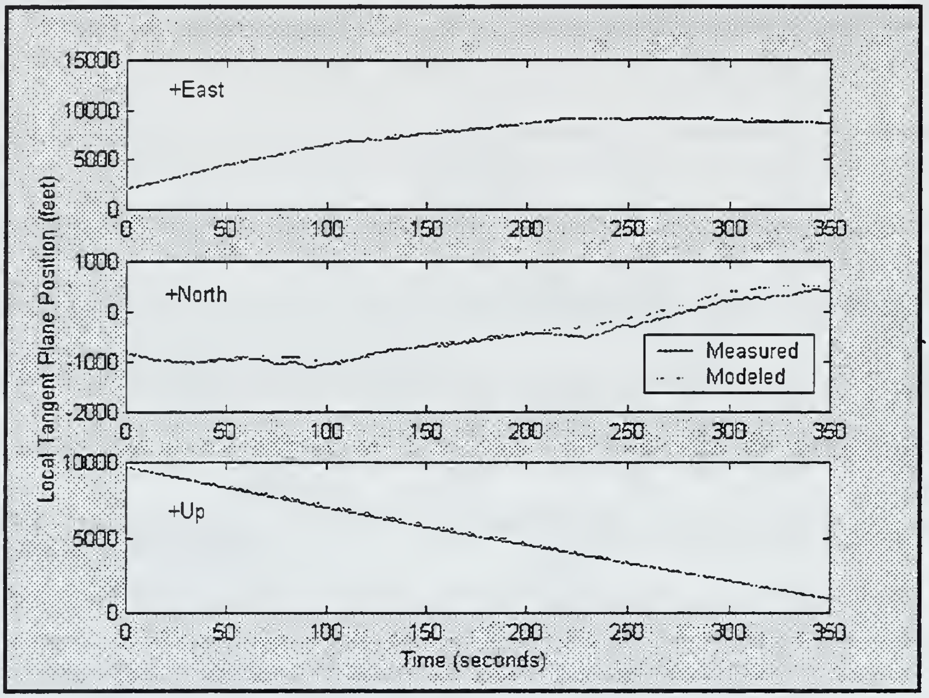

Figure 48. Measured vs. Modeled Position

The response of the system to a control input was identified during flight test. For a single control input, a glide ratio of 0.4 to 0.5 was found with a time constant of about 4-5 seconds. The glide ratio was decreased to approximately 0.2 when two simultaneous controls were actuated. This response was incorporated into the system model by adding the resultant horizontal velocity components. Recall the flight test results demonstrated an apparent decrease in descent rate upon control activation resulting from the decreased oscillation angles. This reduced vertical velocity is an apparent benefit to the system allowing more time in the air to be controlled to the desired impact point. However, the implementation of the point mass model does not predict oscillation angle. Therefore, no vertical velocity change was incorporated into the model on control input. The modeled response to double and single control inputs is illustrated in Figure 49.

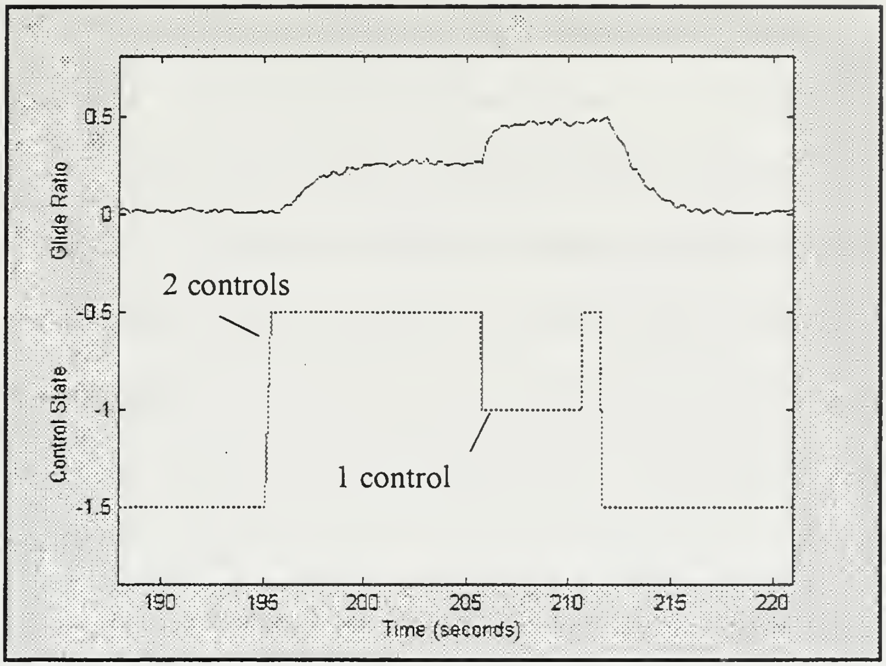

Figure 49. Modeled Control Input Response

As observed in flight test (Figure 50), a glide ratio of approximately 0.2 for two simultaneous control inputs and 0.4 to 0.5 for a single control input result. A time constant of approximately 3 to 5 seconds is observed.

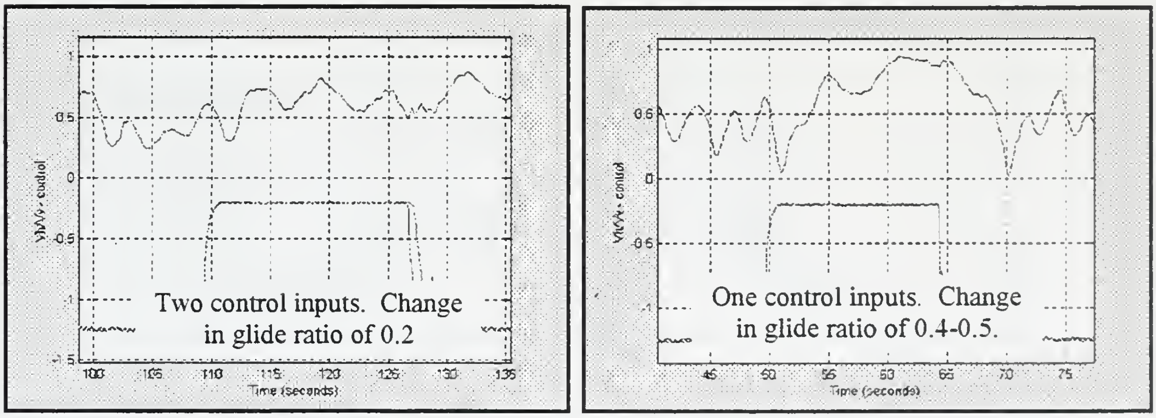

Figure 50. Measured Control Input Response (Two Controls and Single Control)

The modeled data closely represents the measured system response.

# XI. SIMULATION

## A. OVERVIEW

The individual modeling efforts have been presented. Three major components are included in the overall system model: 1) Dynamics Model, 2) Sensor Model, and 3) Control System Model. In addition, the reference trajectory generator was implemented using the same equations of motion utilized in the dynamics model. This trajectory generator has the additional benefit of being a tool for calculating the Computed Air Release Point. Figure 51 provides a block diagram of the overall control concept. This control methodology was implemented in Simulink® (Appendix C) and integrated with the sensor models and dynamics model. Single simulation runs can be executed. It is desirable to assess to obtain a statistical base for many trials.

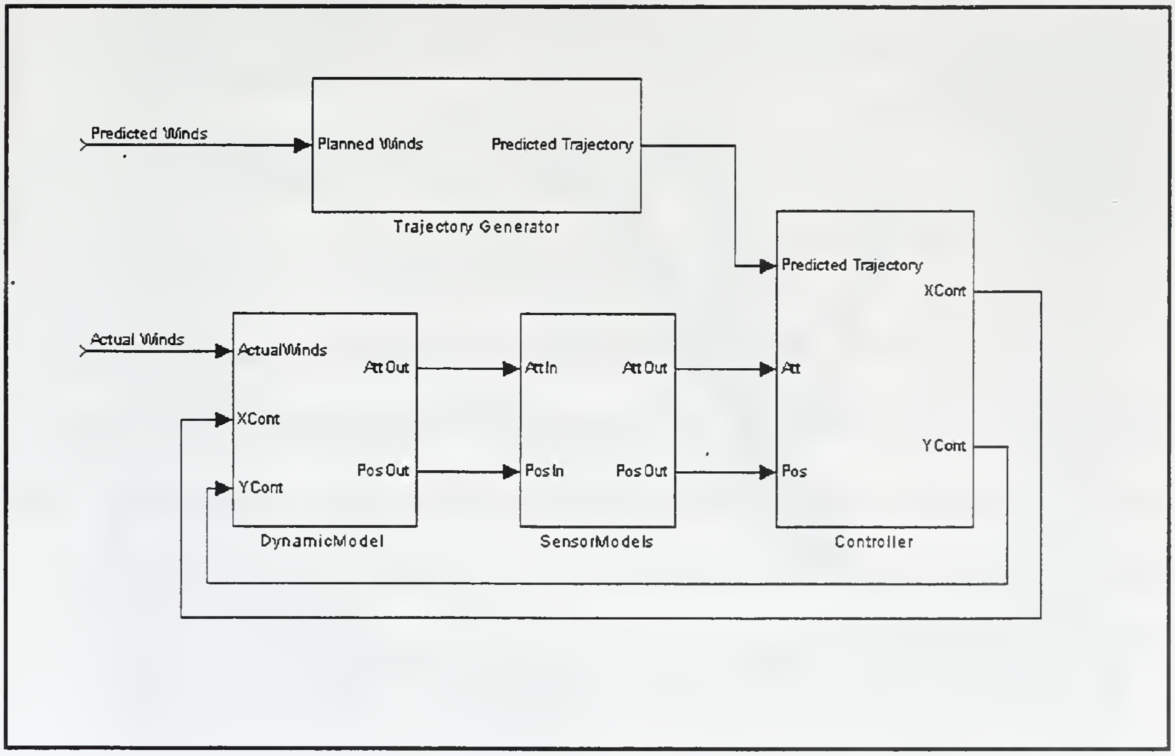

Figure 51. Control Concept

## B. INITIALIZATION

To obtain the statistical base desired, an initialization file was created where numerous parameters utilized in the simulation were selected randomly. The initialization file then provided the parameters required for numerous simulations. A MATLAB® script file called INIT was created to select the desired parameters. When executed, the user is prompted to input the number of simulation runs desired and to select the "actual winds" to be used. The program then randomly selects the parameters identified in Table 4.

| Parameter | Method | Possible Results |
|---|---|---|
| **Planned Wind File** | Uniform Distribution | any valid wind file from the same day as the selected "actual winds" |
| **SAON**<br>selects which sensor model is used | Uniform Distribution | YES/NO |
| **CARP Offset**<br>distance from desired release point | Uniform Distribution | 0, 1000, 2000, 3000 feet each axis |
| **PSIDOT**<br>parachute turn rate | Normal Distribution | Mean: 1.89 degrees<br>STDEV: 1 degree |
| **RELEASEALT**<br>altitude at parachute release | Based on maximum height of actual wind file | 9500 feet, 20000 feet |
| **CompassBias** | Uniform Distribution | ± 2 degrees |
| **SASEED**<br>seeds used in GPS error models | Uniform Distribution | 0 to 9999 |

Table 4. Simulation Parameter

Another script file, titled CARLO is then executed. This execution file imports the parameters in the initialization file, executes the simulation CARP to calculate the predicted trajectory and the simulation C9POINTMASS to perform the simulation. The results are then stored in individual data files. Summary statistics are calculated by a script titled MONTE called from within the CARLO routine and stored in a text file.

## C. RESULTS

Appendix A contains the initialized states and results for each of the 600 simulations conducted. These data include the achieved accuracy improvement of the controlled system over that of an uncontrolled system. The simulations produced excellent results with an accuracy of 210 feet (64 meters), Circular Error Probable (CEP). The total average horizontal error was 309 feet (94 meters) with an average of 15 control inputs being required. The maximum number of control inputs for all 600 simulations was 33. Appendix B presents sample plots from several simulations.

Figures 52 through 54 present three dimensional plots of several of the simulation results. These figures illustrate the initial release points and flight paths to impact with the center of the coordinate system (0,0) being the planned impact point. With the exception of a few trials, the system guided to the desired target.

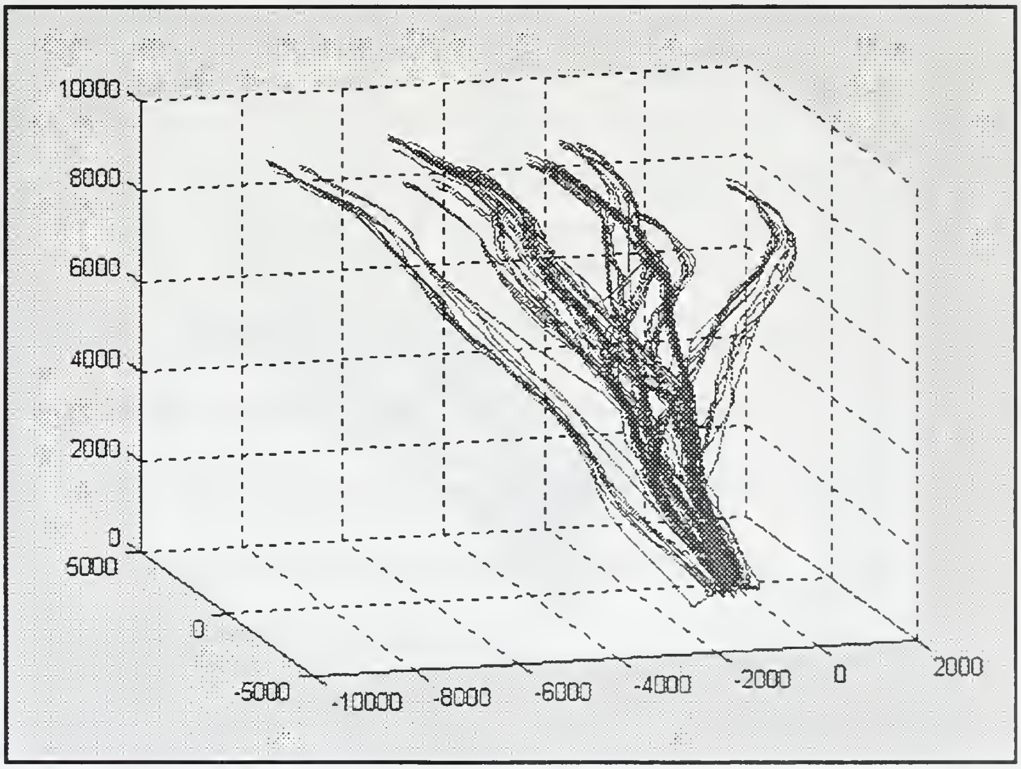

Figure 52. Simulation Results, 10000 foot Release, 100 trials

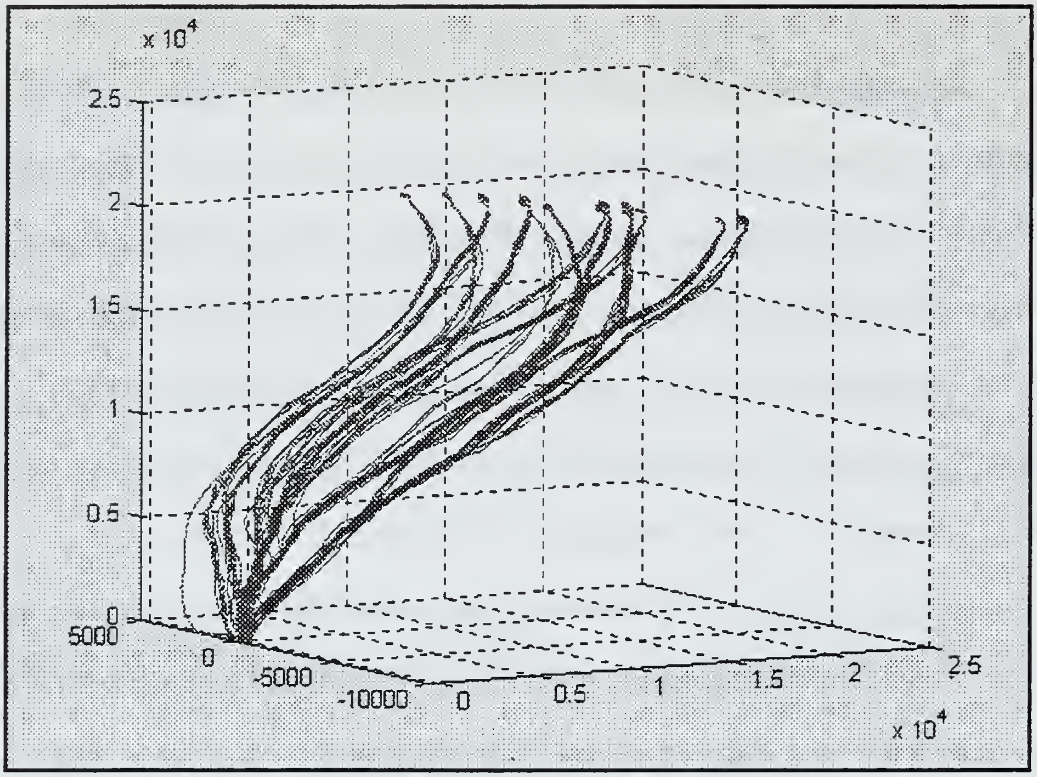

Figure 53. Simulation Results, 20000 foot Release, 100 trials

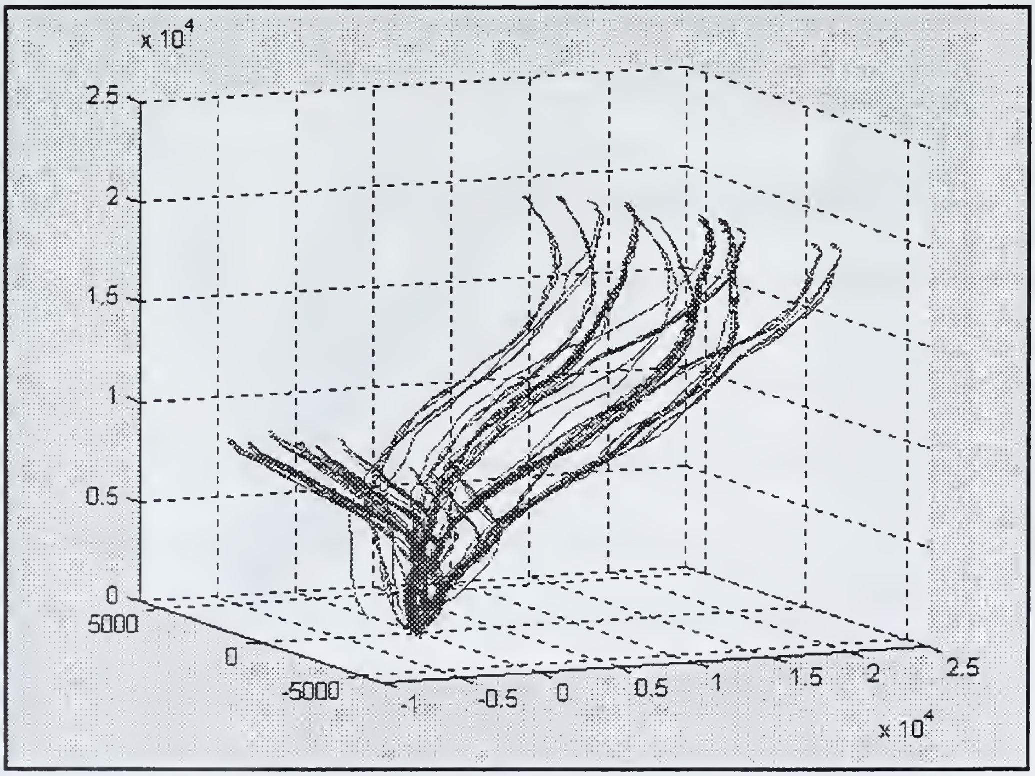

Figure 54. Simulation Results, 50: 10000 foot Release, 50: 20000 foot Release

To assess each of the randomized variables, the statistics were summarized by the time from the predicted winds to the actual winds, the GPS errors introduced (state of selective availability (ON = included)), and the distance from the predicted CARP to simulated release point. Table 5 presents these results.

| Release Alt | Age of | SA | Number | Mean Horizontal Error (feet) | | Control Inputs | | |
|---|---|---|---|---|---|---|---|---|
| (feet) | Wind (hrs) | On/Off | Of Runs | Uncontrolled | Controlled | Average | Max | STDEV |
| 9500 | 1 | 0 | 75 | 1935 | 159 | 14 | 3 | 22 |
| 9500 | 1 | 1 | 91 | 2323 | 213 | 14 | 3 | 21 |
| 9500 | 2 | 0 | 52 | 2169 | 157 | 13 | 3 | 21 |
| 9500 | 2 | 1 | 50 | 2232 | 192 | 13 | 3 | 18 |
| 9500 | 3 | 0 | 28 | 2355 | 56 | 15 | 3 | 20 |
| 9500 | 3 | 1 | 28 | 3340 | 136 | 16 | 3 | 22 |
| 9500 | 5 | 0 | 38 | 3188 | 401 | 12 | 5 | 20 |
| 9500 | 5 | 1 | 51 | 3412 | 448 | 11 | 5 | 20 |
| 9500 | 6 | 0 | 14 | 3351 | 427 | 10 | 3 | 17 |
| 9500 | 6 | 1 | 22 | 3816 | 573 | 10 | 4 | 15 |
| 9500 | 7 | 0 | 29 | 4044 | 818 | 9 | 3 | 13 |
| 9500 | 7 | 1 | 22 | 4326 | 886 | 10 | 4 | 16 |
| 20000 | 3 | 0 | 16 | 3501 | 82 | 24 | 4 | 30 |
| 20000 | 3 | 1 | 15 | 3372 | 173 | 22 | 5 | 31 |
| 20000 | 5 | 0 | 11 | 3179 | 312 | 19 | 5 | 28 |
| 20000 | 5 | 1 | 10 | 2923 | 352 | 21 | 4 | 25 |
| 20000 | 7 | 0 | 15 | 5886 | 138 | 22 | 6 | 33 |
| 20000 | 7 | 1 | 13 | 5999 | 208 | 23 | 6 | 33 |
| 20000 | 9 | 0 | 12 | 7492 | 828 | 13 | 5 | 19 |
| 20000 | 9 | 1 | 8 | 8081 | 701 | 18 | 5 | 24 |

Table 5. Simulation Results

The predominant factor influencing accuracy of the control system was the time from the predicted winds used to establish the planned trajectory to that of the time of the simulated airdrop. Figure 55 plots the resultant accuracy with the "age" of wind and shows that the impact accuracy is greatly reduced when the actual winds are within approximately three hours of the predicted winds.

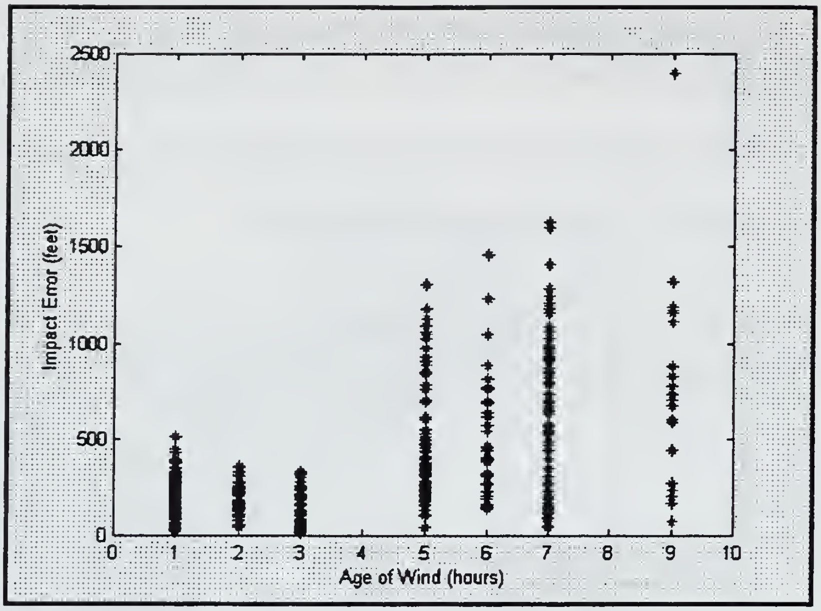

Figure 55. Influence of Age of Wind on Accuracy

Figure 56 presents an example of the magnitude of wind error for the three and five hour old winds. For the first set of winds (three hours), the actual winds closely match those of the predicted winds (within 15 feet per second). The second example (five hours) shows differences in wind speed up to 30-40 feet per second with changes in significant changes in direction below 2,000 feet in altitude. The system simply does not have enough drive to overcome differences of this magnitude between the planned winds and the actual winds.

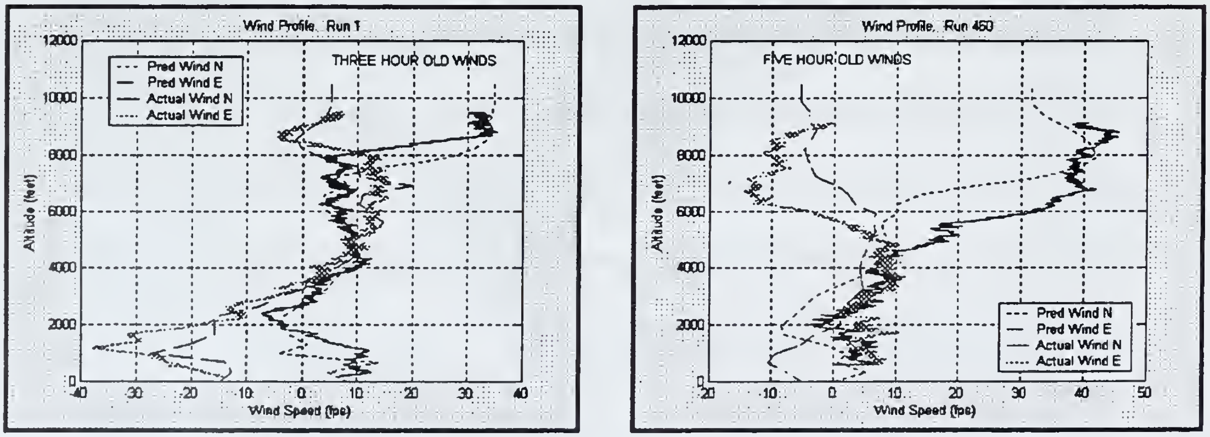

Figure 56. Wind Comparison

The effects of GPS navigation errors are not as apparent as that of age of wind. Figure 57 presents the accuracy with the status of GPS errors (Selective Availability). This plot shows no direct correlation between the state of GPS errors and the resultant impact accuracy.

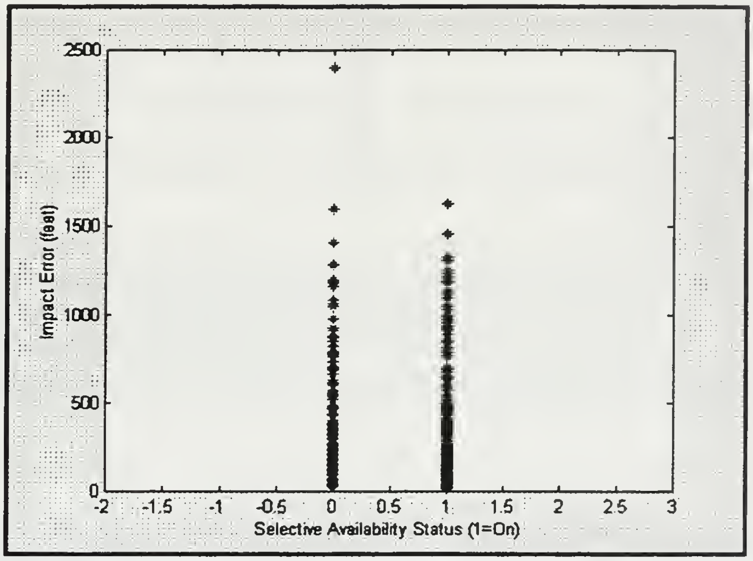

Figure 57. Influence of Selective Availability Errors on System Accuracy

Evaluating the trials that had impact errors less than 100 feet, a slight correlation is observed between Selective Availability status and impact errors. For SA Off trials, the resultant impact errors had a smaller variance than that for SA On (Figure 58). This shows that the GPS navigation errors do contribute to the overall accuracy of the AGAS system but do not have the same degree of impact as the age of wind data.

The effect of the magnitude of the offset of the actual release position from that of the planned release point also does not show a direct correlation with the magnitude of the impact accuracy (Figures 58 and 59).

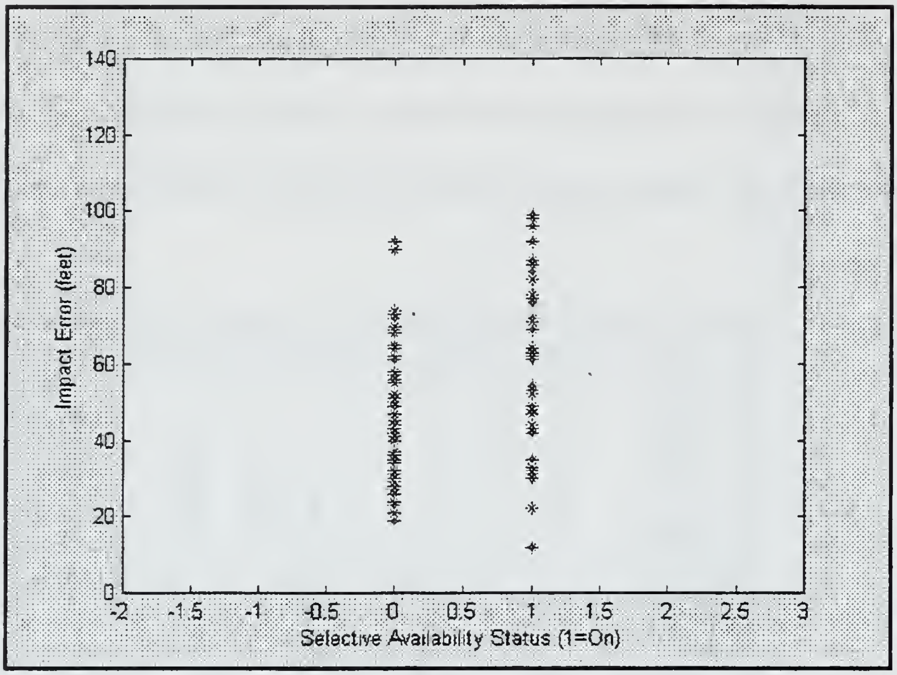

Figure 58. Influence of Selective Availability Errors on System Accuracy

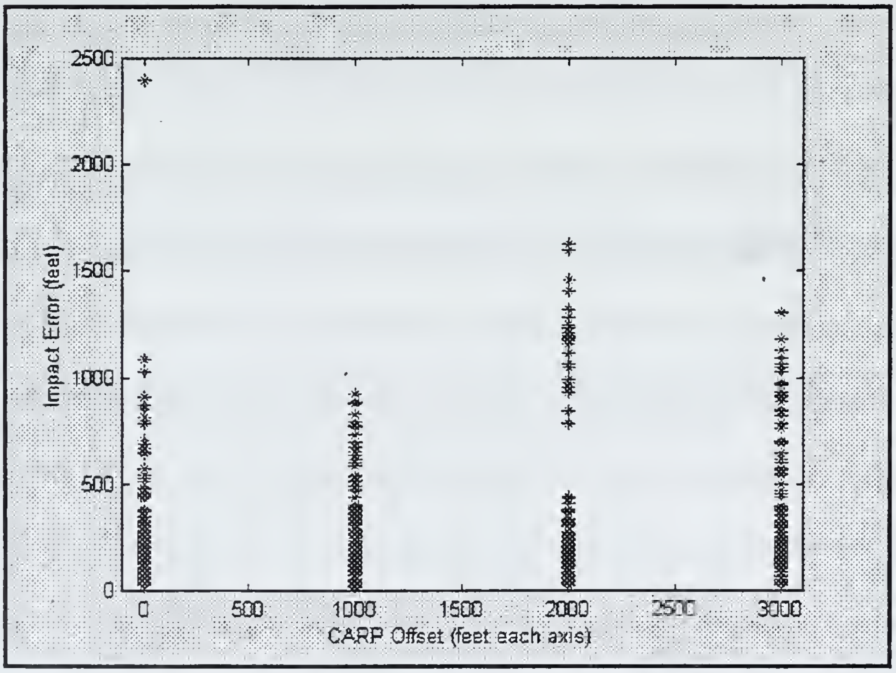

Figure 59. Influence of CARP Errors on System Accuracy

# XII. CONCLUSIONS AND RECOMMENDATIONS

## A. CONCLUSIONS

This study demonstrated that the AGAS concept is capable of providing a cost effective option for precision airdrop. Simulations demonstrate that accuracies of 210 feet (64 meters), Circular Error Probable (CEP), can be achieved. The development is warranted in going into the next stage of development. Additional efforts are needed to optimize the control system in an effort to further reduce the amount of stored gas required on the operational system.

The flight test program provided adequate flight dynamic data for the AGAS system. The instrumentation system developed for this program proved invaluable. The wind measurement techniques employed by use of a "calibration" parachute system provided the best possible wind measurement system for this application. Use of the measured GPS ground track velocities as the wind estimate was validated to provide sufficient wind measurements.

The MMLE3 parameter estimation algorithms as implemented in MATLAB386 are not sufficient for predicting the stability derivatives for this parachute. A numerical sensitivity to the magnitude of the particular parameters is suspected to be the cause. It is unlikely that these techniques, had they provided a solution, would have produced a reliable solution due to the non-linearity of the aerodynamics of a parachute system.

An efficient Monte-Carlo type simulation was developed using a point mass model for parachute dynamics, sensor models for GPS and heading information, and a Bang-Bang type control system.

The point mass concept for system modeling is adequate for this evaluation. The position and velocity results from the model matched well with the measured flight test results under the same wind conditions. However, to optimize the control system, a full six degree of freedom model is likely required to capture the proper heading response. A complete set of general 6-DOF equations of motion were developed and presented herein. However, additional work is needed to either estimate the stability derivatives for the parachute system or develop a physics-based aerodynamic model such as that proposed by Colin Tory.[26]

Six hundred simulations were conducted with randomly selected initialization parameters. These results demonstrated that the Affordable Guided Airdrop System, as described herein, shows strong potential of providing a low-cost alternative for precision airdrop. Three critical factors will drive the final design of the AGAS. First, the accuracy of the estimated winds when determining the planned trajectory is the dominant factor in the accuracy of the AGAS concept. Winds of up to 6 hours old (as compared to the 'actual' winds used in the simulation) resulted in large horizontal errors from the desired impact points. Secondly, the rotation rate of the parachute system is important. Rotation rates with a mean of 1.89 degrees per second and a standard deviation of 1 degree per second allowed effective control. If the rotation rates of the production system are increased from that, sufficient control may not be possible. Finally, the number of control inputs required to achieve the desired accuracy is marginal under the current control concept. However, no attempts were made to optimize the control algorithms for minimum fuel usage.

## B. RECOMMENDATIONS

This study demonstrated the feasibility of the AGAS concept to provide a low cost alternative for precision airdrop. However, the success of the final design rides on the three critical factors presented above. Therefore, the following recommendations are offered for follow-on work:

1. Complete the incorporation of 6-DOF equations of motion. Nonlinear parameter estimation techniques would need to be investigated or a physics-based approach would be needed.

2. Fully characterize the performance of the AGAS concept using the G-12 and/or G-11 parachute systems. The remote controlled activation technique used on the C-9 test program should be applied to the G-12 system as soon as G-12 actuators are available.

3. Investigate optimizing the control algorithms for minimum fuel usage. The current methodology provides minimum horizontal errors without regard to fuel consumption. The fuel consumption for these algorithms is marginal. A technique for evaluating multiple control algorithms is the application of a ground based guidance computer. The navigation data from the system could be downlinked via radio modem to the guidance computer, the control algorithms could determine the desired activation of the actuator, and these control commands could be uplinked to the test item. Figure 60 illustrates this concept.

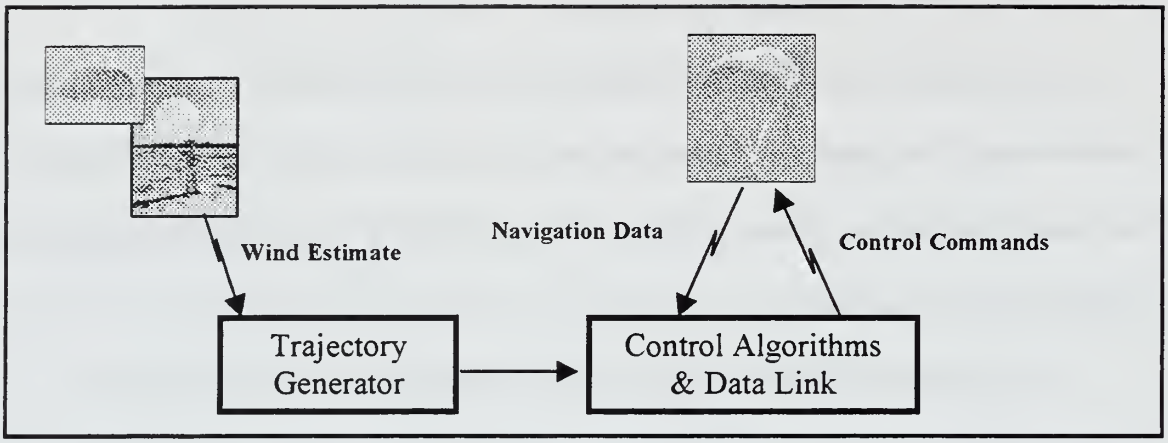

Figure 60. Autonomous Guidance Test Concept

# REFERENCES

---

[1] "Summary Report: New World Vistas, Air and Space Power for the 21st Century," United States Air Force Science Advisory Board, 1997.

[2] G. Brown, R. Haggard, R. Almassy, R. Benney, S. Dellicker, "The Affordable Guided Airdrop System," AIAA 99-1742, 15th CAES/AIAA Aerodynamic Decelerator Systems Technology Conference, June 1999.

[3] R. Benney, G. Brown, K. Stein, "A New Pneumatic Actuator: Its Use in Airdrop Applications", AIAA 99-1719, 15th CAES/AIAA Aerodynamic Decelerator Systems Technology Conference, June 1999.

[4] Irving H. Shames, Engineering Mechanics, 3rd Edition, Prentice Hall, Inc., New Jersey, 1980.

[5] Vertigo, Incorporated, "Test Report: BZA Parachute Ground Effects Summary", 02 October 1997.

[6] Hock, T. F. and J. L. Franklin, 1999: "The NCAR GPS Dropwindsonde", Bulletin American Meteorological Society, Vol. 80, Number 3, 407-420.

[7] T. Yavus and D.J. Cockrell, "Experimental Determination of Parachute Apparent Mass and Its Significance in Predicting Dynamic Stability", AIAA, No. 81-1920.

[8] M.S. Braasch, "A Signal Model for GPS", Journal of The Institute of Navigation, Vol. 37, No. 4, Winter 1990-1991.

[9] I. Kaminer, "Lecture Notes, AA3276 Introduction to Avionics", Naval Postgraduate School, 1997.

[10] System Identification Toolbox User's Manual, The Mathworks, Incorporated, 1997.

[11] Final Report: Development and Demonstration of a Ram-Air Parafoil Precision Guided Airdrop System, Volume 3, Draper Laboratory under Army Contract DAAK60-94-C-0041, October 1996.

[12] I. Kaminer, "Lecture Notes, AA4276: Avionics Systems Design", Naval Postgraduate School, 1998.

[13] Carlos J. Silvestre and Antonio M. Pascoal, "Modeling of an Autonomous Underwater Vehicle", University of Lisbon, January 22, 1992.

---

[14] Sir Horace Lamb, Hydrodynamics 6th Edition, Cambridge University Press, Reprinted by Dover Publications, New York, 1945.

[15] D.J. Cockrell and K.F. Doherr, "Preliminary Consideration of Parameter Identification Analysis from Parachute Aerodynamic Flight Test Data", AIAA Paper 81-1940.

[16] T. Yavus and D.J. Cockrell, "Experimental Determination of Parachute Apparent Mass and Its Significance in Predicting Dynamic Stability", AIAA Paper 81-1920.

[17] K.F. Doherr and C. Saliaris, "On the Influence of Stochastic and Acceleration Dependent Aerodynamic Forces on the Dynamic Stability of Parachutes", AIAA Paper 81-1941.

[18] W. Gockel, "Computer Based Modeling and Analysis of a Parafoil-Load Vehicle", 14th AIAA Aerodynamic Decelerator Systems Technology Conference and Seminar, June 1997.

[19] I. Kaminer, "Lecture Notes: AA4276 Avionics Design", Naval Postgraduate School, 1998.

[20] D.J. Cockrell and K.F. Doherr, "Preliminary Considerations of Parameter Identification Analysis From Parachute Aerodynamic Flight Test Data", AIAA Paper No. 81-1940.

[21] Richard E. Maine and Kenneth W. Illif, "Application of Parameter Estimation to Aircraft Stability and Control," NASA Reference Publication 1169, June 1986.

[23] Karl Doherr, "Information on the Identification of Stability Derivatives", Email Message, February 1999.

[24] Robert G. Graham, "Implementation of a Personal Computer Based Parameter Estimation Program", Naval Postgraduate School, March 1992.

[26] Colin Tory, "Computer Model of a Fully Deployed Parachute", Journal of Aircraft, Vol 14, No. 7, July 1977.

# APPENDIX A. SIMULATION RESULTS

| Run No. | Hours from Pred Wind | SA On | CARP X Offset | CARP Y Offset | Psi Dot | Release Alt | Predicted CARP | | Error No Control | Error Controlled | Control Inputs |
|---|---|---|---|---|---|---|---|---|---|---|---|
| 1 | 3 | 0 | -2000 | 2000 | 1.4 | 9500 | -3677 | -84 | 2769 | 115 | 9 |
| 2 | 7 | 0 | -2000 | 2000 | 0.2 | 9500 | -6688 | -516 | 5432 | 783 | 7 |
| 3 | 3 | 0 | 3000 | -3000 | 2.0 | 9500 | -3677 | -84 | 4593 | 24 | 16 |
| 4 | 3 | 1 | -2000 | 2000 | 2.1 | 9500 | -3677 | -84 | 2775 | 48 | 16 |
| 5 | 3 | 1 | 3000 | -3000 | 0.7 | 9500 | -3677 | -84 | 4599 | 104 | 11 |
| 6 | 1 | 1 | 3000 | -3000 | 3.0 | 9500 | -3864 | 687 | 3966 | 176 | 17 |
| 7 | 6 | 1 | 3000 | -3000 | 3.0 | 9500 | -6197 | -963 | 4667 | 540 | 13 |
| 8 | 6 | 1 | -2000 | 2000 | 1.8 | 9500 | -6197 | -963 | 5056 | 1233 | 6 |
| 9 | 7 | 0 | 0 | 0 | 2.2 | 9500 | -6688 | -516 | 3564 | 485 | 11 |
| 10 | 6 | 1 | 1000 | 1000 | 2.0 | 9500 | -6197 | -963 | 2151 | 442 | 9 |
| 11 | 7 | 0 | 3000 | -3000 | 1.7 | 9500 | -6688 | -516 | 4178 | 396 | 13 |
| 12 | 7 | 1 | 0 | 0 | 2.6 | 9500 | -6688 | -516 | 3564 | 910 | 11 |
| 13 | 7 | 0 | -2000 | 2000 | 1.3 | 9500 | -6688 | -516 | 5428 | 1179 | 4 |
| 14 | 7 | 1 | -2000 | 2000 | 4.0 | 9500 | -6688 | -516 | 5427 | 990 | 14 |
| 15 | 3 | 0 | -2000 | 2000 | 1.7 | 9500 | -3677 | -84 | 2767 | 61 | 12 |
| 16 | 3 | 1 | 0 | 0 | 2.0 | 9500 | -3677 | -84 | 1024 | 105 | 19 |
| 17 | 1 | 1 | -2000 | 2000 | 2.9 | 9500 | -3864 | 687 | 3248 | 113 | 13 |
| 18 | 1 | 0 | 3000 | -3000 | 1.9 | 9500 | -3864 | 687 | 3964 | 35 | 11 |
| 19 | 3 | 1 | 1000 | 1000 | 1.8 | 9500 | -3677 | -84 | 484 | 152 | 18 |
| 20 | 6 | 1 | 3000 | -3000 | 1.0 | 9500 | -6197 | -963 | 4666 | 137 | 10 |
| 21 | 7 | 1 | 0 | 0 | 2.1 | 9500 | -6688 | -516 | 3562 | 485 | 13 |
| 22 | 7 | 1 | -2000 | 2000 | 0.5 | 9500 | -6688 | -516 | 5427 | 1627 | 1 |
| 23 | 7 | 0 | -2000 | 2000 | 2.6 | 9500 | -6688 | -516 | 5424 | 1066 | 9 |
| 24 | 3 | 1 | 1000 | 1000 | 3.5 | 9500 | -3677 | -84 | 484 | 251 | 21 |
| 25 | 1 | 1 | 0 | 0 | 1.2 | 9500 | -3864 | 687 | 774 | 250 | 13 |
| 26 | 3 | 1 | 1000 | 1000 | 2.7 | 9500 | -3677 | -84 | 482 | 86 | 16 |
| 27 | 1 | 1 | 1000 | 1000 | 3.1 | 9500 | -3864 | 687 | 789 | 42 | 18 |
| 28 | 1 | 0 | 1000 | 1000 | 0.3 | 9500 | -3864 | 687 | 791 | 44 | 12 |
| 29 | 3 | 1 | 3000 | -3000 | 0.4 | 9500 | -3677 | -84 | 4594 | 49 | 6 |
| 30 | 3 | 0 | 0 | 0 | 2.4 | 9500 | -3677 | -84 | 1023 | 51 | 16 |
| 31 | 3 | 1 | 0 | 0 | 1.5 | 9500 | -3677 | -84 | 1028 | 128 | 14 |
| 32 | 1 | 1 | 1000 | 1000 | 2.5 | 9500 | -3864 | 687 | 790 | 226 | 13 |
| 33 | 6 | 1 | 0 | 0 | 2.7 | 9500 | -6197 | -963 | 3474 | 460 | 13 |
| 34 | 3 | 0 | -2000 | 2000 | 2.6 | 9500 | -3677 | -84 | 2770 | 55 | 16 |
| 35 | 3 | 1 | 1000 | 1000 | 3.1 | 9500 | -3677 | -84 | 483 | 12 | 15 |
| 36 | 1 | 0 | 3000 | -3000 | 2.5 | 9500 | -3864 | 687 | 3963 | 29 | 15 |
| 37 | 7 | 0 | 1000 | 1000 | 3.0 | 9500 | -6688 | -516 | 2370 | 735 | 11 |
| 38 | 6 | 1 | 1000 | 1000 | 0.6 | 9500 | -6197 | -963 | 2150 | 886 | 6 |
| 39 | 1 | 0 | 0 | 0 | 1.8 | 9500 | -3864 | 687 | 778 | 65 | 20 |
| 40 | 3 | 0 | -2000 | 2000 | 1.7 | 9500 | -3677 | -84 | 2770 | 72 | 14 |
| 41 | 1 | 1 | 0 | 0 | 0.2 | 9500 | -3864 | 687 | 777 | 204 | 13 |
| 42 | 1 | 1 | -2000 | 2000 | 2.1 | 9500 | -3864 | 687 | 3252 | 69 | 21 |
| 43 | 3 | 1 | 0 | 0 | 0.8 | 9500 | -3677 | -84 | 1026 | 169 | 19 |
| 44 | 3 | 0 | -2000 | 2000 | 3.3 | 9500 | -3677 | -84 | 2774 | 68 | 14 |
| 45 | 1 | 1 | -2000 | 2000 | 1.0 | 9500 | -3864 | 687 | 3247 | 181 | 11 |
| 46 | 3 | 1 | 1000 | 1000 | 2.4 | 9500 | -3677 | -84 | 481 | 54 | 18 |
| 47 | 7 | 1 | 3000 | -3000 | 2.1 | 9500 | -6688 | -516 | 4176 | 468 | 9 |
| 48 | 1 | 0 | -2000 | 2000 | 0.9 | 9500 | -3864 | 687 | 3247 | 21 | 14 |
| 49 | 7 | 0 | 1000 | 1000 | -0.3 | 9500 | -6688 | -516 | 2374 | 538 | 6 |
| 50 | 1 | 0 | 0 | 0 | 1.8 | 9500 | -3864 | 687 | 776 | 36 | 15 |
| 51 | 6 | 0 | 1000 | 1000 | 0.8 | 9500 | -6197 | -963 | 2147 | 614 | 4 |
| 52 | 3 | 1 | 1000 | 1000 | 2.5 | 9500 | -3677 | -84 | 482 | 205 | 17 |
| 53 | 6 | 1 | -2000 | 2000 | 2.4 | 9500 | -6197 | -963 | 5055 | 1045 | 8 |

| Run No. | Hours from Pred Wind | SA On | CARP X Offset | CARP Y Offset | Psi Dot | Release Alt | Predicted CARP | | Error No Control | Error Controlled | Control Inputs |
|---|---|---|---|---|---|---|---|---|---|---|---|
| 54 | 1 | 1 | 3000 | -3000 | 3.5 | 9500 | -3864 | 687 | 3964 | 35 | 19 |
| 55 | 6 | 0 | 3000 | -3000 | 2.4 | 9500 | -6197 | -963 | 4668 | 458 | 13 |
| 56 | 1 | 0 | 1000 | 1000 | 1.2 | 9500 | -3864 | 687 | 798 | 58 | 13 |
| 57 | 3 | 0 | 0 | 0 | 2.2 | 9500 | -3677 | -84 | 1028 | 70 | 18 |
| 58 | 7 | 0 | 0 | 0 | 0.8 | 9500 | -6688 | -516 | 3564 | 570 | 11 |
| 59 | 3 | 1 | 0 | 0 | 1.8 | 9500 | -3677 | -84 | 1020 | 130 | 19 |
| 60 | 7 | 0 | 1000 | 1000 | 1.8 | 9500 | -6688 | -516 | 2369 | 794 | 8 |
| 61 | 7 | 0 | 0 | 0 | 1.9 | 9500 | -6688 | -516 | 3565 | 1083 | 13 |
| 62 | 1 | 1 | 0 | 0 | 1.5 | 9500 | -3864 | 687 | 778 | 192 | 16 |
| 63 | 7 | 1 | -2000 | 2000 | 2.9 | 9500 | -6688 | -516 | 5433 | 1210 | 9 |
| 64 | 7 | 0 | 3000 | -3000 | 0.0 | 9500 | -6688 | -516 | 4183 | 824 | 5 |
| 65 | 6 | 1 | 1000 | 1000 | 2.3 | 9500 | -6197 | -963 | 2147 | 399 | 7 |
| 66 | 7 | 1 | -2000 | 2000 | 2.7 | 9500 | -6688 | -516 | 5428 | 842 | 10 |
| 67 | 1 | 0 | -2000 | 2000 | 2.6 | 9500 | -3864 | 687 | 3241 | 26 | 13 |
| 68 | 1 | 0 | 3000 | -3000 | 2.4 | 9500 | -3864 | 687 | 3966 | 35 | 14 |
| 69 | 7 | 1 | 3000 | -3000 | 1.9 | 9500 | -6688 | -516 | 4166 | 918 | 13 |
| 70 | 7 | 0 | 1000 | 1000 | 2.5 | 9500 | -6688 | -516 | 2374 | 924 | 12 |
| 71 | 1 | 1 | 0 | 0 | 2.4 | 9500 | -3864 | 687 | 774 | 262 | 17 |
| 72 | 3 | 0 | 3000 | -3000 | 1.6 | 9500 | -3677 | -84 | 4595 | 70 | 15 |
| 73 | 7 | 0 | 3000 | -3000 | 1.5 | 9500 | -6688 | -516 | 4181 | 540 | 10 |
| 74 | 6 | 1 | 3000 | -3000 | 1.6 | 9500 | -6197 | -963 | 4668 | 188 | 12 |
| 75 | 3 | 1 | 0 | 0 | 0.4 | 9500 | -3677 | -84 | 1016 | 63 | 18 |
| 76 | 6 | 0 | 1000 | 1000 | 1.6 | 9500 | -6197 | -963 | 2147 | 148 | 11 |
| 77 | 3 | 0 | 3000 | -3000 | 2.0 | 9500 | -3677 | -84 | 4594 | 45 | 15 |
| 78 | 6 | 1 | 0 | 0 | 2.2 | 9500 | -6197 | -963 | 3472 | 228 | 15 |
| 79 | 6 | 1 | 3000 | -3000 | 3.3 | 9500 | -6197 | -963 | 4665 | 381 | 14 |
| 80 | 7 | 0 | 1000 | 1000 | 1.5 | 9500 | -6688 | -516 | 2378 | 517 | 13 |
| 81 | 3 | 1 | 0 | 0 | 2.5 | 9500 | -3677 | -84 | 1025 | 159 | 22 |
| 82 | 6 | 0 | 1000 | 1000 | 2.6 | 9500 | -6197 | -963 | 2152 | 389 | 9 |
| 83 | 7 | 1 | -2000 | 2000 | 2.8 | 9500 | -6688 | -516 | 5429 | 933 | 10 |
| 84 | 1 | 0 | 0 | 0 | 0.9 | 9500 | -3864 | 687 | 775 | 30 | 16 |
| 85 | 7 | 0 | 3000 | -3000 | 2.1 | 9500 | -6688 | -516 | 4176 | 628 | 11 |
| 86 | 1 | 1 | 3000 | -3000 | 2.1 | 9500 | -3864 | 687 | 3967 | 64 | 12 |
| 87 | 3 | 1 | 0 | 0 | 0.8 | 9500 | -3677 | -84 | 1028 | 209 | 15 |
| 88 | 1 | 1 | -2000 | 2000 | 1.1 | 9500 | -3864 | 687 | 3245 | 192 | 19 |
| 89 | 3 | 0 | 0 | 0 | 2.9 | 9500 | -3677 | -84 | 1024 | 56 | 19 |
| 90 | 7 | 1 | 0 | 0 | 1.7 | 9500 | -6688 | -516 | 3568 | 787 | 19 |
| 91 | 6 | 0 | 1000 | 1000 | 2.2 | 9500 | -6197 | -963 | 2147 | 163 | 11 |
| 92 | 1 | 0 | 1000 | 1000 | 1.9 | 9500 | -3864 | 687 | 803 | 37 | 19 |
| 93 | 3 | 0 | 3000 | -3000 | 1.2 | 9500 | -3677 | -84 | 4600 | 49 | 16 |
| 94 | 7 | 1 | 3000 | -3000 | 1.9 | 9500 | -6688 | -516 | 4171 | 966 | [illegible] |
| 95 | 6 | 0 | 3000 | -3000 | 2.9 | 9500 | -6197 | -963 | 4688 | 163 | 11 |
| 96 | 3 | 1 | 0 | 0 | 0.9 | 9500 | -3677 | -84 | 1024 | 158 | 19 |
| 97 | 6 | 0 | 3000 | -3000 | 2.6 | 9500 | -6197 | -963 | 4667 | 458 | 12 |
| 98 | 3 | 1 | 0 | 0 | 2.4 | 9500 | -3677 | -84 | 1024 | 22 | 21 |
| 99 | 7 | 1 | 3000 | -3000 | 1.9 | 9500 | -6688 | -516 | 4180 | 642 | [illegible] |
| 100 | 1 | 1 | 3000 | -3000 | 1.6 | 9500 | -3864 | 687 | 3963 | 333 | 11 |
| 101 | 1 | 1 | 1000 | 1000 | 0.7 | 9500 | -7283 | -867 | 585 | 108 | 11 |
| 102 | 1 | 0 | 0 | 0 | -0.4 | 9500 | -7283 | -867 | 881 | 231 | 16 |
| 103 | 1 | 0 | -2000 | 2000 | 2.9 | 9500 | -7283 | -867 | 3134 | 168 | 19 |
| 104 | 1 | 1 | 1000 | 1000 | 1.9 | 9500 | -7283 | -867 | 585 | 246 | 17 |
| 105 | 1 | 0 | 1000 | 1000 | 2.2 | 9500 | -7283 | -867 | 585 | 214 | 18 |
| 106 | 5 | 1 | 1000 | 1000 | 2.1 | 9500 | -4748 | 41 | 3194 | 159 | 18 |
| 107 | 2 | 0 | 0 | 0 | 1.9 | 9500 | -7533 | -91 | 897 | 167 | 14 |
| 108 | 2 | 1 | 0 | 0 | 0.8 | 9500 | -7533 | -91 | 905 | 253 | 13 |

| Run No. | Hours from Pred Wind | SA On | CARP X Offset | CARP Y Offset | Psi Dot | Release Alt | Predicted CARP | | Error No Control | Error Controlled | Control Inputs |
|---|---|---|---|---|---|---|---|---|---|---|---|
| 109 | 5 | 1 | 3000 | -3000 | 0.9 | 9500 | -4748 | 41 | 5723 | 458 | 4 |
| 110 | 1 | 0 | 1000 | 1000 | 1.5 | 9500 | -7283 | -867 | 589 | 330 | 10 |
| 111 | 1 | 1 | 3000 | -3000 | 0.7 | 9500 | -7283 | -867 | 4142 | 252 | 14 |
| 112 | 5 | 1 | 1000 | 1000 | 0.8 | 9500 | -4748 | 41 | 3216 | 327 | 8 |
| 113 | 1 | 1 | 3000 | -3000 | 3.3 | 9500 | -7283 | -867 | 4141 | 396 | 13 |
| 114 | 5 | 0 | 0 | 0 | 1.9 | 9500 | -4748 | 41 | 2002 | 346 | 10 |
| 115 | 5 | 1 | 0 | 0 | 0.6 | 9500 | -4748 | 41 | 2005 | 384 | 5 |
| 116 | 1 | 1 | 3000 | -3000 | 1.8 | 9500 | -7283 | -867 | 4145 | 212 | 11 |
| 117 | 5 | 1 | 3000 | -3000 | 0.7 | 9500 | -4748 | 41 | 5723 | 886 | 3 |
| 118 | 2 | 1 | 0 | 0 | 0.5 | 9500 | -7533 | -91 | 893 | 243 | 8 |
| 119 | 2 | 1 | 0 | 0 | 1.6 | 9500 | -7533 | -91 | 905 | 276 | 12 |
| 120 | 5 | 1 | -2000 | 2000 | 2.8 | 9500 | -4748 | 41 | 2185 | 246 | 17 |
| 121 | 2 | 0 | 0 | 0 | 2.0 | 9500 | -7533 | -91 | 896 | 164 | 9 |
| 122 | 2 | 0 | -2000 | 2000 | 2.5 | 9500 | -7533 | -91 | 3675 | 162 | 15 |
| 123 | 5 | 0 | -2000 | 2000 | 0.7 | 9500 | -4748 | 41 | 2198 | 373 | 10 |
| 124 | 2 | 0 | 0 | 0 | 1.4 | 9500 | -7533 | -91 | 895 | 166 | 10 |
| 125 | 2 | 0 | 1000 | 1000 | 1.6 | 9500 | -7533 | -91 | 1349 | 169 | 15 |
| 126 | 2 | 1 | 1000 | 1000 | 0.6 | 9500 | -7533 | -91 | 1355 | 98 | 10 |
| 127 | 5 | 0 | -2000 | 2000 | 0.5 | 9500 | -4748 | 41 | 2193 | 227 | 11 |
| 128 | 1 | 0 | 0 | 0 | 2.8 | 9500 | -7283 | -867 | 863 | 203 | 12 |
| 125 | 5 | 0 | 0 | 0 | 1.9 | 9500 | -4748 | 41 | 1998 | 431 | 10 |
| 130 | 5 | 1 | -2000 | 2000 | 1.2 | 9500 | -4748 | 41 | 2192 | 246 | 12 |
| 131 | 5 | 1 | 1000 | 1000 | 2.7 | 9500 | -4748 | 41 | 3211 | 207 | 20 |
| 132 | 2 | 1 | 0 | 0 | 2.1 | 9500 | -7533 | -91 | 901 | 274 | 9 |
| 133 | 5 | 0 | 3000 | -3000 | 0.5 | 9500 | -4748 | 41 | 5722 | 707 | 9 |
| 134 | 2 | 0 | 3000 | -3000 | 3.2 | 9500 | -7533 | -91 | 3431 | 154 | 10 |
| 135 | 1 | 1 | 0 | 0 | 2.1 | 9500 | -7283 | -867 | 862 | 288 | 10 |
| 136 | 5 | 0 | -2000 | 2000 | 3.3 | 9500 | -4748 | 41 | 2188 | 237 | 18 |
| 137 | 5 | 1 | -2000 | 2000 | 3.0 | 9500 | -4748 | 41 | 2186 | 439 | 19 |
| 138 | 2 | 0 | 3000 | -3000 | 1.2 | 9500 | -7533 | -91 | 3430 | 134 | 10 |
| 139 | 5 | 0 | 1000 | 1000 | 0.6 | 9500 | -4748 | 41 | 3216 | 282 | 10 |
| 140 | 2 | 0 | 0 | 0 | 1.8 | 9500 | -7533 | -91 | 901 | 145 | 12 |
| 141 | 2 | 0 | 0 | 0 | 1.5 | 9500 | -7533 | -91 | 902 | 147 | 12 |
| 142 | 2 | 0 | -2000 | 2000 | 1.0 | 9500 | -7533 | -91 | 3674 | 147 | 11 |
| 143 | 1 | 1 | -2000 | 2000 | 2.3 | 9500 | -7283 | -867 | 3136 | 432 | 10 |
| 144 | 5 | 1 | -2000 | 2000 | 3.3 | 9500 | -4748 | 41 | 2193 | 245 | 16 |
| 145 | 5 | 1 | -2000 | 2000 | 1.3 | 9500 | -4748 | 41 | 2192 | 304 | 9 |
| 146 | 1 | 1 | 1000 | 1000 | 1.0 | 9500 | -7283 | -867 | 602 | 312 | 10 |
| 147 | 2 | 1 | 3000 | -3000 | 1.6 | 9500 | -7533 | -91 | 3432 | 53 | 10 |
| 148 | 2 | 0 | 3000 | -3000 | 2.5 | 9500 | -7533 | -91 | 3433 | 148 | 12 |
| 149 | 2 | 0 | 3000 | -3000 | 1.0 | 9500 | -7533 | -91 | 3431 | 171 | 13 |
| 150 | 5 | 1 | 0 | 0 | 0.6 | 9500 | -4748 | 41 | 1999 | 515 | 9 |
| 151 | 2 | 1 | -2000 | 2000 | 1.7 | 9500 | -7533 | -91 | 3671 | 157 | 10 |
| 152 | 5 | 0 | 3000 | -3000 | 1.8 | 9500 | -4748 | 41 | 5724 | 909 | 7 |
| 153 | 1 | 0 | 1000 | 1000 | 2.3 | 9500 | -7283 | -867 | 574 | 181 | 22 |
| 154 | 5 | 1 | 3000 | -3000 | 1.3 | 9500 | -4748 | 41 | 5726 | 1048 | 5 |
| 155 | 1 | 1 | 1000 | 1000 | 1.7 | 9500 | -7283 | -867 | 589 | 285 | 14 |
| 156 | 5 | 0 | 1000 | 1000 | 1.4 | 9500 | -4748 | 41 | 3210 | 204 | 14 |
| 157 | 1 | 1 | -2000 | 2000 | 1.8 | 9500 | -7283 | -867 | 3134 | 123 | 12 |
| 158 | 1 | 1 | 3000 | -3000 | 3.4 | 9500 | -7283 | -867 | 4140 | 107 | 11 |
| 159 | 5 | 0 | 1000 | 1000 | 1.2 | 9500 | -4748 | 41 | 3210 | 468 | 11 |
| 160 | 5 | 1 | 0 | 0 | 0.5 | 9500 | -4748 | 41 | 1993 | 212 | 12 |
| 161 | 5 | 1 | 3000 | -3000 | 2.3 | 9500 | -4748 | 41 | 5722 | 931 | 8 |
| 162 | 2 | 0 | 1000 | 1000 | 0.9 | 9500 | -7533 | -91 | 1337 | 165 | 17 |
| 163 | 1 | 1 | -2000 | 2000 | 1.9 | 9500 | -7283 | -867 | 3134 | 227 | 12 |

| Run No. | Hours from Pred Wind | SA On | CARP X Offset | CARP Y Offset | Psi Dot | Release Alt | Predicted CARP | | Error No Control | Error Controlled | Control Inputs |
|---|---|---|---|---|---|---|---|---|---|---|---|
| 164 | 2 | 0 | 1000 | 1000 | 1.2 | 9500 | -7533 | -91 | 1345 | 135 | 15 |
| 165 | 1 | 1 | 0 | 0 | 2.4 | 9500 | -7283 | -867 | 881 | 102 | 16 |
| 166 | 1 | 1 | 1000 | 1000 | 2.4 | 9500 | -7283 | -867 | 577 | 512 | 20 |
| 167 | 2 | 1 | 3000 | -3000 | 1.6 | 9500 | -7533 | -91 | 3432 | 315 | 12 |
| 168 | 1 | 1 | -2000 | 2000 | -0.2 | 9500 | -7283 | -867 | 3132 | 230 | 8 |
| 169 | 1 | 0 | 1000 | 1000 | 2.0 | 9500 | -7283 | -867 | 597 | 279 | 18 |
| 170 | 5 | 1 | -2000 | 2000 | 3.4 | 9500 | -4748 | 41 | 2188 | 299 | 18 |
| 171 | 2 | 1 | -2000 | 2000 | 2.9 | 9500 | -7533 | -91 | 3673 | 77 | 14 |
| 172 | 2 | 1 | 1000 | 1000 | 0.3 | 9500 | -7533 | -91 | 1355 | 184 | 11 |
| 173 | 1 | 1 | -2000 | 2000 | 1.8 | 9500 | -7283 | -867 | 3136 | 188 | 15 |
| 174 | 1 | 0 | 1000 | 1000 | 1.2 | 9500 | -7283 | -867 | 582 | 181 | 17 |
| 175 | 5 | 0 | 1000 | 1000 | 0.8 | 9500 | -4748 | 41 | 3203 | 230 | 11 |
| 176 | 5 | 1 | 3000 | -3000 | 0.6 | 9500 | -4748 | 41 | 5724 | 1129 | 4 |
| 177 | 2 | 0 | 1000 | 1000 | 2.1 | 9500 | -7533 | -91 | 1328 | 173 | 21 |
| 178 | 2 | 0 | -2000 | 2000 | 1.4 | 9500 | -7533 | -91 | 3672 | 167 | 8 |
| 179 | 2 | 0 | 3000 | -3000 | 1.9 | 9500 | -7533 | -91 | 3433 | 148 | 17 |
| 180 | 1 | 1 | 1000 | 1000 | 1.5 | 9500 | -7283 | -867 | 590 | 333 | 12 |
| 181 | 1 | 1 | 3000 | -3000 | 1.4 | 9500 | -7283 | -867 | 4141 | 388 | 12 |
| 182 | 1 | 1 | 3000 | -3000 | 2.2 | 9500 | -7283 | -867 | 4141 | 194 | 16 |
| 183 | 5 | 0 | 3000 | -3000 | 2.6 | 9500 | -4748 | 41 | 5722 | 761 | 9 |
| 184 | 5 | 1 | -2000 | 2000 | 4.0 | 9500 | -4748 | 41 | 2191 | 278 | 19 |
| 185 | 5 | 1 | -2000 | 2000 | 0.5 | 9500 | -4748 | 41 | 2187 | 315 | 12 |
| 186 | 1 | 1 | -2000 | 2000 | 0.8 | 9500 | -7283 | -867 | 3136 | 328 | 10 |
| 187 | 1 | 1 | -2000 | 2000 | 2.9 | 9500 | -7283 | -867 | 3136 | 133 | 14 |
| 188 | 1 | 0 | 0 | 0 | 1.5 | 9500 | -7283 | -867 | 872 | 265 | 13 |
| 189 | 1 | 0 | 0 | 0 | 0.5 | 9500 | -7283 | -867 | 876 | 220 | 14 |
| 190 | 1 | 0 | -2000 | 2000 | 2.2 | 9500 | -7283 | -867 | 3131 | 234 | 13 |
| 191 | 1 | 1 | -2000 | 2000 | 3.4 | 9500 | -7283 | -867 | 3130 | 179 | 16 |
| 192 | 2 | 1 | 0 | 0 | 2.6 | 9500 | -7533 | -91 | 898 | 177 | 13 |
| 193 | 2 | 0 | 3000 | -3000 | 3.8 | 9500 | -7533 | -91 | 3435 | 177 | 17 |
| 194 | 2 | 1 | -2000 | 2000 | 2.4 | 9500 | -7533 | -91 | 3672 | 164 | 13 |
| 195 | 2 | 1 | 0 | 0 | 3.7 | 9500 | -7533 | -91 | 902 | 132 | 17 |
| 196 | 2 | 0 | 1000 | 1000 | 1.5 | 9500 | -7533 | -91 | 1337 | 161 | 16 |
| 197 | 1 | 0 | 0 | 0 | 0.7 | 9500 | -7283 | -867 | 879 | 189 | 12 |
| 198 | 3 | 1 | 0 | 0 | 1.6 | 9500 | -4748 | 41 | 1980 | 331 | 12 |
| 199 | 1 | 0 | 0 | 0 | 3.0 | 9500 | -7283 | -867 | 876 | 193 | 14 |
| 200 | 2 | 1 | 0 | 0 | 0.7 | 9500 | -7533 | -91 | 897 | 161 | 12 |
| 201 | 3 | 0 | -2000 | 2000 | 1.4 | 20000 | 13238 | 1503 | 10883 | 1174 | 11 |
| 202 | 3 | 0 | 0 | 0 | 0.2 | 20000 | 13238 | 1503 | 8052 | 2397 | 3 |
| 203 | 7 | 1 | 3000 | -3000 | 2.0 | 20000 | 14857 | 1019 | 2335 | 274 | 19 |
| 204 | 5 | 1 | 3000 | -3000 | 2.1 | 20000 | 16319 | -1584 | 739 | 393 | 22 |
| 205 | 3 | 0 | 3000 | -3000 | 0.7 | 20000 | 17012 | -2036 | 1289 | 37 | 19 |
| 206 | 3 | 0 | -2000 | 2000 | 3.0 | 20000 | 17012 | -2036 | 5820 | 110 | 28 |
| 207 | 3 | 1 | 1000 | 1000 | 3.0 | 20000 | 17012 | -2036 | 3195 | 32 | 30 |
| 208 | 5 | 1 | -2000 | 2000 | 1.8 | 20000 | 16319 | -1584 | 6537 | 411 | 19 |
| 209 | 5 | 0 | -2000 | 2000 | 2.2 | 20000 | 13238 | 1503 | 10884 | 1156 | 17 |
| 210 | 7 | 1 | 1000 | 1000 | 2.0 | 20000 | 14857 | 1019 | 6781 | 544 | 20 |
| 211 | 3 | 1 | 1000 | 1000 | 1.7 | 20000 | 17012 | -2036 | 3191 | 318 | 19 |
| 212 | 7 | 0 | 3000 | -3000 | 2.6 | 20000 | 14857 | 1019 | 2338 | 205 | 23 |
| 213 | 5 | 1 | 3000 | -3000 | 1.3 | 20000 | 16319 | -1584 | 737 | 496 | 20 |
| 214 | 7 | 0 | 1000 | 1000 | 4.0 | 20000 | 14857 | 1019 | 6783 | 117 | 33 |
| 215 | 7 | 0 | 3000 | -3000 | 1.7 | 20000 | 14857 | 1019 | 2336 | 226 | 21 |
| 216 | 7 | 1 | 1000 | 1000 | 2.0 | 20000 | 14857 | 1019 | 6781 | 96 | 24 |
| 217 | 9 | 1 | -2000 | 2000 | 2.9 | 20000 | 13238 | 1503 | 10885 | 1322 | 22 |
| 218 | 9 | 0 | 1000 | 1000 | 1.9 | 20000 | 13238 | 1503 | 8113 | 602 | 17 |

| Run No. | Hours from Pred Wind | SA On | CARP X Offset | CARP Y Offset | Psi Dot | Release Alt | Predicted CARP | | Error No Control | Error Controlled | Control Inputs |
|---|---|---|---|---|---|---|---|---|---|---|---|
| 219 | 3 | 0 | 3000 | -3000 | 1.8 | 20000 | 17012 | -2036 | 1288 | 35 | 20 |
| 220 | 7 | 0 | 1000 | 1000 | 1.0 | 20000 | 14857 | 1019 | 6777 | 130 | 16 |
| 221 | 7 | 0 | -2000 | 2000 | 2.1 | 20000 | 14857 | 1019 | 9389 | 73 | 18 |
| 222 | 3 | 1 | 3000 | -3000 | 0.5 | 20000 | 17012 | -2036 | 1289 | 199 | 15 |
| 223 | 3 | 0 | 3000 | -3000 | 2.6 | 20000 | 17012 | -2036 | 1281 | 121 | 30 |
| 224 | 7 | 1 | 0 | 0 | 3.5 | 20000 | 14857 | 1019 | 6568 | 188 | 33 |
| 225 | 5 | 0 | 3000 | -3000 | 1.2 | 20000 | 16319 | -1584 | 738 | 382 | 17 |
| 226 | 9 | 1 | 3000 | -3000 | 2.7 | 20000 | 13238 | 1503 | 3831 | 76 | 24 |
| 227 | 3 | 1 | 1000 | 1000 | 3.1 | 20000 | 17012 | -2036 | 3196 | 275 | 31 |
| 228 | 5 | 1 | 1000 | 1000 | 0.3 | 20000 | 16319 | -1584 | 3802 | 406 | 19 |
| 229 | 7 | 0 | 3000 | -3000 | 0.4 | 20000 | 14857 | 1019 | 2333 | 189 | 19 |
| 230 | 3 | 1 | -2000 | 2000 | 2.4 | 20000 | 17012 | -2036 | 5820 | 78 | 19 |
| 231 | 5 | 0 | 0 | 0 | 1.5 | 20000 | 16319 | -1584 | 3727 | 443 | 20 |
| 232 | 5 | 1 | 0 | 0 | 2.5 | 20000 | 16319 | -1584 | 3726 | 231 | 20 |
| 233 | 7 | 0 | 0 | 0 | 2.7 | 20000 | 14857 | 1019 | 6563 | 90 | 23 |
| 234 | 3 | 0 | -2000 | 2000 | 2.6 | 20000 | 17012 | -2036 | 5817 | 106 | 21 |
| 235 | 3 | 0 | 1000 | 1000 | 3.1 | 20000 | 17012 | -2036 | 3192 | 70 | 27 |
| 236 | 7 | 1 | -2000 | 2000 | 2.5 | 20000 | 14857 | 1019 | 9388 | 128 | 21 |
| 237 | 3 | 0 | -2000 | 2000 | 3.0 | 20000 | 17012 | -2036 | 5821 | 131 | 29 |
| 238 | 5 | 1 | 0 | 0 | 0.6 | 20000 | 16319 | -1584 | 3722 | 477 | 19 |
| 239 | 3 | 0 | 0 | 0 | 1.8 | 20000 | 17012 | -2036 | 2999 | 47 | 21 |
| 240 | 3 | 1 | 0 | 0 | 1.7 | 20000 | 17012 | -2036 | 2999 | 209 | 19 |
| 241 | 5 | 0 | 1000 | 1000 | 0.2 | 20000 | 16319 | -1584 | 3803 | 222 | 19 |
| 242 | 7 | 0 | 0 | 0 | 2.1 | 20000 | 14857 | 1019 | 6564 | 92 | 26 |
| 243 | 9 | 0 | 0 | 0 | 0.8 | 20000 | 13238 | 1503 | 8055 | 706 | 8 |
| 244 | 7 | 1 | -2000 | 2000 | 3.3 | 20000 | 14857 | 1019 | 9388 | 302 | 26 |
| 245 | 3 | 1 | 1000 | 1000 | 1.0 | 20000 | 17012 | -2036 | 3200 | 235 | 20 |
| 246 | 7 | 0 | 0 | 0 | 2.4 | 20000 | 14857 | 1019 | 6566 | 144 | 26 |
| 247 | 5 | 1 | 1000 | 1000 | 2.1 | 20000 | 16319 | -1584 | 3805 | 490 | 22 |
| 248 | 5 | 0 | 1000 | 1000 | 0.9 | 20000 | 16319 | -1584 | 3806 | 480 | 20 |
| 249 | 5 | 0 | -2000 | 2000 | -0.3 | 20000 | 16319 | -1584 | 6534 | 242 | 10 |
| 250 | 7 | 0 | 0 | 0 | 1.8 | 20000 | 14857 | 1019 | 6563 | 135 | 19 |
| 251 | 5 | 0 | 1000 | 1000 | 0.8 | 20000 | 16319 | -1584 | 3806 | 355 | 22 |
| 252 | 9 | 1 | 1000 | 1000 | 2.5 | 20000 | 13238 | 1503 | 8113 | 673 | 21 |
| 253 | 3 | 1 | -2000 | 2000 | 2.4 | 20000 | 17012 | -2036 | 5819 | 44 | 23 |
| 254 | 7 | 1 | 1000 | 1000 | 3.5 | 20000 | 14857 | 1019 | 6782 | 141 | 32 |
| 255 | 7 | 1 | 1000 | 1000 | 2.4 | 20000 | 14857 | 1019 | 6784 | 54 | 27 |
| 256 | 9 | 0 | 1000 | 1000 | 1.2 | 20000 | 13238 | 1503 | 8111 | 883 | 12 |
| 257 | 7 | 1 | 3000 | -3000 | 2.2 | 20000 | 14857 | 1019 | 2336 | 260 | 21 |
| 258 | 7 | 1 | 3000 | -3000 | 0.8 | 20000 | 14857 | 1019 | 2336 | 167 | 12 |
| 259 | 3 | 1 | 1000 | 1000 | 1.8 | 20000 | 17012 | -2036 | 3191 | 77 | 17 |
| 260 | 9 | 1 | 3000 | -3000 | 1.8 | 20000 | 13238 | 1503 | 3826 | 203 | 18 |
| 261 | 5 | 1 | 1000 | 1000 | 1.9 | 20000 | 16319 | -1584 | 3807 | 175 | 25 |
| 262 | 7 | 1 | 3000 | -3000 | 1.5 | 20000 | 14857 | 1019 | 2341 | 153 | 23 |
| 263 | 5 | 1 | 3000 | -3000 | 2.9 | 20000 | 16319 | -1584 | 738 | 354 | 23 |
| 264 | 9 | 1 | 1000 | 1000 | 0.0 | 20000 | 13238 | 1503 | 8113 | 442 | 17 |
| 265 | 7 | 0 | 3000 | -3000 | 2.3 | 20000 | 14857 | 1019 | 2339 | 184 | 26 |
| 266 | 5 | 1 | 1000 | 1000 | 2.7 | 20000 | 16319 | -1584 | 3807 | 261 | 25 |
| 267 | 5 | 0 | 1000 | 1000 | 2.6 | 20000 | 16319 | -1584 | 3805 | 372 | 28 |
| 268 | 3 | 1 | 3000 | -3000 | 2.4 | 20000 | 17012 | -2036 | 1279 | 190 | 29 |
| 269 | 7 | 0 | 1000 | 1000 | 1.9 | 20000 | 14857 | 1019 | 6781 | 45 | 23 |
| 270 | 3 | 0 | 1000 | 1000 | 2.5 | 20000 | 17012 | -2036 | 3193 | 51 | 22 |
| 271 | 9 | 1 | 1000 | 1000 | 2.4 | 20000 | 13238 | 1503 | 8113 | 588 | 21 |
| 272 | 3 | 1 | 3000 | -3000 | 1.6 | 20000 | 17012 | -2036 | 1284 | 211 | 20 |
| 273 | 9 | 1 | -2000 | 2000 | 1.5 | 20000 | 13238 | 1503 | 10883 | 1188 | 12 |

| Run No. | Hours from Pred Wind | SA On | CARP X Offset | CARP Y Offset | Psi Dot | Release Alt | Predicted CARP | | Error No Control | Error Controlled | Control Inputs |
|---|---|---|---|---|---|---|---|---|---|---|---|
| 274 | 5 | 0 | 3000 | -3000 | 1.6 | 20000 | 16319 | -1584 | 738 | 274 | 22 |
| 275 | 9 | 0 | 3000 | -3000 | 0.4 | 20000 | 13238 | 1503 | 3823 | 172 | 11 |
| 276 | 7 | 1 | -2000 | 2000 | 1.6 | 20000 | 14857 | 1019 | 9387 | 54 | 17 |
| 277 | 3 | 0 | 1000 | 1000 | 2.0 | 20000 | 17012 | -2036 | 3192 | 169 | 20 |
| 278 | 3 | 0 | -2000 | 2000 | 2.2 | 20000 | 17012 | -2036 | 5818 | 110 | 18 |
| 279 | 3 | 1 | -2000 | 2000 | 3.3 | 20000 | 17012 | -2036 | 5823 | 71 | 25 |
| 280 | 9 | 0 | 1000 | 1000 | 1.5 | 20000 | 13238 | 1503 | 8112 | 735 | 14 |
| 281 | 5 | 0 | -2000 | 2000 | 2.5 | 20000 | 16319 | -1584 | 6540 | 176 | 21 |
| 282 | 3 | 0 | 1000 | 1000 | 2.6 | 20000 | 17012 | -2036 | 3193 | 58 | 30 |
| 283 | 7 | 0 | 1000 | 1000 | 2.8 | 20000 | 14857 | 1019 | 6782 | 110 | 27 |
| 284 | 9 | 0 | 3000 | -3000 | 0.9 | 20000 | 13238 | 1503 | 3825 | 269 | 11 |
| 285 | 9 | 0 | 1000 | 1000 | 2.1 | 20000 | 13238 | 1503 | 8113 | 775 | 18 |
| 286 | 7 | 0 | 1000 | 1000 | 2.1 | 20000 | 14857 | 1019 | 6781 | 171 | 26 |
| 287 | 5 | 0 | 3000 | -3000 | 0.8 | 20000 | 16319 | -1584 | 738 | 303 | 14 |
| 288 | 7 | 0 | -2000 | 2000 | 1.1 | 20000 | 14857 | 1019 | 9386 | 152 | 14 |
| 289 | 3 | 1 | -2000 | 2000 | 2.9 | 20000 | 17012 | -2036 | 5820 | 329 | 23 |
| 290 | 3 | 0 | 0 | 0 | 1.7 | 20000 | 17012 | -2036 | 3005 | 101 | 23 |
| 291 | 3 | 1 | 3000 | -3000 | 2.2 | 20000 | 17012 | -2036 | 1283 | 69 | 29 |
| 292 | 9 | 0 | 3000 | -3000 | 1.9 | 20000 | 13238 | 1503 | 3827 | 236 | 19 |
| 293 | 3 | 0 | 0 | 0 | 1.2 | 20000 | 17012 | -2036 | 2996 | 23 | 20 |
| 294 | 5 | 0 | 3000 | -3000 | 1.3 | 20000 | 16319 | -1584 | 735 | 182 | 20 |
| 295 | 3 | 0 | -2000 | 2000 | 2.3 | 20000 | 17012 | -2036 | 5822 | 74 | 22 |
| 296 | 3 | 1 | 1000 | 1000 | 0.9 | 20000 | 17012 | -2036 | 3194 | 253 | 15 |
| 297 | 7 | 1 | 1000 | 1000 | 2.6 | 20000 | 14857 | 1019 | 6782 | 343 | 26 |
| 298 | 3 | 0 | 3000 | -3000 | 2.4 | 20000 | 17012 | -2036 | 1288 | 72 | 30 |
| 299 | 9 | 0 | 1000 | 1000 | 1.0 | 20000 | 13238 | 1503 | 8110 | 831 | 10 |
| 300 | 9 | 1 | -2000 | 2000 | 1.6 | 20000 | 13238 | 1503 | 10883 | 1117 | 12 |
| 301 | 7 | 1 | -2000 | 2000 | 2.5 | 9500 | -6688 | -516 | 5428 | 1250 | 9 |
| 302 | 7 | 0 | -2000 | 2000 | 1.2 | 9500 | -6688 | -516 | 5427 | 1193 | 4 |
| 303 | 1 | 0 | -2000 | 2000 | 2.4 | 9500 | -3864 | 687 | 3238 | 45 | 15 |
| 304 | 1 | 0 | 1000 | 1000 | 0.8 | 9500 | -3864 | 687 | 789 | 31 | 14 |
| 305 | 6 | 1 | 1000 | 1000 | 1.9 | 9500 | -6197 | -963 | 2150 | 696 | 10 |
| 306 | 7 | 0 | 0 | 0 | -0.2 | 9500 | -6688 | -516 | 3563 | 670 | 7 |
| 307 | 1 | 1 | 1000 | 1000 | 1.4 | 9500 | -3864 | 687 | 800 | 62 | 14 |
| 308 | 3 | 1 | 3000 | -3000 | 2.3 | 9500 | -3677 | -84 | 4596 | 47 | 16 |
| 309 | 3 | 0 | 0 | 0 | 1.5 | 9500 | -3677 | -84 | 1025 | 62 | 18 |
| 310 | 3 | 0 | 1000 | 1000 | 3.1 | 9500 | -3677 | -84 | 486 | 28 | 18 |
| 311 | 1 | 0 | 3000 | -3000 | 1.2 | 9500 | -3864 | 687 | 3967 | 43 | 6 |
| 312 | 3 | 0 | 0 | 0 | -0.5 | 9500 | -3677 | -84 | 1025 | 70 | 14 |
| 313 | 3 | 1 | 3000 | -3000 | 0.6 | 9500 | -3677 | -84 | 4599 | 242 | 10 |
| 314 | 6 | 1 | 3000 | -3000 | 2.8 | 9500 | -6197 | -963 | 4665 | 310 | 12 |
| 315 | 7 | 0 | -2000 | 2000 | 1.7 | 9500 | -6688 | -516 | 5425 | 1406 | 6 |
| 316 | 6 | 1 | 3000 | -3000 | 2.2 | 9500 | -6197 | -963 | 4665 | 137 | 14 |
| 317 | 6 | 1 | 1000 | 1000 | 2.8 | 9500 | -6197 | -963 | 2151 | 262 | 11 |
| 318 | 3 | 1 | 3000 | -3000 | -0.3 | 9500 | -3677 | -84 | 4592 | 243 | 10 |
| 319 | 6 | 1 | 3000 | -3000 | 1.2 | 9500 | -6197 | -963 | 4667 | 690 | 6 |
| 320 | 1 | 1 | -2000 | 2000 | 1.1 | 9500 | -3864 | 687 | 3246 | 52 | 11 |
| 321 | 3 | 0 | 3000 | -3000 | 0.8 | 9500 | -3677 | -84 | 4596 | 90 | 10 |
| 322 | 1 | 0 | 1000 | 1000 | 1.7 | 9500 | -3864 | 687 | 794 | 21 | 14 |
| 323 | 1 | 1 | -2000 | 2000 | 3.4 | 9500 | -3864 | 687 | 3249 | 205 | 20 |
| 324 | 1 | 1 | 3000 | -3000 | 1.8 | 9500 | -3864 | 687 | 3965 | 194 | 11 |
| 325 | 3 | 0 | 3000 | -3000 | 3.1 | 9500 | -3677 | -84 | 4590 | 19 | 16 |
| 326 | 1 | 0 | -2000 | 2000 | 1.2 | 9500 | -3864 | 687 | 3249 | 28 | 17 |
| 327 | 1 | 1 | 0 | 0 | 1.9 | 9500 | -3864 | 687 | 776 | 33 | 16 |
| 328 | 3 | 0 | 0 | 0 | 1.1 | 9500 | -3677 | -84 | 1024 | 55 | 17 |

| Run No. | Hours from Pred Wind | SA On | CARP X Offset | CARP Y Offset | Psi Dot | Release Alt | Predicted CARP | | Error No Control | Error Controlled | Control Inputs |
|---|---|---|---|---|---|---|---|---|---|---|---|
| 329 | 7 | 1 | 0 | 0 | 2.4 | 9500 | -6688 | -516 | 3564 | 796 | 13 |
| 330 | 7 | 1 | -2000 | 2000 | 1.6 | 9500 | -6688 | -516 | 5426 | 951 | 6 |
| 331 | 6 | 0 | -2000 | 2000 | 2.3 | 9500 | -6197 | -963 | 5053 | 1050 | 8 |
| 332 | 3 | 1 | 1000 | 1000 | 2.5 | 9500 | -3677 | -84 | 485 | 194 | 15 |
| 333 | 3 | 1 | 0 | 0 | 1.8 | 9500 | -3677 | -84 | 1030 | 184 | 15 |
| 334 | 7 | 0 | 3000 | -3000 | 2.7 | 9500 | -6688 | -516 | 4179 | 573 | 11 |
| 335 | 6 | 0 | 3000 | -3000 | 4.2 | 9500 | -6197 | -963 | 4670 | 313 | 17 |
| 336 | 3 | 0 | 0 | 0 | 2.4 | 9500 | -3677 | -84 | 1028 | 57 | 18 |
| 337 | 6 | 1 | 1000 | 1000 | 1.8 | 9500 | -6197 | -963 | 2152 | 640 | 10 |
| 338 | 7 | 0 | 3000 | -3000 | 2.8 | 9500 | -6688 | -516 | 4181 | 565 | 11 |
| 339 | 6 | 0 | 1000 | 1000 | 1.9 | 9500 | -6197 | -963 | 2152 | 769 | 9 |
| 340 | 1 | 0 | 0 | 0 | 0.7 | 9500 | -3864 | 687 | 774 | 41 | 16 |
| 341 | 6 | 1 | 0 | 0 | 2.3 | 9500 | -6197 | -963 | 3471 | 321 | 11 |
| 342 | 3 | 1 | 0 | 0 | 1.8 | 9500 | -3677 | -84 | 1025 | 299 | 17 |
| 343 | 1 | 0 | 0 | 0 | 1.6 | 9500 | -3864 | 687 | 776 | 26 | 21 |
| 344 | 1 | 1 | 3000 | -3000 | 3.1 | 9500 | -3864 | 687 | 3967 | 150 | 15 |
| 345 | 7 | 0 | -2000 | 2000 | 3.7 | 9500 | -6688 | -516 | 5430 | 1156 | 12 |
| 346 | 7 | 0 | 0 | 0 | 1.3 | 9500 | -6688 | -516 | 3563 | 870 | 11 |
| 347 | 1 | 1 | 1000 | 1000 | 2.0 | 9500 | -3864 | 687 | 803 | 136 | 17 |
| 348 | 7 | 0 | -2000 | 2000 | 1.0 | 9500 | -6688 | -516 | 5426 | 1284 | 4 |
| 349 | 7 | 1 | 0 | 0 | 2.5 | 9500 | -6688 | -516 | 3562 | 854 | 10 |
| 350 | 7 | 1 | -2000 | 2000 | -0.5 | 9500 | -6688 | -516 | 5428 | 1184 | 3 |
| 351 | 7 | 1 | 0 | 0 | 2.8 | 9500 | -6688 | -516 | 3563 | 648 | 12 |
| 352 | 1 | 1 | -2000 | 2000 | 2.1 | 9500 | -3864 | 687 | 3251 | 87 | 14 |
| 353 | 1 | 0 | -2000 | 2000 | 2.1 | 9500 | -3864 | 687 | 3248 | 42 | 13 |
| 354 | 7 | 1 | 1000 | 1000 | 3.1 | 9500 | -6688 | -516 | 2372 | 653 | 10 |
| 355 | 1 | 0 | -2000 | 2000 | 1.6 | 9500 | -3864 | 687 | 3246 | 32 | 14 |
| 356 | 1 | 1 | 0 | 0 | 1.7 | 9500 | -3864 | 687 | 779 | 124 | 17 |
| 357 | 6 | 1 | -2000 | 2000 | 0.6 | 9500 | -6197 | -963 | 5055 | 1462 | 1 |
| 358 | 1 | 0 | 3000 | -3000 | 0.2 | 9500 | -3864 | 687 | 3960 | 69 | 12 |
| 359 | 7 | 1 | 3000 | -3000 | 1.1 | 9500 | -6688 | -516 | 4179 | 693 | 7 |
| 360 | 3 | 0 | 0 | 0 | 2.1 | 9500 | -3677 | -84 | 1028 | 52 | 16 |
| 361 | 3 | 0 | 1000 | 1000 | 1.3 | 9500 | -3677 | -84 | 483 | 34 | 17 |
| 362 | 7 | 0 | -2000 | 2000 | 0.5 | 9500 | -6688 | -516 | 5428 | 1600 | 1 |
| 363 | 1 | 0 | 1000 | 1000 | 2.9 | 9500 | -3864 | 687 | 793 | 50 | 14 |
| 364 | 3 | 1 | 1000 | 1000 | 1.1 | 9500 | -3677 | -84 | 485 | 31 | 18 |
| 365 | 6 | 1 | 3000 | -3000 | 1.8 | 9500 | -6197 | -963 | 4669 | 572 | 11 |
| 366 | 1 | 0 | 0 | 0 | 1.8 | 9500 | -3864 | 687 | 777 | 36 | 15 |
| 367 | 3 | 0 | -2000 | 2000 | 1.6 | 9500 | -3677 | -84 | 2769 | 57 | 12 |
| 368 | 3 | 0 | 0 | 0 | 2.2 | 9500 | -3677 | -84 | 1022 | 64 | 20 |
| 369 | 1 | 0 | -2000 | 2000 | 1.6 | 9500 | -3864 | 687 | 3244 | 46 | 14 |
| 370 | 6 | 1 | 3000 | -3000 | 0.2 | 9500 | -6197 | -963 | 4671 | 765 | 4 |
| 371 | 7 | 0 | 0 | 0 | 0.8 | 9500 | -6688 | -516 | 3565 | 686 | 12 |
| 372 | 6 | 0 | 1000 | 1000 | 2.1 | 9500 | -6197 | -963 | 2148 | 406 | 9 |
| 373 | 3 | 1 | 1000 | 1000 | 0.6 | 9500 | -3677 | -84 | 482 | 30 | 20 |
| 374 | 1 | 0 | 1000 | 1000 | 1.5 | 9500 | -3864 | 687 | 794 | 19 | 15 |
| 375 | 7 | 0 | 3000 | -3000 | 0.9 | 9500 | -6688 | -516 | 4182 | 440 | 12 |
| 376 | 3 | 0 | 1000 | 1000 | 0.7 | 9500 | -3677 | -84 | 481 | 72 | 16 |
| 377 | 6 | 1 | 0 | 0 | 0.8 | 9500 | -6197 | -963 | 3470 | 817 | 6 |
| 378 | 7 | 0 | 0 | 0 | 1.4 | 9500 | -6688 | -516 | 3561 | 543 | 8 |
| 379 | 7 | 0 | 1000 | 1000 | 2.0 | 9500 | -6688 | -516 | 2372 | 700 | 8 |
| 380 | 1 | 1 | 1000 | 1000 | 1.7 | 9500 | -3864 | 687 | 793 | 276 | 15 |
| 381 | 6 | 0 | 1000 | 1000 | 2.9 | 9500 | -6197 | -963 | 2153 | 271 | 10 |
| 382 | 1 | 0 | -2000 | 2000 | 1.6 | 9500 | -3864 | 687 | 3243 | 40 | 13 |
| 383 | 6 | 0 | 3000 | -3000 | 0.3 | 9500 | -6197 | -963 | 4669 | 206 | 6 |

| Run No. | Hours from Pred Wind | SA On | CARP X Offset | CARP Y Offset | Psi Dot | Release Alt | Predicted CARP | | Error No Control | Error Controlled | Control Inputs |
|---|---|---|---|---|---|---|---|---|---|---|---|
| 384 | 1 | 0 | 0 | 0 | 1.9 | 9500 | -3864 | 687 | 775 | 57 | 18 |
| 385 | 1 | 1 | 1000 | 1000 | 1.9 | 9500 | -3864 | 687 | 792 | 177 | 15 |
| 386 | 3 | 1 | 1000 | 1000 | 2.2 | 9500 | -3677 | -84 | 484 | 121 | 16 |
| 387 | 1 | 1 | 3000 | -3000 | 2.3 | 9500 | -3864 | 687 | 3961 | 194 | 14 |
| 388 | 3 | 0 | -2000 | 2000 | 3.1 | 9500 | -3677 | -84 | 2775 | 27 | 17 |
| 389 | 3 | 0 | -2000 | 2000 | 1.3 | 9500 | -3677 | -84 | 2772 | 61 | 16 |
| 390 | 1 | 1 | 1000 | 1000 | 2.1 | 9500 | -3864 | 687 | 791 | 92 | 13 |
| 391 | 7 | 1 | 0 | 0 | 1.8 | 9500 | -6688 | -516 | 3564 | 1025 | 14 |
| 392 | 3 | 1 | 0 | 0 | 1.3 | 9500 | -3677 | -84 | 1028 | 321 | 14 |
| 393 | 1 | 1 | 0 | 0 | 4.0 | 9500 | -3864 | 687 | 779 | 198 | 19 |
| 394 | 3 | 0 | -2000 | 2000 | 1.6 | 9500 | -3677 | -84 | 2769 | 24 | 11 |
| 395 | 1 | 1 | 3000 | -3000 | 0.4 | 9500 | -3864 | 687 | 3963 | 125 | 8 |
| 396 | 1 | 1 | 3000 | -3000 | 3.6 | 9500 | -3864 | 687 | 3965 | 209 | 18 |
| 397 | 7 | 0 | -2000 | 2000 | 2.2 | 9500 | -6688 | -516 | 5429 | 975 | 7 |
| 398 | 3 | 0 | -2000 | 2000 | 0.7 | 9500 | -3677 | -84 | 2767 | 46 | 14 |
| 399 | 6 | 0 | 0 | 0 | 2.5 | 9500 | -6197 | -963 | 3472 | 542 | 11 |
| 400 | 7 | 1 | 0 | 0 | 3.1 | 9500 | -6688 | -516 | 3564 | 655 | 16 |
| 401 | 5 | 1 | 3000 | -3000 | 1.0 | 9500 | -4748 | 41 | 5722 | 933 | 4 |
| 402 | 5 | 0 | -2000 | 2000 | 2.0 | 9500 | -4748 | 41 | 2195 | 233 | 13 |
| 403 | 1 | 0 | 0 | 0 | 1.7 | 9500 | -7283 | -867 | 873 | 212 | 10 |
| 404 | 5 | 1 | 1000 | 1000 | 0.7 | 9500 | -4748 | 41 | 3228 | 324 | 5 |
| 405 | 1 | 1 | 3000 | -3000 | 3.0 | 9500 | -7283 | -867 | 4138 | 384 | 14 |
| 406 | 5 | 1 | 3000 | -3000 | 1.8 | 9500 | -4748 | 41 | 5723 | 700 | 6 |
| 407 | 5 | 0 | 1000 | 1000 | 2.4 | 9500 | -4748 | 41 | 3208 | 369 | 15 |
| 408 | 1 | 1 | 3000 | -3000 | 1.1 | 9500 | -7283 | -867 | 4138 | 322 | 10 |
| 409 | 1 | 1 | 1000 | 1000 | 1.2 | 9500 | -7283 | -867 | 582 | 82 | 17 |
| 410 | 2 | 0 | 3000 | -3000 | 2.2 | 9500 | -7533 | -91 | 3433 | 161 | 14 |
| 411 | 2 | 1 | 1000 | 1000 | 2.0 | 9500 | -7533 | -91 | 1346 | 123 | 14 |
| 412 | 2 | 0 | 1000 | 1000 | 3.7 | 9500 | -7533 | -91 | 1356 | 153 | 13 |
| 413 | 1 | 1 | 0 | 0 | 1.6 | 9500 | -7283 | -867 | 867 | 448 | 12 |
| 414 | 2 | 0 | 1000 | 1000 | 4.1 | 9500 | -7533 | -91 | 1331 | 143 | 20 |
| 415 | 1 | 1 | 3000 | -3000 | 3.4 | 9500 | -7283 | -867 | 4137 | 374 | 13 |
| 416 | 5 | 1 | 3000 | -3000 | -0.1 | 9500 | -4748 | 41 | 5722 | 599 | 2 |
| 417 | 5 | 0 | 1000 | 1000 | 0.2 | 9500 | -4748 | 41 | 3210 | 357 | 9 |
| 418 | 2 | 1 | -2000 | 2000 | 1.9 | 9500 | -7533 | -91 | 3671 | 221 | 6 |
| 419 | 5 | 1 | 3000 | -3000 | 1.7 | 9500 | -4748 | 41 | 5724 | 1094 | 6 |
| 420 | 5 | 1 | 1000 | 1000 | 1.9 | 9500 | -4748 | 41 | 3218 | 493 | 6 |
| 421 | 5 | 1 | 0 | 0 | 2.7 | 9500 | -4748 | 41 | 1981 | 112 | 13 |
| 422 | 2 | 1 | 3000 | -3000 | 1.1 | 9500 | -7533 | -91 | 3429 | 259 | 13 |
| 423 | 2 | 1 | -2000 | 2000 | 1.1 | 9500 | -7533 | -91 | 3677 | 208 | 13 |
| 424 | 2 | 1 | -2000 | 2000 | 1.6 | 9500 | -7533 | -91 | 3671 | 109 | 12 |
| 425 | 1 | 1 | 3000 | -3000 | 1.9 | 9500 | -7283 | -867 | 4141 | 52 | 11 |
| 426 | 5 | 1 | 1000 | 1000 | 2.1 | 9500 | -4748 | 41 | 3196 | 135 | 15 |
| 427 | 1 | 1 | 1000 | 1000 | 2.9 | 9500 | -7283 | -867 | 586 | 124 | 20 |
| 428 | 2 | 1 | 3000 | -3000 | 2.5 | 9500 | -7533 | -91 | 3432 | 177 | 13 |
| 429 | 2 | 0 | -2000 | 2000 | 0.1 | 9500 | -7533 | -91 | 3676 | 140 | 13 |
| 430 | 2 | 0 | 1000 | 1000 | 2.5 | 9500 | -7533 | -91 | 1355 | 166 | 13 |
| 431 | 2 | 1 | 1000 | 1000 | 2.7 | 9500 | -7533 | -91 | 1353 | 349 | 13 |
| 432 | 2 | 1 | 1000 | 1000 | 2.9 | 9500 | -7533 | -91 | 1354 | 251 | 13 |
| 433 | 1 | 0 | 0 | 0 | 3.2 | 9500 | -7283 | -867 | 869 | 251 | 13 |
| 434 | 5 | 1 | -2000 | 2000 | 2.2 | 9500 | -4748 | 41 | 2186 | 130 | 15 |
| 435 | 5 | 0 | -2000 | 2000 | 1.2 | 9500 | -4748 | 41 | 2192 | 319 | 12 |
| 436 | 1 | 1 | 1000 | 1000 | 1.7 | 9500 | -7283 | -867 | 599 | 210 | 12 |
| 437 | 2 | 0 | 1000 | 1000 | -0.6 | 9500 | -7533 | -91 | 1352 | 141 | 15 |
| 438 | 5 | 1 | -2000 | 2000 | 2.3 | 9500 | -4748 | 41 | 2190 | 156 | 13 |

| Run No. | Hours from Pred Wind | SA On | CARP X Offset | CARP Y Offset | Psi Dot | Release Alt | Predicted CARP | | Error No Control | Error Controlled | Control Inputs |
|---|---|---|---|---|---|---|---|---|---|---|---|
| 439 | 2 | 1 | 3000 | -3000 | 2.0 | 9500 | -7533 | -91 | 3430 | 310 | 11 |
| 440 | 2 | 1 | 0 | 0 | 1.3 | 9500 | -7533 | -91 | 898 | 128 | 13 |
| 441 | 2 | 0 | 1000 | 1000 | 1.2 | 9500 | -7533 | -91 | 1357 | 155 | 13 |
| 442 | 1 | 1 | -2000 | 2000 | 0.8 | 9500 | -7283 | -867 | 3134 | 117 | 10 |
| 443 | 1 | 0 | 3000 | -3000 | 1.8 | 9500 | -7283 | -867 | 4141 | 178 | 12 |
| 444 | 5 | 0 | -2000 | 2000 | 2.2 | 9500 | -4748 | 41 | 2180 | 260 | 18 |
| 445 | 2 | 0 | 0 | 0 | 1.5 | 9500 | -7533 | -91 | 905 | 216 | 14 |
| 446 | 2 | 1 | 0 | 0 | 1.4 | 9500 | -7533 | -91 | 902 | 316 | 14 |
| 447 | 2 | 0 | 0 | 0 | 1.8 | 9500 | -7533 | -91 | 904 | 133 | 16 |
| 448 | 1 | 0 | 3000 | -3000 | 1.7 | 9500 | -7283 | -867 | 4140 | 214 | 15 |
| 449 | 2 | 0 | -2000 | 2000 | 0.9 | 9500 | -7533 | -91 | 3674 | 152 | 9 |
| 450 | 1 | 1 | 0 | 0 | 3.1 | 9500 | -7283 | -867 | 869 | 374 | 11 |
| 451 | 1 | 1 | 1000 | 1000 | 2.3 | 9500 | -7283 | -867 | 584 | 181 | 18 |
| 452 | 1 | 0 | 3000 | -3000 | 3.1 | 9500 | -7283 | -867 | 4139 | 276 | 18 |
| 453 | 2 | 1 | 3000 | -3000 | 1.4 | 9500 | -7533 | -91 | 3431 | 233 | 9 |
| 454 | 5 | 0 | 1000 | 1000 | 0.7 | 9500 | -4748 | 41 | 3220 | 334 | 5 |
| 455 | 5 | 0 | 1000 | 1000 | 2.7 | 9500 | -4748 | 41 | 3214 | 202 | 16 |
| 456 | 5 | 1 | 3000 | -3000 | 1.9 | 9500 | -4748 | 41 | 5722 | 781 | 7 |
| 457 | 1 | 1 | 0 | 0 | 1.1 | 9500 | -7283 | -867 | 883 | 221 | 20 |
| 458 | 2 | 1 | -2000 | 2000 | 1.8 | 9500 | -7533 | -91 | 3675 | 238 | 13 |
| 459 | 2 | 1 | 0 | 0 | -0.2 | 9500 | -7533 | -91 | 900 | 152 | 10 |
| 460 | 5 | 0 | 0 | 0 | 2.9 | 9500 | -4748 | 41 | 1986 | 353 | 14 |
| 461 | 2 | 0 | 1000 | 1000 | 0.9 | 9500 | -7533 | -91 | 1348 | 163 | 17 |
| 462 | 2 | 0 | -2000 | 2000 | 1.2 | 9500 | -7533 | -91 | 3674 | 137 | 9 |
| 463 | 2 | 1 | -2000 | 2000 | 3.2 | 9500 | -7533 | -91 | 3671 | 244 | 13 |
| 464 | 1 | 1 | 3000 | -3000 | 0.9 | 9500 | -7283 | -867 | 4139 | 353 | 9 |
| 465 | 2 | 1 | -2000 | 2000 | 1.4 | 9500 | -7533 | -91 | 3673 | 250 | 10 |
| 466 | 5 | 1 | -2000 | 2000 | 1.3 | 9500 | -4748 | 41 | 2190 | 369 | 10 |
| 467 | 2 | 1 | 0 | 0 | 3.5 | 9500 | -7533 | -91 | 910 | 72 | 18 |
| 468 | 2 | 1 | 3000 | -3000 | 1.9 | 9500 | -7533 | -91 | 3431 | 359 | 15 |
| 469 | 1 | 0 | 0 | 0 | 0.8 | 9500 | -7283 | -867 | 879 | 175 | 17 |
| 470 | 1 | 1 | 1000 | 1000 | 0.7 | 9500 | -7283 | -867 | 590 | 144 | 18 |
| 471 | 1 | 0 | 1000 | 1000 | 3.6 | 9500 | -7283 | -867 | 587 | 253 | 15 |
| 472 | 2 | 0 | -2000 | 2000 | 3.8 | 9500 | -7533 | -91 | 3674 | 242 | 17 |
| 473 | 1 | 1 | 3000 | -3000 | 3.5 | 9500 | -7283 | -867 | 4141 | 127 | 16 |
| 474 | 2 | 1 | 0 | 0 | 0.6 | 9500 | -7533 | -91 | 895 | 123 | 8 |
| 475 | 5 | 0 | 3000 | -3000 | 1.6 | 9500 | -4748 | 41 | 5724 | 1178 | 6 |
| 476 | 1 | 1 | 0 | 0 | 1.7 | 9500 | -7283 | -867 | 879 | 285 | 14 |
| 477 | 1 | 0 | 3000 | -3000 | 2.2 | 9500 | -7283 | -867 | 4138 | 258 | 10 |
| 478 | 1 | 1 | -2000 | 2000 | 1.3 | 9500 | -7283 | -867 | 3138 | 245 | 11 |
| 479 | 5 | 0 | 3000 | -3000 | 0.9 | 9500 | -4748 | 41 | 5723 | 619 | 4 |
| 480 | 2 | 0 | 0 | 0 | 1.4 | 9500 | -7533 | -91 | 898 | 160 | 11 |
| 481 | 5 | 0 | 3000 | -3000 | 2.9 | 9500 | -4748 | 41 | 5723 | 851 | 11 |
| 482 | 5 | 1 | 1000 | 1000 | 4.2 | 9500 | -4748 | 41 | 3210 | 377 | 18 |
| 483 | 5 | 0 | -2000 | 2000 | 2.1 | 9500 | -4748 | 41 | 2191 | 195 | 17 |
| 484 | 1 | 0 | 0 | 0 | 1.6 | 9500 | -7283 | -867 | 869 | 252 | 9 |
| 485 | 5 | 1 | 1000 | 1000 | 2.6 | 9500 | -4748 | 41 | 3212 | 173 | 16 |
| 486 | 5 | 0 | 3000 | -3000 | 1.4 | 9500 | -4748 | 41 | 5723 | 550 | 5 |
| 487 | 1 | 1 | 0 | 0 | 3.7 | 9500 | -7283 | -867 | 871 | 166 | 21 |
| 488 | 1 | 0 | 1000 | 1000 | 3.0 | 9500 | -7283 | -867 | 575 | 217 | 21 |
| 489 | 5 | 0 | 0 | 0 | 0.6 | 9500 | -4748 | 41 | 2006 | 451 | 3 |
| 490 | 2 | 1 | -2000 | 2000 | 1.2 | 9500 | -7533 | -91 | 3670 | 158 | 9 |
| 491 | 2 | 0 | 3000 | -3000 | 3.2 | 9500 | -7533 | -91 | 3433 | 151 | 17 |
| 492 | 2 | 0 | 3000 | -3000 | 2.2 | 9500 | -7533 | -91 | 3433 | 166 | 14 |
| 493 | 2 | 1 | 1000 | 1000 | 2.2 | 9500 | -7533 | -91 | 1349 | 99 | 12 |

| Run No. | Hours from Pred Wind | SA On | CARP X Offset | CARP Y Offset | Psi Dot | Release Alt | Predicted CARP | | Error No Control | Error Controlled | Control Inputs |
|---|---|---|---|---|---|---|---|---|---|---|---|
| 494 | 1 | 0 | 3000 | -3000 | 0.1 | 9500 | -7283 | -867 | 4141 | 125 | 10 |
| 495 | 2 | 1 | 1000 | 1000 | 2.1 | 9500 | -7533 | -91 | 1352 | 163 | 14 |
| 496 | 1 | 1 | 0 | 0 | 2.5 | 9500 | -7283 | -867 | 866 | 243 | 14 |
| 497 | 2 | 0 | -2000 | 2000 | 1.2 | 9500 | -7533 | -91 | 3672 | 144 | 9 |
| 498 | 5 | 0 | -2000 | 2000 | 0.8 | 9500 | -4748 | 41 | 2189 | 308 | 15 |
| 499 | 2 | 1 | -2000 | 2000 | 1.7 | 9500 | -7533 | -91 | 3674 | 99 | 14 |
| 500 | 5 | 1 | 1000 | 1000 | 0.8 | 9500 | -4748 | 41 | 3208 | 382 | 11 |
| 501 | 5 | 1 | -2000 | 2000 | 0.4 | 9500 | -4748 | 41 | 2183 | 43 | 11 |
| 502 | 2 | 1 | 1000 | 1000 | 2.5 | 9500 | -7533 | -91 | 1360 | 72 | 12 |
| 503 | 2 | 0 | 3000 | -3000 | 0.5 | 9500 | -7533 | -91 | 3434 | 154 | 6 |
| 504 | 1 | 1 | 1000 | 1000 | 1.2 | 9500 | -7283 | -867 | 592 | 149 | 14 |
| 505 | 1 | 0 | -2000 | 2000 | 1.7 | 9500 | -7283 | -867 | 3134 | 156 | 10 |
| 506 | 5 | 0 | 1000 | 1000 | 2.1 | 9500 | -4748 | 41 | 3202 | 174 | 16 |
| 507 | 5 | 0 | 0 | 0 | 1.8 | 9500 | -4748 | 41 | 1994 | 317 | 12 |
| 508 | 1 | 1 | 0 | 0 | 3.6 | 9500 | -7283 | -867 | 869 | 237 | 14 |
| 509 | 5 | 1 | 3000 | -3000 | 3.5 | 9500 | -4748 | 41 | 5723 | 1025 | 12 |
| 510 | 2 | 0 | 1000 | 1000 | 2.5 | 9500 | -7533 | -91 | 1359 | 148 | 12 |
| 511 | 2 | 1 | 0 | 0 | 1.9 | 9500 | -7533 | -91 | 899 | 42 | 13 |
| 512 | 1 | 1 | 3000 | -3000 | 1.0 | 9500 | -7283 | -867 | 4141 | 251 | 11 |
| 513 | 1 | 0 | 1000 | 1000 | 1.4 | 9500 | -7283 | -867 | 588 | 232 | 16 |
| 514 | 1 | 0 | 0 | 0 | 0.4 | 9500 | -7283 | -867 | 867 | 244 | 11 |
| 515 | 5 | 1 | 1000 | 1000 | 1.5 | 9500 | -4748 | 41 | 3202 | 102 | 15 |
| 516 | 2 | 1 | -2000 | 2000 | 1.4 | 9500 | -7533 | -91 | 3675 | 61 | 11 |
| 517 | 1 | 0 | -2000 | 2000 | 3.6 | 9500 | -7283 | -867 | 3135 | 188 | 15 |
| 518 | 5 | 0 | -2000 | 2000 | 2.6 | 9500 | -4748 | 41 | 2193 | 197 | 12 |
| 519 | 1 | 1 | 0 | 0 | 1.9 | 9500 | -7283 | -867 | 875 | 223 | 13 |
| 520 | 5 | 1 | 0 | 0 | 1.6 | 9500 | -4748 | 41 | 1981 | 102 | 12 |
| 521 | 1 | 1 | 3000 | -3000 | 1.9 | 9500 | -7283 | -867 | 4140 | 114 | 12 |
| 522 | 1 | 1 | 3000 | -3000 | 2.6 | 9500 | -7283 | -867 | 4140 | 257 | 13 |
| 523 | 1 | 1 | -2000 | 2000 | 4.1 | 9500 | -7283 | -867 | 3133 | 249 | 15 |
| 524 | 2 | 1 | 1000 | 1000 | 2.2 | 9500 | -7533 | -91 | 1347 | 274 | 15 |
| 525 | 1 | 1 | 1000 | 1000 | 2.7 | 9500 | -7283 | -867 | 601 | 380 | 14 |
| 526 | 2 | 1 | -2000 | 2000 | 2.5 | 9500 | -7533 | -91 | 3672 | 158 | 16 |
| 527 | 1 | 0 | 0 | 0 | 2.4 | 9500 | -7283 | -867 | 879 | 210 | 15 |
| 528 | 2 | 0 | 0 | 0 | 2.8 | 9500 | -7533 | -91 | 902 | 140 | 17 |
| 529 | 5 | 1 | 1000 | 1000 | 3.1 | 9500 | -4748 | 41 | 3209 | 99 | 15 |
| 530 | 1 | 0 | 3000 | -3000 | 1.9 | 9500 | -7283 | -867 | 4141 | 213 | 12 |
| 531 | 5 | 1 | 1000 | 1000 | 1.9 | 9500 | -4748 | 41 | 3209 | 262 | 13 |
| 532 | 1 | 1 | 3000 | -3000 | 2.1 | 9500 | -7283 | -867 | 4140 | 210 | 10 |
| 533 | 5 | 1 | 3000 | -3000 | 2.8 | 9500 | -4748 | 41 | 5724 | 973 | 10 |
| 534 | 1 | 0 | 3000 | -3000 | 3.1 | 9500 | -7283 | -867 | 4139 | 291 | 12 |
| 535 | 2 | 1 | 1000 | 1000 | 1.3 | 9500 | -7533 | -91 | 1360 | 224 | 10 |
| 536 | 1 | 1 | -2000 | 2000 | 2.8 | 9500 | -7283 | -867 | 3134 | 277 | 13 |
| 537 | 1 | 0 | -2000 | 2000 | 1.7 | 9500 | -7283 | -867 | 3135 | 213 | 9 |
| 538 | 1 | 1 | 0 | 0 | 1.9 | 9500 | -7283 | -867 | 874 | 314 | 11 |
| 539 | 1 | 0 | 3000 | -3000 | 2.4 | 9500 | -7283 | -867 | 4141 | 168 | 17 |
| 540 | 1 | 1 | 0 | 0 | 2.8 | 9500 | -7283 | -867 | 860 | 105 | 12 |
| 541 | 5 | 1 | -2000 | 2000 | 1.3 | 9500 | -4748 | 41 | 2191 | 379 | 11 |
| 542 | 2 | 0 | -2000 | 2000 | 0.4 | 9500 | -7533 | -91 | 3673 | 168 | 10 |
| 543 | 2 | 0 | 0 | 0 | 1.9 | 9500 | -7533 | -91 | 899 | 126 | 8 |
| 544 | 2 | 0 | -2000 | 2000 | 2.4 | 9500 | -7533 | -91 | 3674 | 127 | 16 |
| 545 | 2 | 0 | 1000 | 1000 | 1.9 | 9500 | -7533 | -91 | 1339 | 138 | 16 |
| 546 | 5 | 0 | -2000 | 2000 | 3.4 | 9500 | -4748 | 41 | 2185 | 262 | 19 |
| 547 | 2 | 1 | 0 | 0 | 1.5 | 9500 | -7533 | -91 | 909 | 127 | 17 |
| 548 | 1 | 0 | 1000 | 1000 | 2.6 | 9500 | -7283 | -867 | 600 | 295 | 13 |

| Run No. | Hours from Pred Wind | SA On | CARP X Offset | CARP Y Offset | Psi Dot | Release Alt | Predicted CARP | | Error No Control | Error Controlled | Control Inputs |
|---|---|---|---|---|---|---|---|---|---|---|---|
| 549 | 2 | 0 | 0 | 0 | 1.1 | 9500 | -7533 | -91 | 903 | 172 | 15 |
| 550 | 2 | 0 | 1000 | 1000 | 0.6 | 9500 | -7533 | -91 | 1354 | 152 | 14 |
| 551 | 1 | 0 | 3000 | -3000 | 2.5 | 9500 | -7283 | -867 | 4143 | 229 | 18 |
| 552 | 1 | 1 | -2000 | 2000 | 0.5 | 9500 | -7283 | -867 | 3138 | 278 | 14 |
| 553 | 1 | 0 | 1000 | 1000 | 0.5 | 9500 | -7283 | -867 | 573 | 198 | 19 |
| 554 | 5 | 1 | -2000 | 2000 | 1.2 | 9500 | -4748 | 41 | 2189 | 340 | 15 |
| 555 | 1 | 0 | 1000 | 1000 | 0.4 | 9500 | -7283 | -867 | 601 | 291 | 12 |
| 556 | 2 | 0 | 1000 | 1000 | 2.4 | 9500 | -7533 | -91 | 1337 | 154 | 17 |
| 557 | 5 | 0 | 3000 | -3000 | 1.6 | 9500 | -4748 | 41 | 5726 | 1064 | 5 |
| 558 | 5 | 1 | 3000 | -3000 | 0.6 | 9500 | -4748 | 41 | 5723 | 1304 | 3 |
| 559 | 2 | 0 | 3000 | -3000 | 1.0 | 9500 | -7533 | -91 | 3432 | 151 | 11 |
| 560 | 2 | 1 | 0 | 0 | 0.9 | 9500 | -7533 | -91 | 911 | 252 | 16 |
| 561 | 2 | 0 | 0 | 0 | 1.8 | 9500 | -7533 | -91 | 899 | 148 | 13 |
| 562 | 1 | 1 | 3000 | -3000 | -0.6 | 9500 | -7283 | -867 | 4142 | 154 | 13 |
| 563 | 1 | 1 | 1000 | 1000 | 1.2 | 9500 | -7283 | -867 | 586 | 235 | 13 |
| 564 | 1 | 0 | -2000 | 2000 | 0.5 | 9500 | -7283 | -867 | 3132 | 222 | 10 |
| 565 | 1 | 1 | -2000 | 2000 | 2.2 | 9500 | -7283 | -867 | 3133 | 297 | 13 |
| 566 | 1 | 1 | 0 | 0 | 2.4 | 9500 | -7283 | -867 | 867 | 184 | 11 |
| 567 | 5 | 0 | 0 | 0 | 2.0 | 9500 | -4748 | 41 | 1997 | 187 | 13 |
| 568 | 1 | 0 | -2000 | 2000 | 1.7 | 9500 | -7283 | -867 | 3136 | 158 | 12 |
| 569 | 1 | 0 | 1000 | 1000 | -0.8 | 9500 | -7283 | -867 | 587 | 293 | 17 |
| 570 | 2 | 0 | -2000 | 2000 | 1.9 | 9500 | -7533 | -91 | 3673 | 152 | 11 |
| 571 | 1 | 1 | -2000 | 2000 | 1.0 | 9500 | -7283 | -867 | 3133 | 270 | 11 |
| 572 | 2 | 1 | -2000 | 2000 | 1.6 | 9500 | -7533 | -91 | 3673 | 307 | 11 |
| 573 | 5 | 1 | -2000 | 2000 | 1.5 | 9500 | -4748 | 41 | 2180 | 265 | 15 |
| 574 | 1 | 0 | 1000 | 1000 | 0.7 | 9500 | -7283 | -867 | 581 | 229 | 17 |
| 575 | 5 | 0 | 1000 | 1000 | 2.4 | 9500 | -4748 | 41 | 3217 | 343 | 13 |
| 576 | 1 | 0 | 1000 | 1000 | 2.1 | 9500 | -7283 | -867 | 593 | 306 | 13 |
| 577 | 2 | 0 | 1000 | 1000 | 1.5 | 9500 | -7533 | -91 | 1354 | 160 | 10 |
| 578 | 1 | 0 | 0 | 0 | 2.7 | 9500 | -7283 | -867 | 866 | 256 | 13 |
| 579 | 5 | 0 | 0 | 0 | 3.4 | 9500 | -4748 | 41 | 1983 | 274 | 20 |
| 580 | 2 | 0 | 0 | 0 | 0.7 | 9500 | -7533 | -91 | 898 | 150 | 11 |
| 581 | 1 | 1 | 3000 | -3000 | 1.8 | 9500 | -7283 | -867 | 4140 | 216 | 12 |
| 582 | 5 | 1 | 0 | 0 | 0.7 | 9500 | -4748 | 41 | 2001 | 525 | 7 |
| 583 | 2 | 0 | 1000 | 1000 | 2.6 | 9500 | -7533 | -91 | 1359 | 173 | 13 |
| 584 | 2 | 1 | 0 | 0 | 2.4 | 9500 | -7533 | -91 | 902 | 84 | 14 |
| 585 | 5 | 1 | -2000 | 2000 | 1.3 | 9500 | -4748 | 41 | 2193 | 380 | 9 |
| 586 | 5 | 1 | 3000 | -3000 | 1.3 | 9500 | -4748 | 41 | 5724 | 842 | 5 |
| 587 | 2 | 1 | 3000 | -3000 | 1.1 | 9500 | -7533 | -91 | 3432 | 331 | 15 |
| 588 | 5 | 0 | -2000 | 2000 | 2.8 | 9500 | -4748 | 41 | 2187 | 260 | 15 |
| 589 | 1 | 0 | 0 | 0 | 1.6 | 9500 | -7283 | -867 | 864 | 249 | 14 |
| 590 | 1 | 1 | 0 | 0 | 1.7 | 9500 | -7283 | -867 | 870 | 309 | 12 |
| 591 | 5 | 1 | 1000 | 1000 | 0.6 | 9500 | -4748 | 41 | 3223 | 285 | 10 |
| 592 | 2 | 1 | 3000 | -3000 | 2.2 | 9500 | -7533 | -91 | 3434 | 157 | 16 |
| 593 | 1 | 0 | -2000 | 2000 | 4.5 | 9500 | -7283 | -867 | 3130 | 172 | 17 |
| 594 | 5 | 0 | 1000 | 1000 | 2.1 | 9500 | -4748 | 41 | 3197 | 185 | 18 |
| 595 | 5 | 1 | 1000 | 1000 | 0.4 | 9500 | -4748 | 41 | 3203 | 222 | 10 |
| 596 | 1 | 0 | 0 | 0 | 2.1 | 9500 | -7283 | -867 | 858 | 348 | 10 |
| 597 | 2 | 1 | 1000 | 1000 | 0.4 | 9500 | -7533 | -91 | 1352 | 316 | 10 |
| 598 | 1 | 0 | 3000 | -3000 | 2.0 | 9500 | -7283 | -867 | 4139 | 257 | 11 |
| 599 | 1 | 0 | 1000 | 1000 | 0.2 | 9500 | -7283 | -867 | 593 | 132 | 18 |
| 600 | 5 | 0 | 0 | 0 | 2.6 | 9500 | -4748 | 41 | 1986 | 217 | 13 |

# APPENDIX B. SAMPLE SIMULATION RESULTS

This appendix contains output for numerous simulation trials to illustrate a sample of the results obtained.

**Run35**
X Error: -2.8414 Y Error: -11.3694 Hor Error: 11.7191
No Control X Error: -466.9893 Y Error: -122.2171 Hor Error: 482.7174
A Inputs: 4 B Inputs: 3 C Inputs: 6 D Inputs: 2
Total Control Inputs: 15

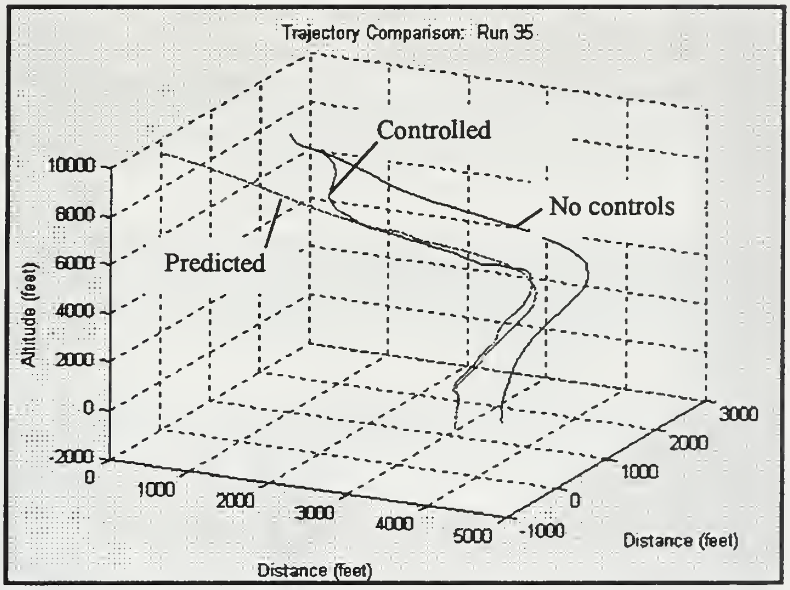

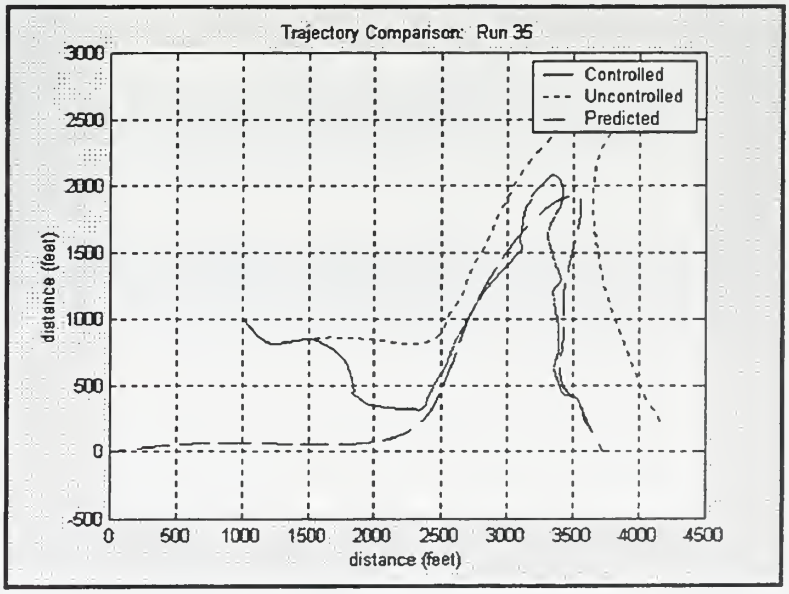

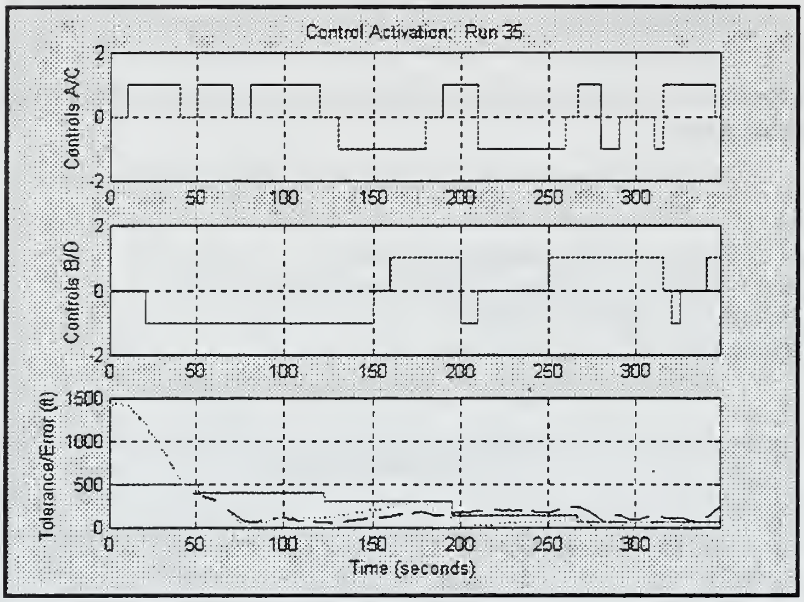
Control Activation: Run 35
Controls A/C
Controls B/D
Tolerance/Error (ft)
2
0
-2
1500
1000
500
0
0
50
100
150
200
250
300
Time (seconds)

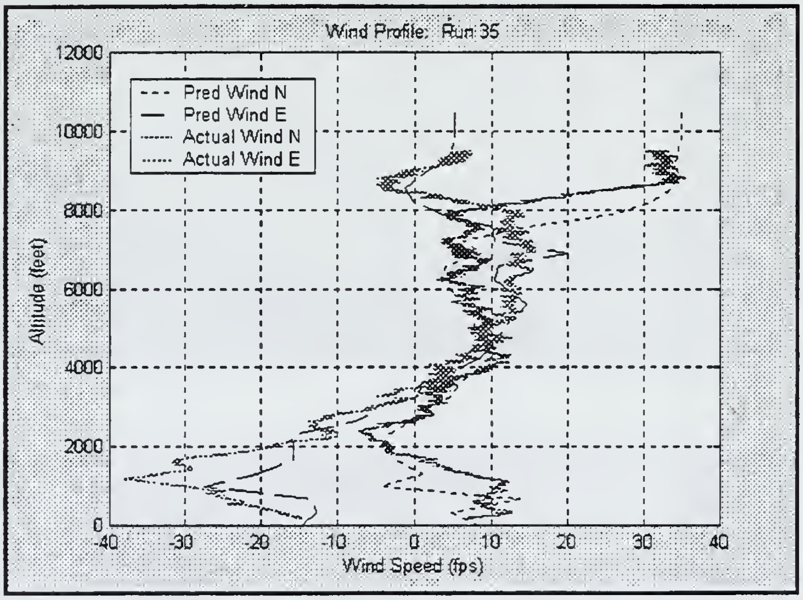
Wind Profile: Run 35
Pred Wind N
Pred Wind E
Actual Wind N
Actual Wind E
Altitude (feet)
12000
10000
8000
6000
4000
2000
0
-40
-30
-20
-10
0
10
20
30
40
Wind Speed (fps)

**Run202**

X Error: 688.6045  Y Error:  -2295.7423  Hor Error:  2396.7913

No Control X Error: 5963.0562  Y Error: -5411.0036 Hor Error: 8052.1425

A Inputs: 1  B Inputs: 1  C Inputs: 0 D Inputs: 1

Total Control Inputs: 3

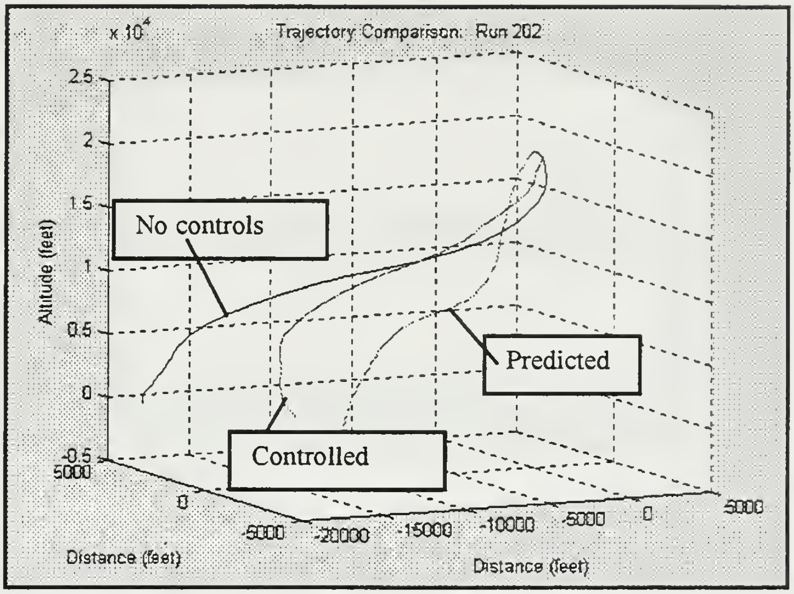

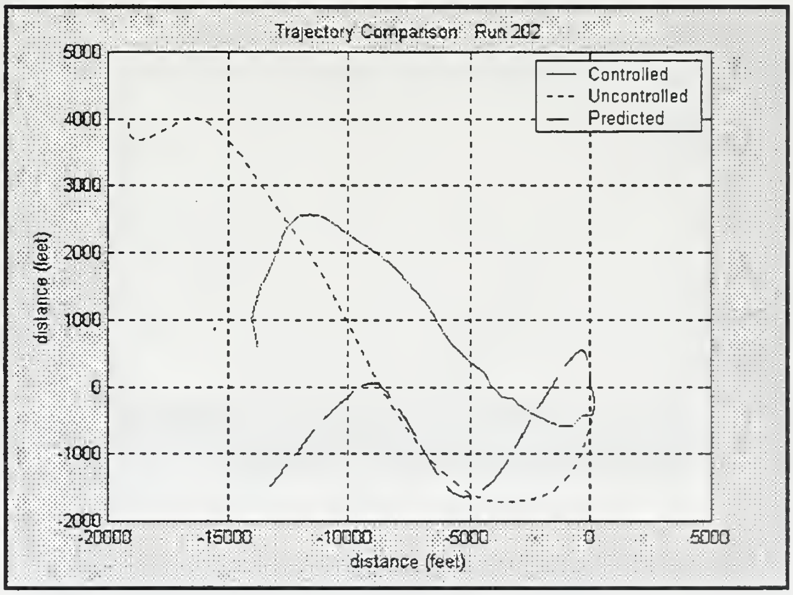

**Run202 (continued)**

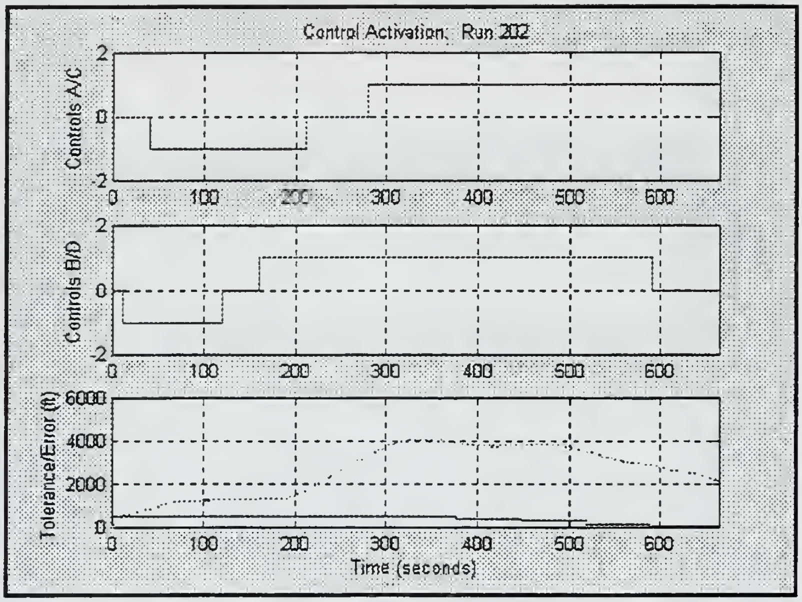

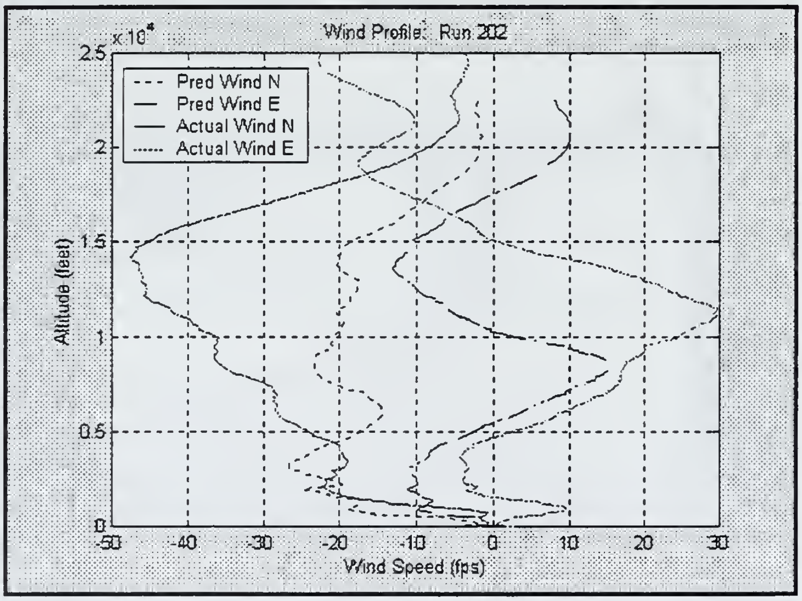

**Run217**

X Error: -209.5789 Y Error: -1305.1452 Hor Error: 1321.8651
No Control X Error: 7971.5228 Y Error: -7412.1185 Hor Error: 10885.0667
A Inputs: 6 B Inputs: 5 C Inputs: 5 D Inputs: 6
Total Control Inputs: 22

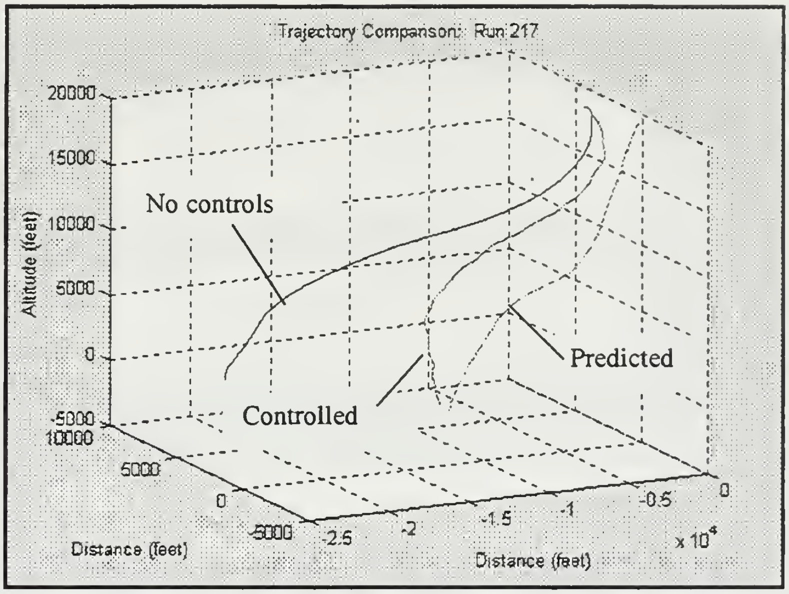

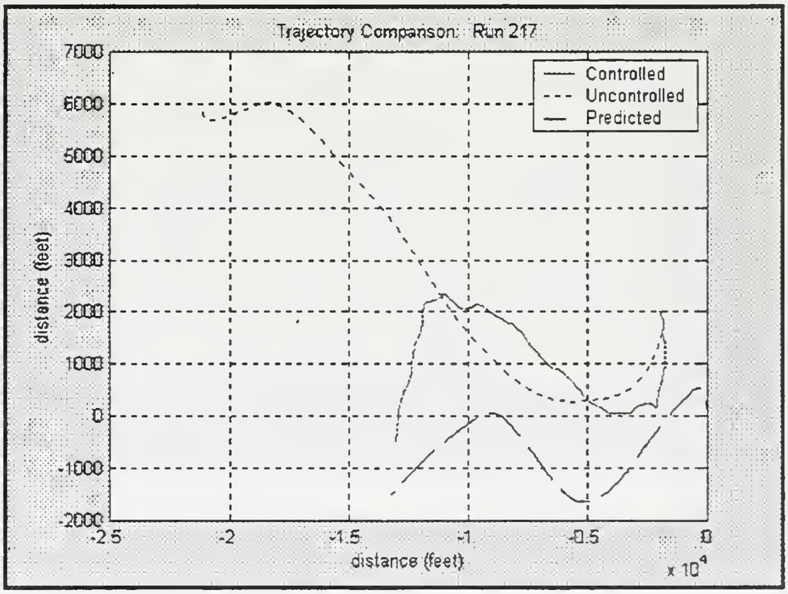

**Run217 (continued)**

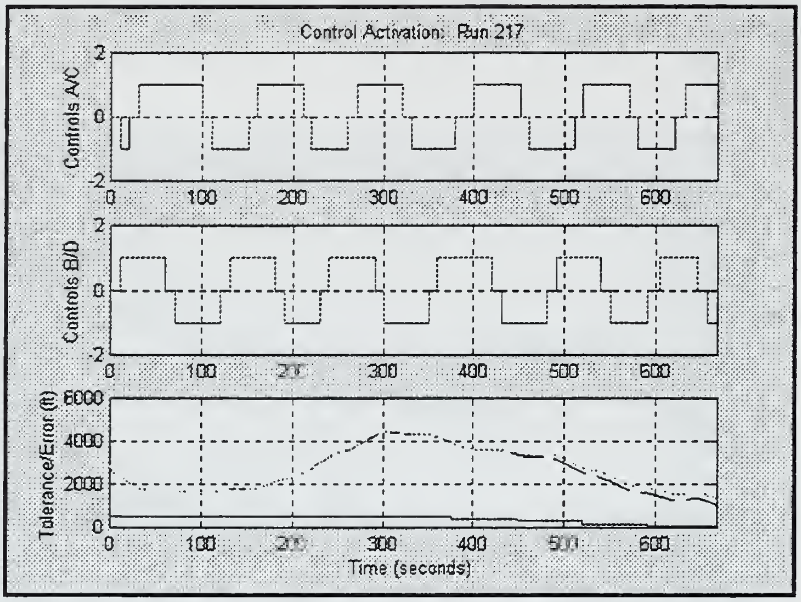

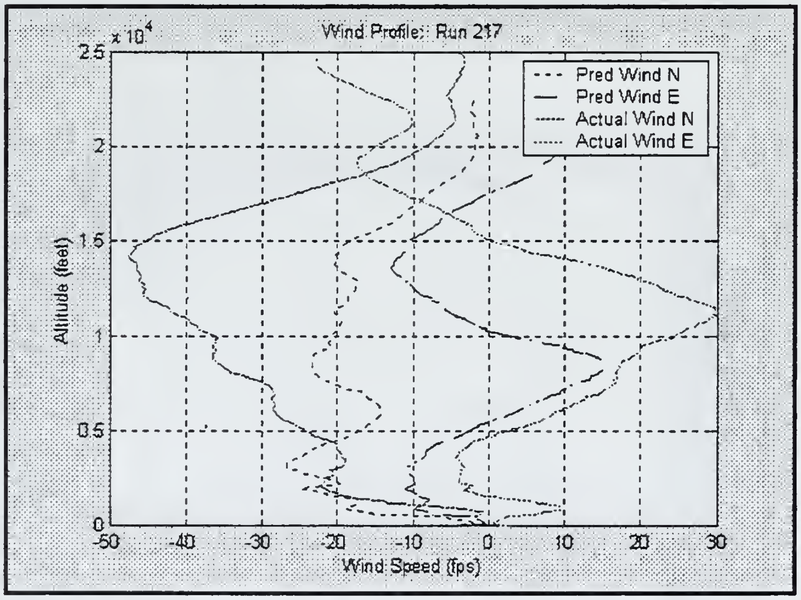

**Run223**

X Error: -115.2622 Y Error: -37.2997 Hor Error: 121.1473

No Control X Error: -684.7159 Y Error: 1083.0916 Hor Error: 1281.3755

A Inputs: 6 B Inputs: 9 C Inputs: 7 D Inputs: 8

Total Control Inputs: 30

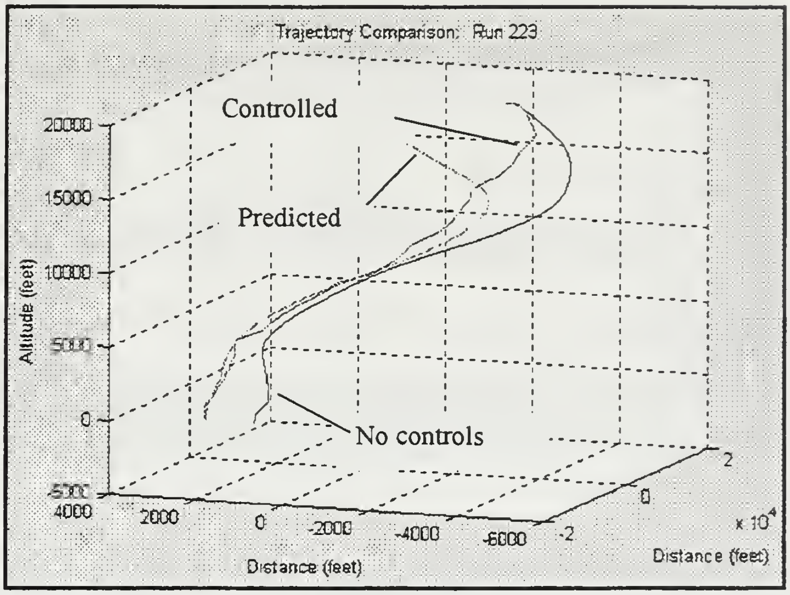

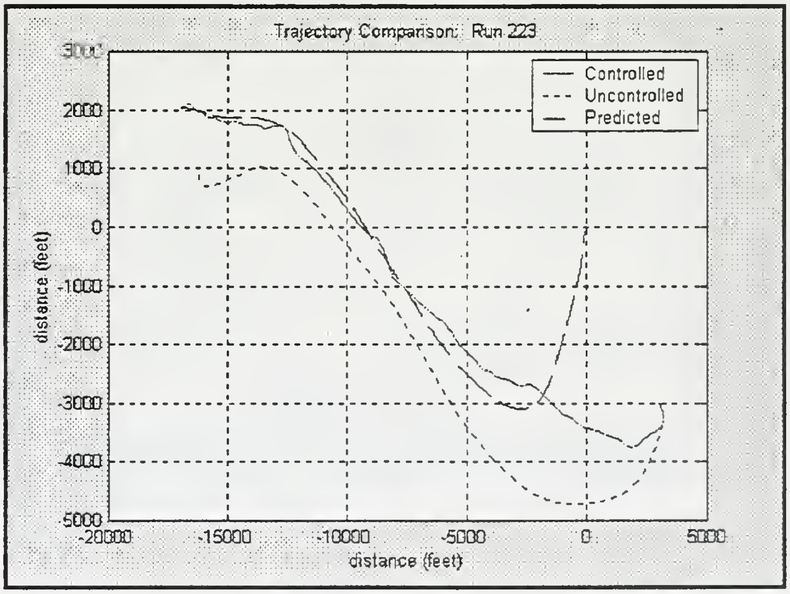

**Run223 (continued)**

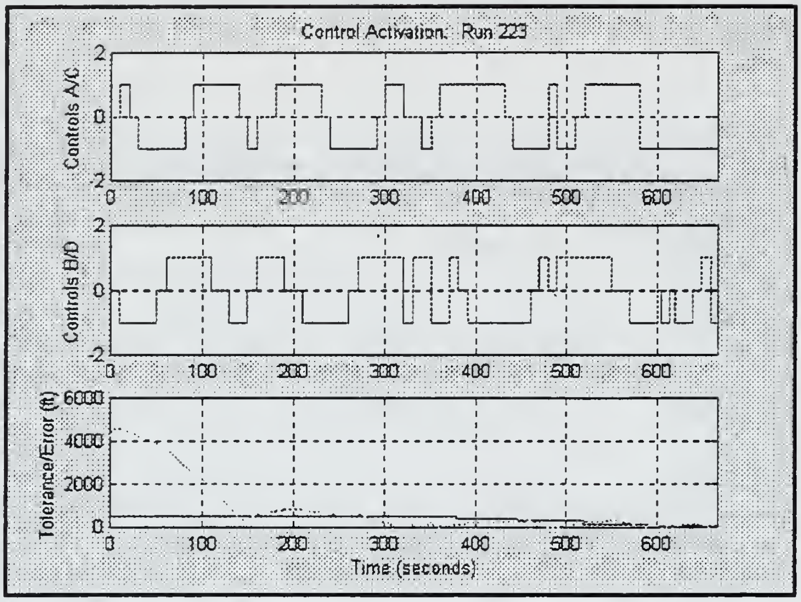

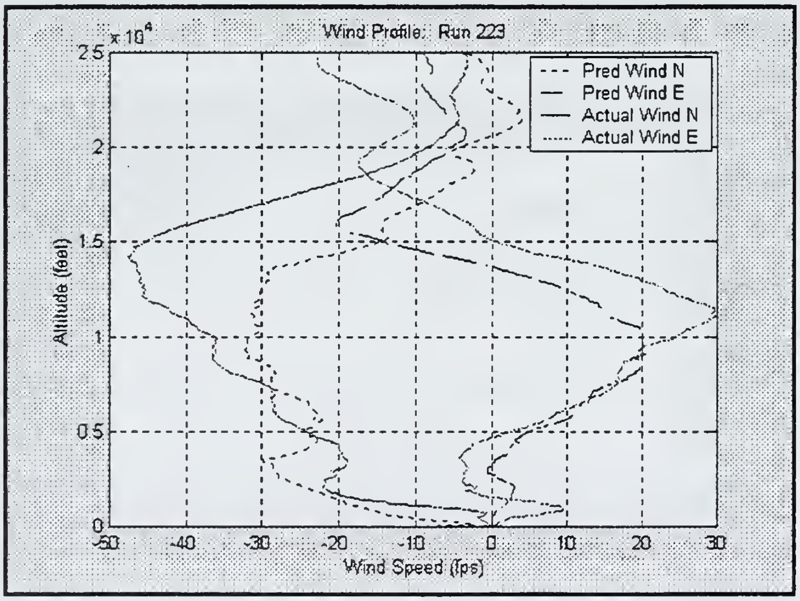

# APPENDIX C. SIMULINK® REALIZATION

The following presents the Simulink® realization for this effort. It is presented in the hierarchy of the implementation of the model.

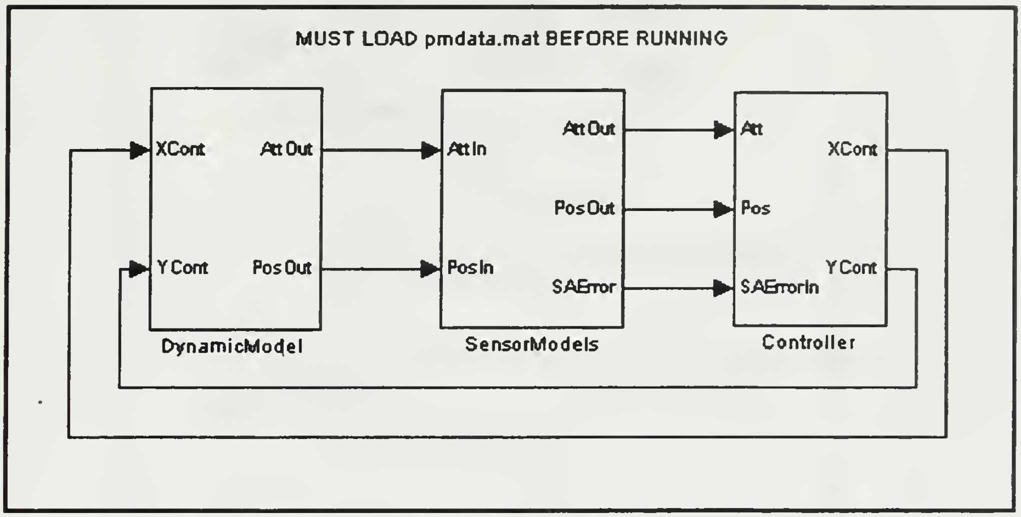

Top-level Model

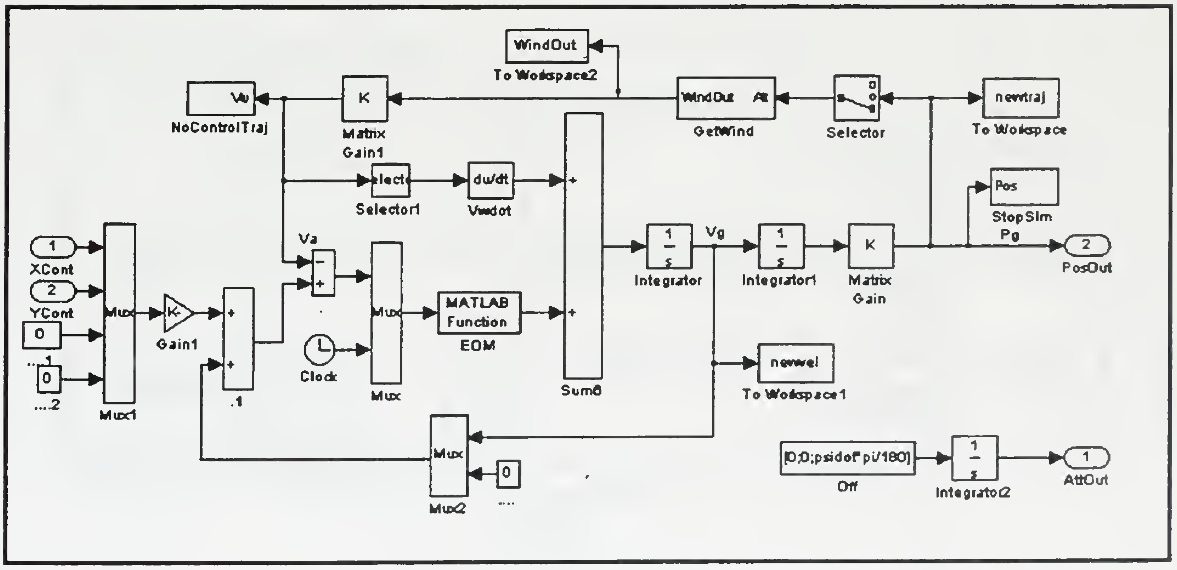

Dynamic Model

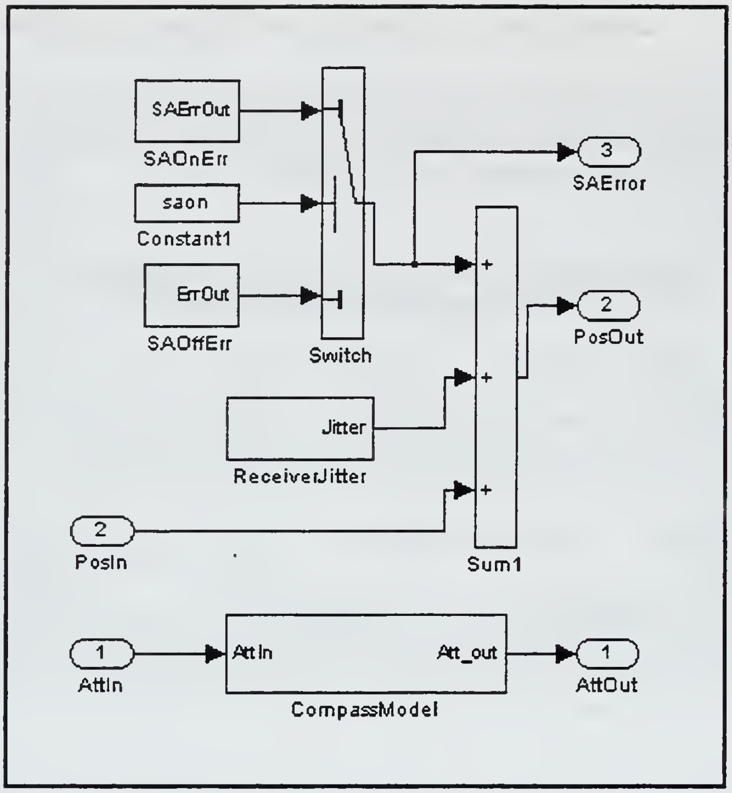

Overall Sensor Model

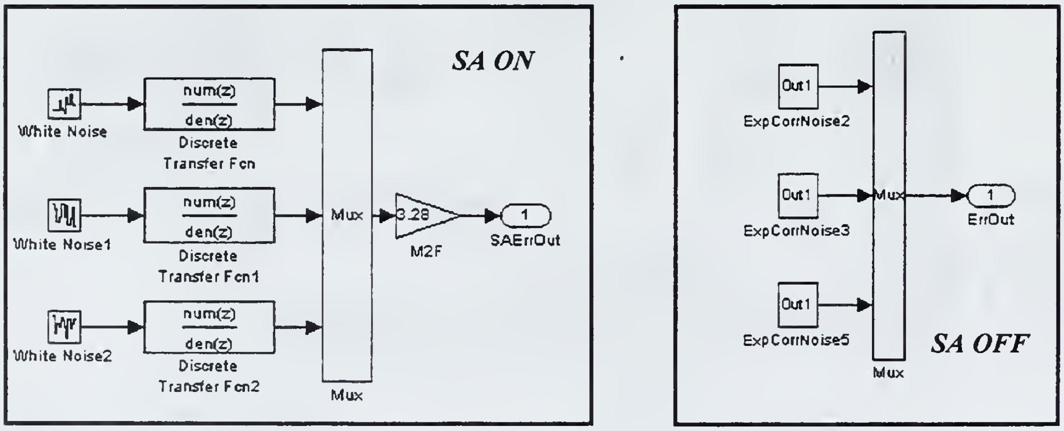

GPS Error Models

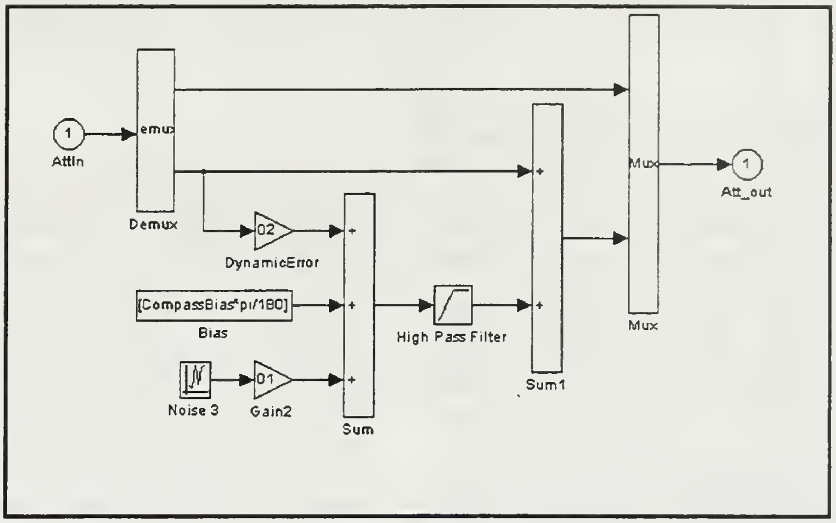

Compass Model

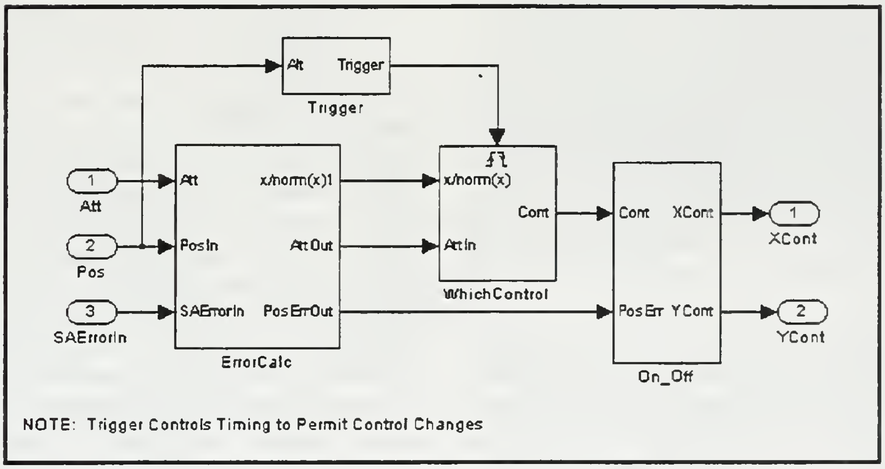

Controller

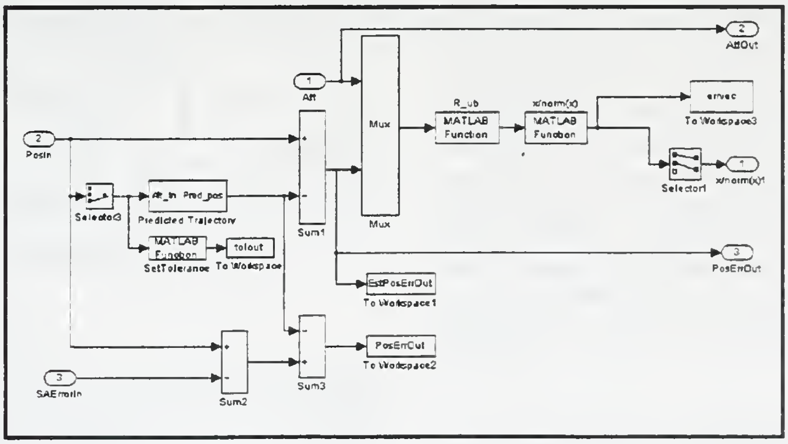

Controller Error and Tolerance Calculation Block

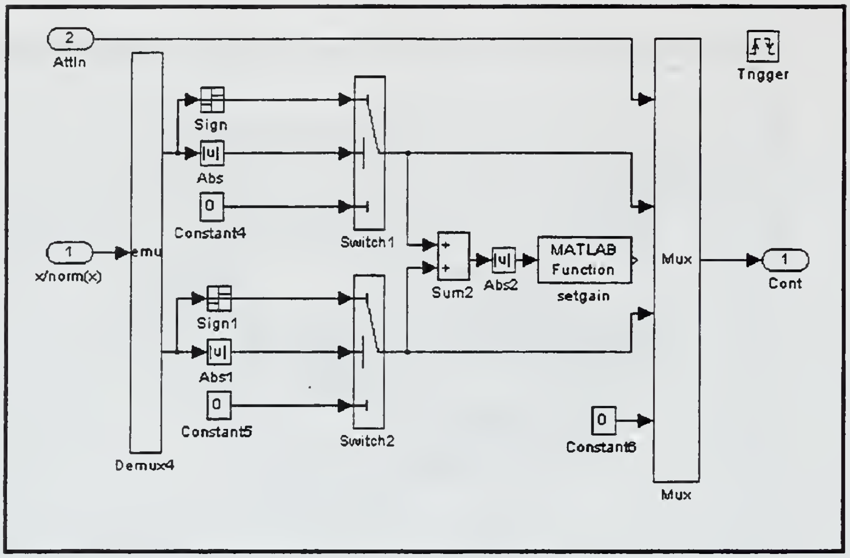

Controller ‘Which Control’ Block: Determines Which Actuator to Affect

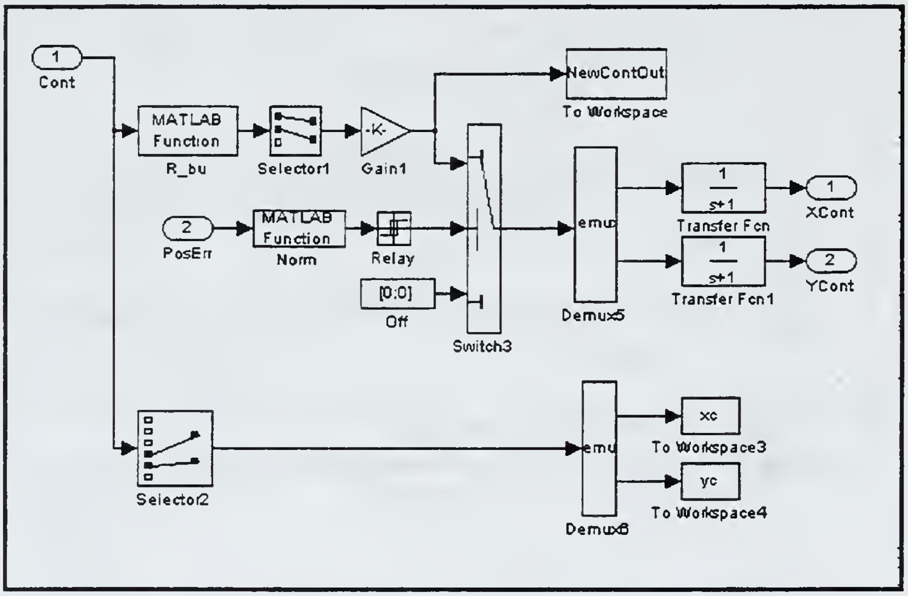

Controller ‘On_Off’ Block: Checks Tolerances and Activates Control

# APPENDIX D. AGAS INSTRUMENTATION DESCRIPTION

## Overview

The AGAS instrumentation package was required to measure and record the state of the AGAS payload to include: position, velocity, acceleration, and three-axis attitude and attitude rates. In addition, the state (extended or retracted) of each of the four actuators was recorded. The position and velocity of the AGAS payload was provided by a differential carrier-phase GPS system known as the Improved Vehicle Tracking System (IVTS). Acceleration data were derived from a triad of accelerometers, and the attitude of the package was measured by an Attitude Heading Reference System (AHRS). Pressure transducers attached to the PMAs provided the state of the actuators. Since time correlation of the data from multiple sources was critical, a timing source was included in the package. All measured data were recorded on removable flash memory devices.

The AGAS instrumentation package contained two PC/104 computer systems. The sensor computer system managed the data acquisition and recording for the AHRS, acceleration and actuator states collected at a 15-Hertz (Hz) rate. The Global Positioning System (GPS) computer system controlled the GPS receiver and acquired and recorded the receiver measurements. The GPS trajectory solution was recorded at a 5-Hz rate. Details of the instrumentation system design are presented in the appendix. The system design is illustrated in Figure 1.

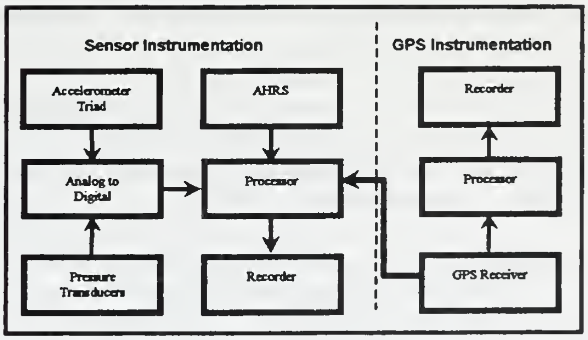

Figure 1. Instrumentation Overview

## System Architecture

The data acquisition system was based on an industry standard embedded computer product family called PC/104. This product family consists of the central processing units, power supplies, and video as well as a large assortment of analog and digital data acquisition and control modules useful in configuring data acquisition systems. The CPU modules are based on Intel® X86 processors and use the Industry Standard Architecture (ISA) bus associated with the IBM® PC/AT series of personal computers. Typical enhancements to the standard computer include solid state mass storage, Basic Input/Output Systems (BIOS) extensions, and reduced power requirements. These modules are highly integrated and have a small footprint, measuring 3.6 X 3.8 inches. The stacking feature of the PC/104 family makes it easy to configure a system to meet unique requirements. A typical PC/104 system is shown in Figure 2.

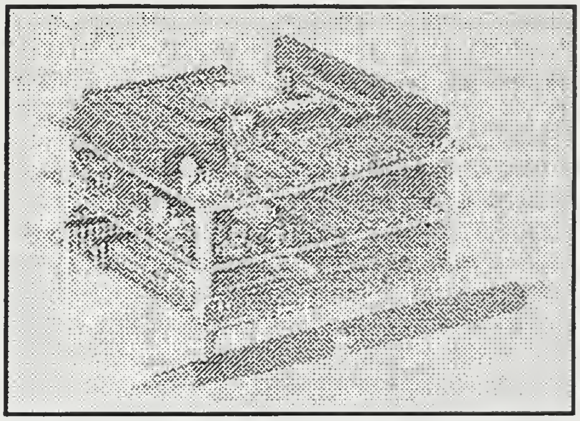

Figure 2. PC-104 Modules

## AGAS Instrumentation Computer System

The sensor computer system contained a central processing unit (CPU) module, an analog-to-digital converter (ADC) module, a power supply module, a timing module and a type II PCMCIA module. The CPU module, is a highly integrated module containing an Intel 486 DX4 processor operating at 100 Mhz, an IDC hard disk controller, a floppy disk controller, two serial ports, a parallel port and 4 megabytes of random access memory. The module also contained a 1 megabyte flash memory which, through BIOS extensions, looked to the processor like a bootable IDC hard disk. This flash memory was programmed with the operating system and the application software that controlled the modules on the stack.

The ADC module is an 8 channel 12-bit converter configured for 5-volt bipolar input. An internal adjustable gain amplifier provides programmable gains of 1, 10, 100, or 1000. The analog to digital conversion rate is a function of the mode used to initiate the conversion, and varies from 2,000 conversions per second in the software conversion mode to a maximum of 100,000 conversions per second if the direct memory access (DMA) conversion mode is used. An interrupt conversion mode is also available, which will provide up to 20,000 conversions per second. In this mode, the interrupt signal may be provided by an external signal or it may be provided from the output of a programmable 32-bit counter contained on the module. This module also contains two 12-bit digital-to-analog converters as well as four digital inputs and four digital outputs.

The timing module is a digital clock that provides accurate time to application software through the PC/104 bus. The clock may also be initialized from the application software through the bus. Time-of-year is available in a binary coded decimal (BCD) format with a resolution of hundreds of nanoseconds. Clock accuracy is maintained by phase-locking the internal clock to an external reference. The reference may be any of the standard timing signals usually found on United States test ranges, such as the Inter-Range Instrumentation Group (IRIG) time code signals or NASA time code signals. In addition the internal clock may be synchronized to an external one pulse per second (1-PPS). Synchronization accuracy to the IRIG or NASA timing signals is specified to be between 20 microseconds and 5 microseconds depending upon which code is being used for the synchronization input. A synchronization accuracy of one microsecond is specified for the 1-PPS input.

The sensor computer system power supply module is a DC to DC converter that provides up to 50 watts of power in the form of +5 volts and +- 12 volts. The power supply module requires a DC input voltage between 6 volts and 40 volts. Each of the power signals is connected to the PC/104 bus to facilitate powering the modules in the stack.

The PCMCIA module located in the sensor computer module stack is a standard type II PCMCIA interface. With the appropriate driver software, flash memory modules inserted into the interface appear to the operating system as an IDC hard drive.

Three modules comprised the GPS system computer: a CPU module, a power supply module, and a PCMCIA module. The hardware on these three modules is identical to the hardware in the sensor system computer modules. The CPU was programmed with the software required to interface with the GPS receiver sensor. A photograph of the packaged instrumentation system is included in Figure 3.

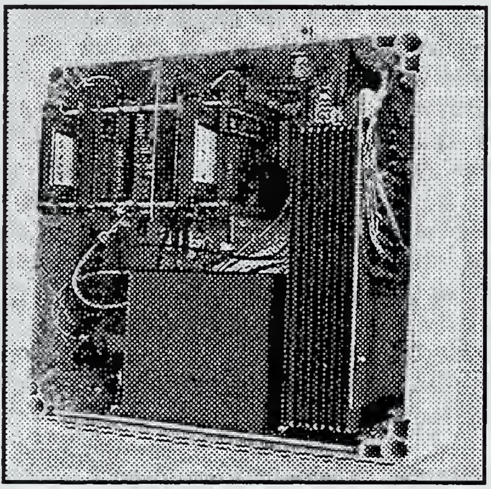

Figure 3. AGAS Instrumentation Package

AGAS Sensors

As mentioned, the AGAS instrumentation package contained four types of sensors: a GPS receiver, an AHRS unit, an accelerometer triad, and muscle state sensors. The GPS sensor consists of an L1 C/A code receiver and antenna. The receiver contains 12 independent channels, which track the GPS satellite signal in parallel. The receiver is capable of making measurements at a 20 Hz rate and providing position and velocity output up to a 10 Hz rate (a 5 Hz rate was used for the AGAS implementation). Two RS-232C I/O ports are available on the receiver to provide for control inputs and data outputs. Either of the I/O ports may be used to input commands and output data, or both may be used at the same time. An auxiliary I/O port provides a 1PPS.

The AHRS used in the AGAS instrumentation system is a solid state device that measures three-axis attitude rate and integrates it to form attitude and heading. The attitude and heading is compared with two reference vertical pendulums and a tri-axial flux-gate magnetometer. The resulting error is filtered and used to adjust the output of the system causing it to converge to the attitude of the vertical pendulums and to magnetic heading. The attitude and attitude rates are available on an RS-232C interface at a rate of just less than 15 Hz. The specified accuracy of the AHRS data is shown in Table 1.

Provided by Cibola Information Services, Yuma, Arizona under contract to US Army Yuma Proving Ground

|  | Static | Dynamic (percent) |
|---|---|---|
| Rate Accuracy (deg/sec) | ± 0.2 | ± 2 |
| Attitude Accuracy (deg) | ± 0.5 | ± 2 |
| Heading Accuracy (deg) | ± 1.0 | ± 2 |

Table 1. AHRS Accuracies

The accelerometers in the AGAS instrumentation system are miniature devices with a full-scale output of ± 10g. The acceleration experienced by these devices is converted to an electrical signal via strain gauges wired as a Wheatstone bridge and attached to the acceleration-sensing element. The frequency response of these devices is nominally 0 to 300 Hz, with a minimum response of 140 Hz. The sensitivity of each element is approximately 8 milli-volts/g. Three accelerometers were mounted in a steel mounting block with their input axis orthogonal. One axis was defined to be the X-axis with the + input of the accelerometer in the direction of +X. This axis was designated as the axis pointing forward. The other two devices were mounted such that the +Y axis was pointing to the right and the +Z axis was pointing down. The mounting block was attached to the mounting structure with the +X axis of the accelerometer triad parallel to the AHRS +X axis.

The last group of sensors in the AGAS sensor system is the riser muscle state sensors. These were simply four pressure transducers, one for each muscle. The four muscles in the control system have two states, extended and contracted. When the muscle is contracted, the pressure in the lines supplying air to the muscles is about 50 psi. When the muscle is extended, the pressure drops to nearly zero. Therefore, the pressure in the lines represents the state of the muscles (zero indicating the control is activated).

AGAS Instrumentation Software

The software residing in the processors shown in the diagram controlled the hardware in the instrumentation package. Both processors ran the MSDOS® operating system, and the application software was written in the C language.

The application software in the GPS processor was the same as that used in the Yuma Proving Ground's Improved Vehicle Tracking System, and in conjunction with the receiver used, will produce sub-meter positioning when the data is post-processed to remove errors. This software initialized the GPS receiver at power on and began to acquire the GPS satellite signal. While the AGAS package was in the aircraft, the GPS receiver tracked the signal via a retransmission system that received the signal external to the aircraft and retransmitted it inside the aircraft. Once the GPS receiver was tracking satellites, the processor collected the navigation data and recorded it on the recorder.

The sensor instrumentation processor also began initializing at power up. Early in this process, it started requesting a time message from the GPS receiver. Once this message was received with status indicating the GPS receiver had solved for GPS time, the sensor instrumentation processor initialized the timing module to the current UTC time. The accuracy of the time in the timing module was subsequently maintained by phase locking its clock to a 1 PPS signal from the GPS receiver. Once accurate time had been established in the timing module, the sensor processor enabled the AHRS output and began acquiring data.

The attitude and attitude rate data from the AHRS was transferred to the processor through an RS-232C interface. Each transfer contained a string of ASCII characters that included a unique header, the current AHRS attitude and attitude rate. The transfer was terminated with the ASCII character representing a carriage return. A period of inactivity on the interface separated the transfers. At the point the software detected the unique character designating the start of a transfer, the current time was sampled and stored. This time became the time of the attitude sample.

As soon as the attitude time sample was stored, the software acquired the accelerometer and pressure data from the ADC. This activity started with another sample of current time, which became the sample times of the data from the A/D converter. After the accelerometer and pressure data were sampled, the software converted the data to ASCII and recorded it in a file designated for A/D converter data.

At this point the software continued with the acquisition of the attitude record. Since the serial port driver operates under interrupt control, the attitude data that arrived at the port during the A/D sample interval was placed in a buffer. These data were retrieved, formatted, and recorded in the file designated for attitude data. This finished one loop of the data acquisition process and the software began to monitor the serial port for the beginning of a new attitude sample. The message rate from the AHRS was approximately 15 Hz, so the sample rate for all data was also at approximately 15 Hz.

# APPENDIX E. MATLAB® SCRIPT FILES

The following presents the MATLAB® script files utilized in this effort. Note that only the critical software code is presented.

## Initialization File

```
%This program initializes the workspace for running the
simulation.


load pmdata
runs=input('Desired Number of Runs: ');


disp('To accept current parameters (one by one) just hit
return');disp(' ');disp(' ');
disp('Current Windfile: ');disp(windfile);
newwindfile=input('Select a Wind File ([day drop#] eg. [310 1]):
');
newwindfile


if isempty(newwindfile)~=1
   windfile=newwindfile;
end


for i=1:runs


if windfile(1,1)==310;
   RAND=ceil(rand(1)*3.999);
   filechoice=[110607 110609 110612 110613];
end
if windfile(1,1)==311;
   RAND=ceil(rand(1)*2.999);
   filechoice=[110707 110711 110714];
end
if windfile(1,1)==0617;
   RAND=ceil(rand(1)*3.999);
   filechoice=[061710 061712 061714 061716];
end
```

```
rawinfile=filechoice(RAND);
saon=floor(rand(1)*1.999);
%sastart=ceil(rand(1)*6.999);
RAND=ceil(rand(1)*3.999);
offset=[0 0;1000 1000;-2000 2000;3000 -3000];
xoffset=offset(RAND,1);yoffset=offset(RAND,2);
psidot=randn(1)+1.85;
BiasDir=floor(rand(1)*1.99);
if BiasDir==1
   CompassSign=1;
else
   CompassSign=-1;
end
CompassBias=(rand(1)*1.999)*CompassSign;

if windfile(1,1)==617;
      releasealt=20000;
   else
      releasealt=9500;
end

if exist('initfile')==0
   initfile=[windfile rawinfile saon releasealt Vi Hi dzalt ...
         xoffset yoffset psidot CompassBias];
   save init initfile
else
   initfile(i,:)=[windfile rawinfile saon releasealt Vi Hi ...
---------dzalt xoffset yoffset psidot CompassBias];
   save init initfile -append
end

clear new* acchange
end
disp('init done')
```

## Equations of Motion – dof3.m

```
function accel=dof3(z);
V=z(1:3);
Vt=norm(V);
%checks to see if density is contained in the input vector.
%If not, sets to standard sea level density
if length(z)==5;
  rho=z(4);
  time=z(5);
else
  rho=0.002377;
  time=z(5);
end
%Atmospherics
qbar=.5*rho*(Vt^2);
g=32.17;
%System aerodynamics/characteristics
opentime=3;   %seconds
Cd=0.75;      %obtained from flight test
Do=28;        %reference diameter in feet
Dp=.67*Do;    %profile diameter
So=pi/4*Do^2; %reference area (flat circular parachute)
W=346;
m=W/g;
%Calculate drag area.  Assumes a linear opening of the parachute
if time<=opentime
  CdSt=[0 0;opentime Cd*So];
  CdSo=interp1(CdSt(:,1),CdSt(:,2),time);
else
  CdSo=Cd*So;
end
```

```
%Calculate mass terms
alpha11=0.25*rho*4/3*pi*(Dp/2)^3;
alpha22=alpha11;
alpha33=2*alpha11;

M1=[(m+alpha11) 0        0;
  0            (m+alpha22)  0;
   0              0          (m+alpha33)];

%accel=[-qbar*CdSo/m*V(1)/Vt;-qbar*CdSo/m*V(2)/Vt;-
qbar*CdSo/m*V(3)/Vt+g];
accel=inv(M1)*([-qbar*CdSo*V(1)/Vt;-qbar*CdSo*V(2)/Vt;...
      -qbar*CdSo*V(3)/Vt]+[0;0;W]);
```

## Monte-Carlo Simulation carlo.m

```
%This file executes the desired simulations
clear
load pmdata;load init;[row col]=size(initfile);

startrun=input('Key-in Starting Run Number ');
for runno=1:row
  windfile=initfile(runno,1:2);
  eval(['Wind=Wind' num2str(windfile(1)) 'd' num2str(windfile(2)) ';'])
  rawinfile=initfile(runno,3);
  eval(['rawin=rawin' num2str(rawinfile) ';'])
  saon=initfile(runno,4);
  if saon==1
    saseed=[floor(rand(1,3)*1000) zeros(1,6)];
  else
    saseed=floor(rand(1,9)*1500);
  end
```

```
    releasealt=initfile(runno,5);
    Vi=initfile(runno,6);
    Hi=initfile(runno,7);
    dzalt=initfile(runno,8);
    xoffset=initfile(runno,9);
    yoffset=initfile(runno,10);
    psidot=initfile(runno,11);
    CompassBias=initfile(runno,12);
    sim('carp')
    disp([num2str(runno) ' CARP Sim(s) Done']);
      CARP=-carptraj(length(carptraj),1:2);
      fliptraj
    sim('c9pointmass')
    %noise1=wavread('c:\windows\media\office97\gunshot.wav');
    %sound(noise1)
    disp([num2str(runno) ' Control Sim(s) Done'])
    monte;
    clear carptraj;
    horimpacterr
    results(runno,:)=[runno+startrun-1 windfile rawinfile saon ...
        xoffset yoffset psidot releasealt Vi Hi dzalt CARP ...
        hornocontimpacterr horimpacterr totcontrols];
end

eval(['save runfile' num2str(startrun) '_' num2str(startrun+runno-1)...
    '.asc results -ascii'])
```

# INITIAL DISTRIBUTION LIST

1. Defense Technical Information Center ........ 2
   8725 John J. Kingman Rd., STE 0944
   Ft. Belvoir, VA 22060-6218

2. Dudley Knox Library ........ 2
   Naval Postgraduate School
   411 Dyer Road
   Monterey, CA 93943-5101

3. Gerald H. Lindsey, Professor ........ 1
   Mail Code: AA/Li
   Dept. of Aeronautics & Astronautics
   Monterey, CA 93943

4. Maximilian F. Platzer, Distinguished Professor ........ 1
   Mail Code: AA/Pl
   Dept. of Aeronautics & Astronautics
   Monterey, CA 93943

5. Issac I. Kaminer, Associate Professor ........ 1
   Mail Code: AA/Ka
   Dept. of Aeronautics & Astronautics
   Monterey, CA 93943

6. Richard M. Howard, Associate Professor ........ 1
   Mail Code: AA/Ho
   Dept. of Aeronautics & Astronautics
   Monterey, CA 93943

7. Isaac M. Ross, Associate Professor ........ 1
   Mail Code: AA/Ro
   Dept. of Aeronautics & Astronautics
   Monterey, CA 93943

8. Dr. Steven Walker ........ 1
   AFOSR/NA
   110 Duncan Avenue
   Bolling AFB
   Washington, DC 20332-8080

9. U.S. Army Soldier & Biological Chemical Command ........................................ 2
Soldier Systems Center Natick
ATTN: SSCNC-UTS (Richard Benney/Sanjay Patel)
Kansas Street
Natick MA 01760-5017

10. Technical Library........................................................................................ 1
US Army Yuma Proving Ground
STEYP-MT-A
Yuma, AZ 85365

11. US Army Yuma Proving Ground ........................................................................ 2
Aviation and Airdrop Systems Division
STEYP-MT-EA
Yuma, AZ 85365

72 290NPG 3030
TH
6/02 22527-200 NLB

DUDLEY KNOX LIBRARY
3 2768 00403411 6